MULTIVARIABLE CONTROL SYSTEM DESIGN FOR A SUBMARINE USING ACTIVE ROLL CONTROL

by

Richard James Martin

B.S., Purdue University
(1978)

SUBMITTED TO THE DEPARTMENTS OF OCEAN ENGINEERING AND MECHANICAL ENGINEERING IN PARTIAL FULFILLMENT OF THE REQUIREMENTS FOR THE DEGREE OF OCEAN ENGINEER AND MASTER OF SCIENCE IN MECHANICAL ENGINEERING

at the

MASSACHUSETTS INSTITUTE OF TECHNOLOGY

May 1985

Signature of Author: _____
Department of Ocean Engineering, April 24, 1985

Certified by _____
Professor Michael Athans, Thesis Co-Supervisor

Certified by _____
Professor Lena Valavani, Thesis Co-Supervisor

Certified by _____
Professor Michael Triantafyllou, Thesis Reader

Accepted by _____
Professor A. D. Carmichael
Chairman, Ocean Engineering Department Committee

Accepted by _____
Professor A. A. Sonin
Chairman, Mechanical Engineering Department Committee

Permission is hereby granted to the Charles Stark Draper Laboratory, Inc., to the Massachusetts Institute of Technology, and to the United States Government and its agencies to reproduce and to distribute copies of this thesis document in whole or in part.

Signature:

MULTIVARIABLE CONTROL SYSTEM DESIGN FOR A SUBMARINE USING ACTIVE ROLL CONTROL

by

Richard James Martin

Submitted to the Departments of Ocean Engineering and Mechanical Engineering in Partial Fulfillment of the Requirements for the Degrees of Ocean Engineer and Master of Science in Mechanical Engineering.

ABSTRACT

A Multivariable Control System is designed for a deeply submerged submarine using the Linear Quadratic Gaussian (LQG) with Loop Transfer Recovery (LTR) methodology. The differential stern, bow, and rudder control surfaces are dynamically coordinated to cause the submarine to follow independent and simultaneous commanded changes in roll, yaw rate, depth rate and pitch attitude. Linear models of the submarine are developed at a ship speed of 30 knots with various rudder angles and then analyzed using the method of modal analysis. The linear models are then augmented with integral control, loop shaping techniques are applied to design a Kalman Filter transfer function, and the LTR technique is applied to recover the Kalman Filter loop shapes. The resulting model-based compensator and plant is tested using a non-linear mathematical model of the submarine, and comparisons are made with an equivalent compensator design that lacks active roll control capability. The performance characteristics of the closed loop design with roll control capability was significantly better than the characteristics of the design without roll control.

THESIS SUPERVISORS: Dr. Michael Athans, Professor of Systems Science and Engineering
Dr. Lena Valavani, Assistant Professor of Aeronautics and Astronautics

ACKNOWLEDGEMENTS

I would like to thank my thesis supervisors, Professors Michael Athans and Lena Valavani, for their support in shaping the ideas of this thesis and for their never-ending patience in its completeness.

I would also like to thank the Charles Stark Draper Laboratory for the use of their facilities over the last three years, including the computer resources and use of modem upon which this thesis strongly depended.

Additionally, I sincerely thank Mr. William Bonnice of Draper, for his technical and programming support for the submarine model.

This research was conducted at the MIT Laboratory for Information and Decision Systems with partial support provided by the Office of Naval Research under contract ONR/N00014-82-K-0582(NR606-003).

TABLE OF CONTENTS

LIST OF FIGURES

LIST OF FIGURES (continued)

LIST OF TABLES

CHAPTER ONE

INTRODUCTION AND SUMMARY

1.1 Background

The advent of the microprocessor is having a significant effect on ship control, as it is in many other fields of engineering. In particular, the present technology for the design and implementation of digitally based multivariable control systems has improved drastically, resulting in a very strong need for the analysis of complex, long standing design problems.

As it stands today, multi-input, multi-output (MIMO) control system design is much more difficult than either classical control system design or single input, single output (SISO) control system design. This MIMO methodology, and in particular the LQG/LTR method, also appears to be relatively unknown to many researchers and engineers involved with control systems design. (This observation was extremely apparent at the Seventh Ship Control Systems Symposium in Bath, UK in September 1984). It appears that the major reason the LQG/LTR methodology is as yet unknown is because of its recent development, and limited application to actual engineering design problems. Another reason, although less significant than the first, is that a significant amount of effort is required to develop a realistic model of the system being considered, to design the controller, and then to evaluate the design.

It is therefore instructive to apply the MIMO methodology to realistic ship examples to display the power and benefits of the methodology, to understand possible shortcomings with the procedures, and to provide results of model tests (in this case a computer program simulation of a full scale submarine). See Appendix A for a description of key issues in submarine control.

1.2 Prior Work

The majority of previous controller designs for submarines have used the SISO design methodology or classical design techniques. There have been a limited number of examples of MIMO designs for full scale submarines. These were performed by Navy graduate students at MIT under the supervision of Professors Lena Valavani and Michael Athans [10 through 13].

In previous designs, the use of pitch, roll, and depth control were not fully utilized. The vertical velocity (w) was generally used to represent one of the state variables considered. Since w(t) is not an inertial reference variable, it represents the true vertical rate only when the submarine has zero pitch and roll angles.

Although the depth rate, $\dot{z}(t)$, is not directly available as a state variable, it can be easily constructed from the geometric relation that

$$\dot{z}(t) = -u \sin\theta + v \cos\theta\sin\phi + w \cos\theta\cos\phi$$

which consists of terms that are readily available.

Additionally, active roll control for a cruciform stern has not been used in previous theses. Active roll control is used in this thesis to demonstrate its advantages.

1.3 Contributions of the Thesis

The major contribution of this thesis is to demonstrate the multivariable LQG/LTR feedback control system design methodology for a submarine. We demonstrate how to design using the LQG/LTR methodology a four input, four output MIMO feedback control system in which the differential stern, bow, and rudder control surfaces are used to cause the submarine to follow independent and simultaneous commands in roll, yaw rate, pitch, and depth rate. A second contribution of this thesis is to demonstrate the improvement in operational capabilities of full scale submarines if active roll control is employed. The closed loop dynamic response of the submarine is improved considerably over a submarine without active roll control. In either case, the LQG/LTR design methodology was found to be robust when evaluated in non-linear simulations, even though there were significant changes between the dynamic characteristics of the linear and non-linear models.

1.4 Outline of the Thesis

Chapter 2 contains a physical description of the submarine and the development of the model employed in this thesis. A brief description of the model implementation at

Draper's computer facility is also discussed. The latter part of the chapter describes the process used to linearize the submarine model, and a discussion of the reasoning used to select the output and control variables.

Chapter 3 contains the analysis of the linear model eigenstructure using modal decomposition. The structure of the pole-zero composition and singular values are also utilized to display the open loop dynamics of the model.

Chapter 4 contains a discussion of the LQG/LTR methodology. The performance specifications of the controller are discussed, and the linear portion of the control system design is presented.

Chapter 5 contains the evaluation of the compensator using both the linear and non-linear submarine simulations. Comparisons are also provided with a compensator which does not have the capability of active roll control, but which is otherwise designed to the same specifications.

Chapter 6 contains the summary, and proposals for future research.

CHAPTER TWO

THE SUBMARINE MODEL

2.1 Introduction

The non-linear submarine dynamical model used in this thesis is implemented at Draper Laboratory both as a real-time simulation facility and as an analytical model generating facility. A summary of the SUBMODEL program can be found in Appendix B. A detailed discussion can be found in reference [14].

The rudder and stern plane configuration to be investigated is the so-called cruciform stern. Existing submarines use a cruciform stern with mechanically coupled upper and lower rudders, and mechanically coupled port and starboard stern planes. The advantage of this stern configuration is that the design allows intuitive actions by the operator for desired ship motion. For example, if it is desired to rise or dive, all the operator has to do is command rise or dive on the stern planes. A similar situation exists if the operator desires to turn. A major drawback to this stern however, is that there is no opportunity to actively control roll on existing submarines. A submarine has the natural tendency to roll in a turn, and since the snap roll of a submarine in a turn is a function of the speed into the turn and the initial displaced rudder angle, it becomes very difficult for the operator to maintain a level trajectory, and even more difficult to

command at the same time a desired pitch and/or depth rate change.

This thesis will investigate the utilization of active roll control, and implementation of a control surface feedback control scheme that will consider the mobility characteristics of depth, course, and speed (in that order). This investigation will be performed using the LQG/LTR methodology for the control system design.

Experience with full scale submarines has shown that roll plays a significant factor in the ability of the operator to maintain ordered depth in turns or rudder malfunctions. This experience has also been shown in computer models of submarines, including the SUBSIM model at Draper laboratory. If methods are utilized to reduce the snap roll, the ability to maintain ordered depth is greatly increased.

This chapter discusses the development, implementation, and linearization of the submarine model upon which the remainder of this thesis is based. The reasoning used to select the output and control variables is also presented.

2.2 Model Development

Submarine hydrodynamics is primarily concerned with the motion of a body through the water. Consequently, there must be a means of defining the body orientation with respect to the fluid flow, and the location of the body with respect to some fixed reference frame.

In defining the motion of a submarine, reference must be made to two sets of coordinate axes; one fixed in the ship and one fixed with respect to the earth.

2.2.1 Ship Coordinates

The axes fixed in the ship (x,y, and z) are in a right-handed orthogonal system where the origin is taken to be the mass center of the ship. The mass center is assumed to lie in the vertical centerplane of the ship and is usually a short distance below the longitudinal axis of symmetry. The mass center is assumed not to move during ship maneuvers. The center of the coordinate system is at the center of mass for motion along any of the three orthogonal axes. Additionally, the moments of inertia, including the inertia due to the water, are taken around the three orthogonal axes and are designated K, M, and N.

2.2.2 Fixed Coordinates

The second set of axes (X, Y, and Z) required to define the motion of the submarine is one which is fixed with respect to the earth. Like the ship axes, these coordinates form a right-handed orthogonal system.

Figure 2.1 shows the reference system used in this thesis.

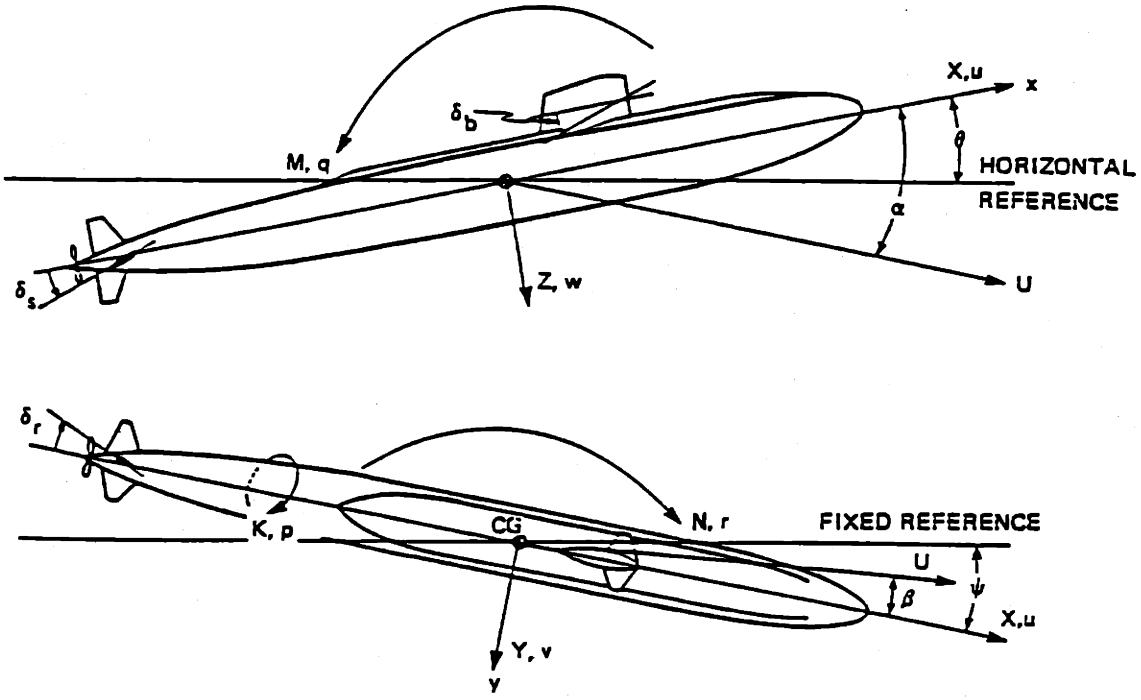

Figure 2.1 Sketch showing positive directions of axes, angles, velocities, forces, and moments.

2.2.3 Definitions of Submarine States and Control Variables

In general, for the purposes of modelling the dynamics of submarine motion, the equations of motion are expressed in the ship coordinate system because hydrodynamic forces and moments are readily computed in this reference frame. On the other hand, when interested in guidance and control of a submarine, it may be desirable to describe the vehicle motion in terms of the fixed coordinate system.
General equations have already been developed for the description of the dynamics of underwater vehicle motion, these equations generally contain expressions for Newtonian forces and moments on the left hand side, and the

expressions for dynamic response on the right hand side. The left hand side of the equations becomes quite involved due to the transformations of the coordinate system from the center of mass to the center of buoyancy; which is more correctly the reference point in these equations because this point is a function of the submarine geometry and is fixed whereas the center of mass may shift due to shifting of weights within the submarine. Details of these transformations can be found in Abkowitz [16]. The right hand side of the equations represent the external forces and moments exerted on the submarine by hydrodynamic, control surface, propulsion, and other effects.

The force and moment equalities of the equations of motion describe the six possible degrees of freedom of submarine motion. Motions of surge, heave, and sway are represented by the three forces in the axial, lateral, and normal directions of motion. Motions of roll, pitch, and yaw are represented by the three moment equations.

The state vector for the submarine must include the six degrees of freedom from the ships coordinate system, the three Euler angles which describe the relationship of the motion of the submarine with respect to the two coordinate systems, and the desired position variables to locate the submarine with respect to the fixed coordinate system. As stated earlier, the critical effort for this thesis will be to maintain ship's depth in hard rudder maneuvers, thus z is included in the state vector, as shown in Table 2.1.

Table 2.1 Definition of Submarine States and Control Variables

Submarine States

$u = x_1(t)$	forward velocity	(ft/sec)
$v = x_2(t)$	lateral velocity	(ft/sec)
$w = x_3(t)$	vertical velocity	(ft/sec)
$p = x_4(t)$	roll rate	(rad/sec)
$q = x_5(t)$	pitch rate	(rad/sec)
$r = x_6(t)$	yaw rate	(rad/sec)
$\phi = x_7(t)$	roll angle	(radians)
$\theta = x_8(t)$	pitch angle	(radians)
$\psi = x_9(t)$	heading angle	(radians)
$z = x_{10}(t)$	depth (+ down)	(feet)

Control Variables

δb	bow/fairwater planes	(rad)
δr	rudder deflection	(rad)
δs_1	port stern plane deflection	(rad)
δs_2	starboard stern plane deflection	(rad)

Further details of the derivation of the non-linear equations of motion and a description of the hydrodynamic coefficients describing the submarine geometry and control surfaces can be found in NSRDC Report 2510 [5].

To reflect current operating procedures, the propeller related thrust control variable RPS will be constrained to turn at a constant specified value during maneuvering situations.

2.3 Model Implementation

Initially, the computer program was developed at the Naval Ship Research and Development Center (NSRDC), and was provided to CSDL along with the 2510 Standard Equations of Motion. These equations have since been improved to include the effects of crossflow drag and vortex contributions. After approximately one year of development, programming, debugging, and documentation, Draper's adapted model was implemented in the simulation laboratory, resulting in a real time simulation environment of the submarine model. A Digital Equipment Corporation VAX 11-780 and graphics display workstation are used to provide visual display of the submarine motion for maneuvering situations. The capability of hard-copy output is also provided.

Later, for the purposes of analytical control system design, the computer program was implemented on the IBM timesharing computer at CSDL. To aid the design engineer, the following capabilities of the system are now included:

1. A user friendly executive routine to allow the modification of parameters and selection of options for simulation runs. The routine submits the user specified program for batch processing.

2. The option of calculating the $\underline{A}$ and $\underline{B}$ matrices that describe the linearization of the model about a specified nominal point, in the form

$$\dot{\underline{x}}(t) = \underline{A}\,\underline{x}(t) + \underline{B}\,\underline{u}(t).$$

3. The options of setting control surfaces, as desired by the designer, as a function of time. The options can be specified in a data file,

calculated using full state feedback, or by calculation using a LQG/LTR derived compensator.

4. Hard copy print-outs, plots, or both, of the state variables over time may be provided of either the non-linear or the linear models.

5. The capability of searching for a local equilibrium point for the non-linear model that is close to the specified desired nominal point.

It is important to note the following limitations of the non-linear model as it is currently implemented:

1. Actuator dynamics, or the actual angle rate limits of the control surfaces are not modelled.

2. Vortex shedding and separation effects of the fluid are not included in the linearized model.

2.4 Model Linearization

The controller design procedure begins with the expression of the equations of motion in linear time invariant state space form. The non-linear, multivariable system that represents the submarine is described by:

$$\frac{d}{dt}\underline{x}(t) = \underline{f}(\underline{x}(t),\underline{u}(t))$$

$$\underline{y}(t) = \underline{g}(\underline{x}(t))$$

where:

$\underline{x}(t)$ is the state vector

$\underline{u}(t)$ is the control vector

$\underline{y}(t)$ is the output vector

These non-linear equations can then be linearized through a fairly straight-forward technique. A nominal point is

chosen for the design by integrating the non-linear equations of motion using a specified set of initial conditions. An equilibrium point is found that corresponds to minimum accelerations for all the state variables determined from the integration of the equations of motion. The values of the state variables at the equilibrium point then specify a nominal point, about which higher order terms may be neglected. From these results, a set of linear differential equations may then be produced, the $\underline{A}$ and $\underline{B}$ matrices calculated, and a state space description of the submarine model produced.

For each nominal point determined, the resulting linear model must be validated by perturbing the nominal point to form a set of initial conditions, and then comparing the results of integrating the non-linear and linear equations of motion. For small perturbations, the non-linear model should always return to the equilibrium point values. The linear model, however, will never reach equilibrium due to the forces imposed by the control surfaces. The comparisons of the two models should, however, provide a means to compare initial derivatives, natural frequencies, and the damping effects.

The nominal point chosen for the design corresponds to a level submarine trajectory at 30 knots. The rudder deflection, δr, can be set at arbitrary angles to cause the submarine to turn at different rates, and to roll at different angles. This attempts to determine the open loop

sensitivity of the submarine to roll, which has a significant effect on the depth of a submarine in a turning maneuver.

Linear models were developed for rudder deflections from 0° to 25°. The models are designated S30R0, S30R1, S30R5, etc., reflecting the speed and rudder deflection.

To adequately validate the linear models, it is necessary to perturb the nominal point of the linear and non-linear models, and compare the time histories of the state parameters. Provided the perturbations are not excessive, the non-linear model will return to the equilibrium point. The linear model, however, will not return to it's equilibrium point resulting from the non-zero forces imposed by the control forces, and the absence of non-linear hydrodynamic effects.

Perturbations were applied to the models differently. For the S30R0 model, the perturbations were as listed below.

state variable	perturbation
u	5 ft/sec
v	0.5 ft/sec
w	0.5 ft/sec
p	-0.005 deg/sec
q	+0.001 deg/sec
r	-0.005 deg/sec
ϕ	-2.0 deg
θ	-4.6 deg
ψ	0.0 deg

The remaining models were perturbed 10% above the nominal values obtained from the intergration of the non-linear dynamics. Remember, these perturbations were not selected

analytically, but were arbitrarily selected to validate the linear models.

The comparisons of selected non-linear and linear models and state variables show excellent correlation, thus, serve to validate the linearized models. Figures 2.2 and 2.3 show the initial derivatives, natural frequency response, and damping factors are almost identical. Similar results were obtained for the other models.

2.5 Output and Control Variable Selections

2.5.1 Constraints of the Methodology

Selection of the output variables requires a careful study of the $\underline{A}$ and $\underline{B}$ matrices and determination of the objectives of the controller design. Four control variables exist if RPS is fixed, and differential stern planes are utilized.

The Loop Transfer Recovery method for the class of Model Based Compensators places a natural constraint on the design process at an early stage. Common sense mathematics of the singular values requires the number of independent control inputs to equal the number of independent output controlled variables. In other words if

$$\underline{y}(t) \in R^m$$

$$\underline{u}(t) \in R^p$$

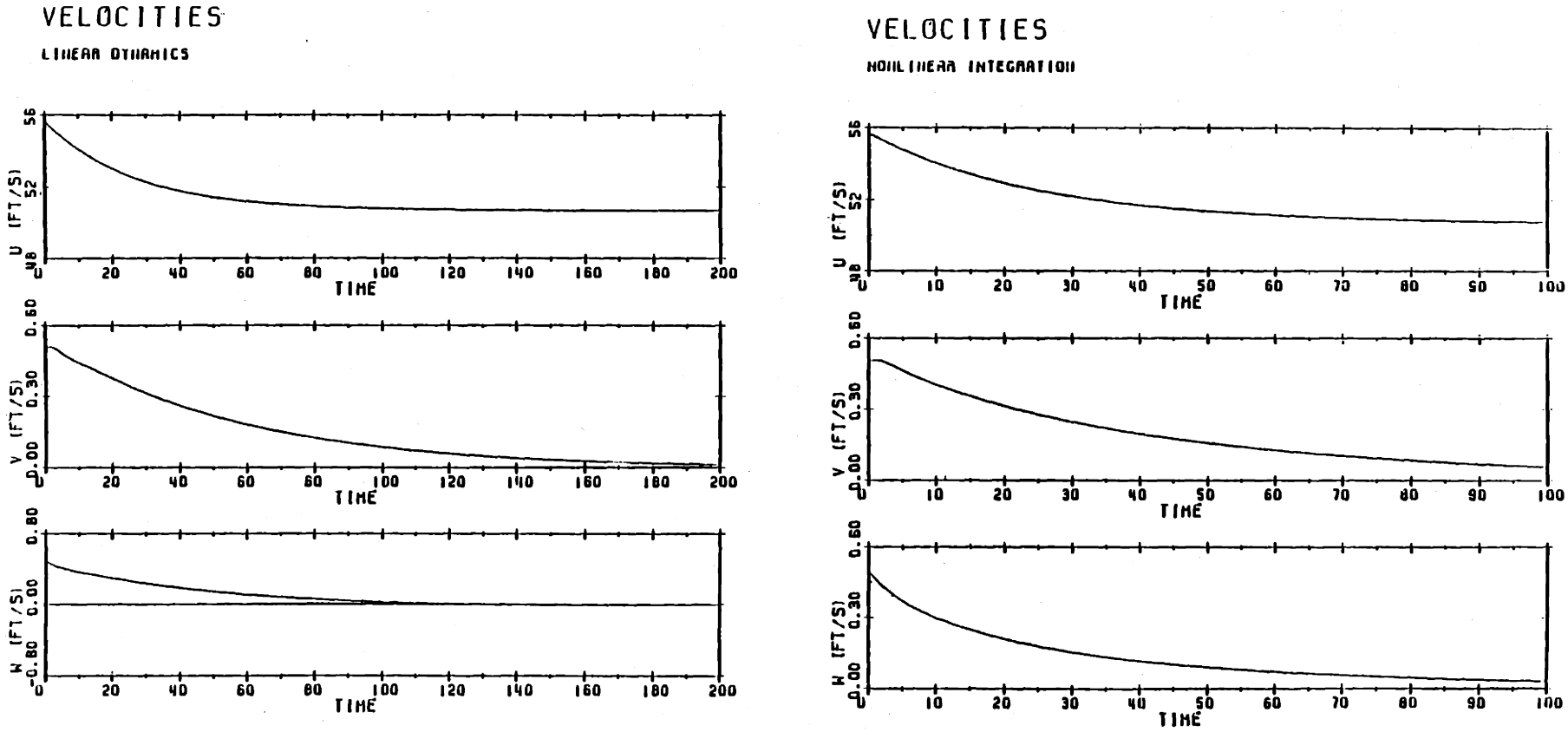

Figure 2.2(a) Comparison of Linear and Non-linear Dynamics for Model S30R0

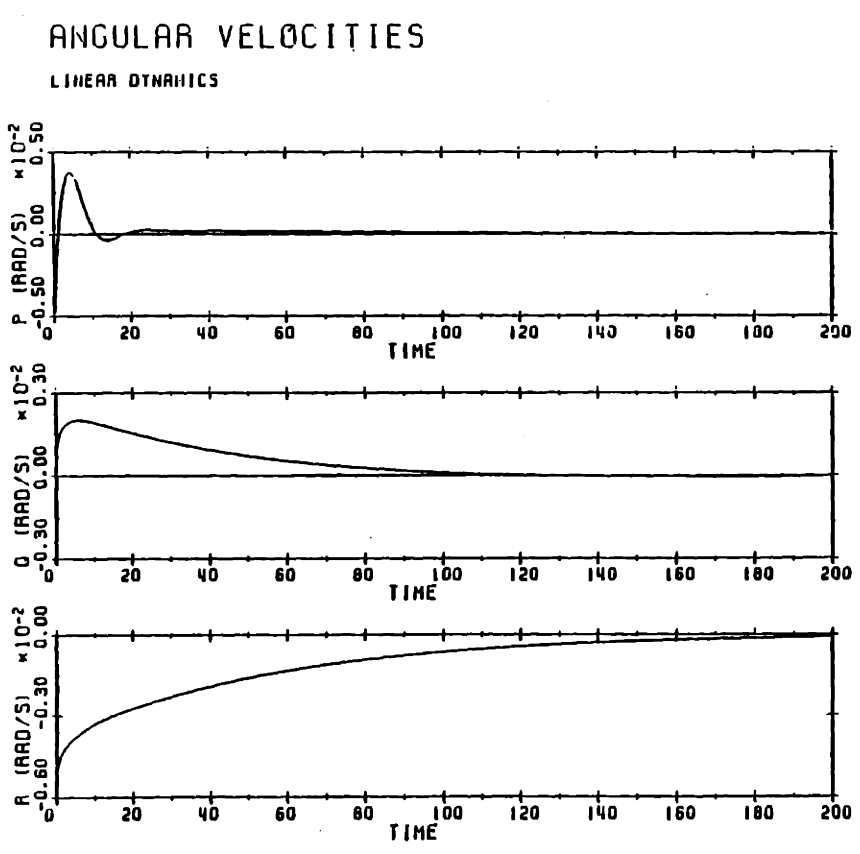

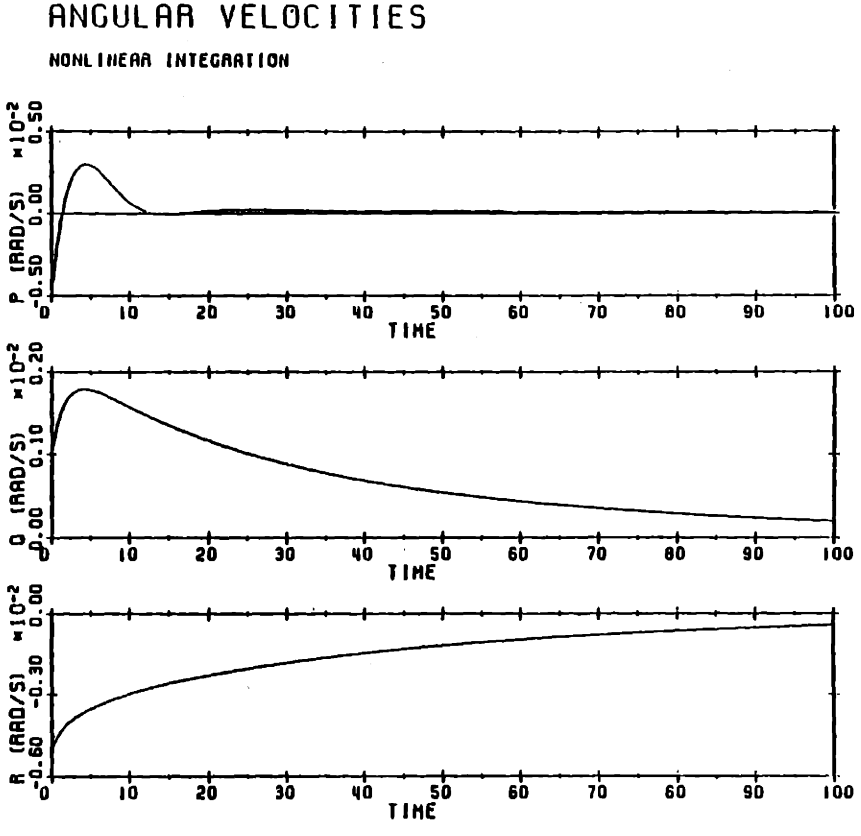

Figure 2.2(b) Comparison of Linear and Non-linear Dynamics for Model S30RO

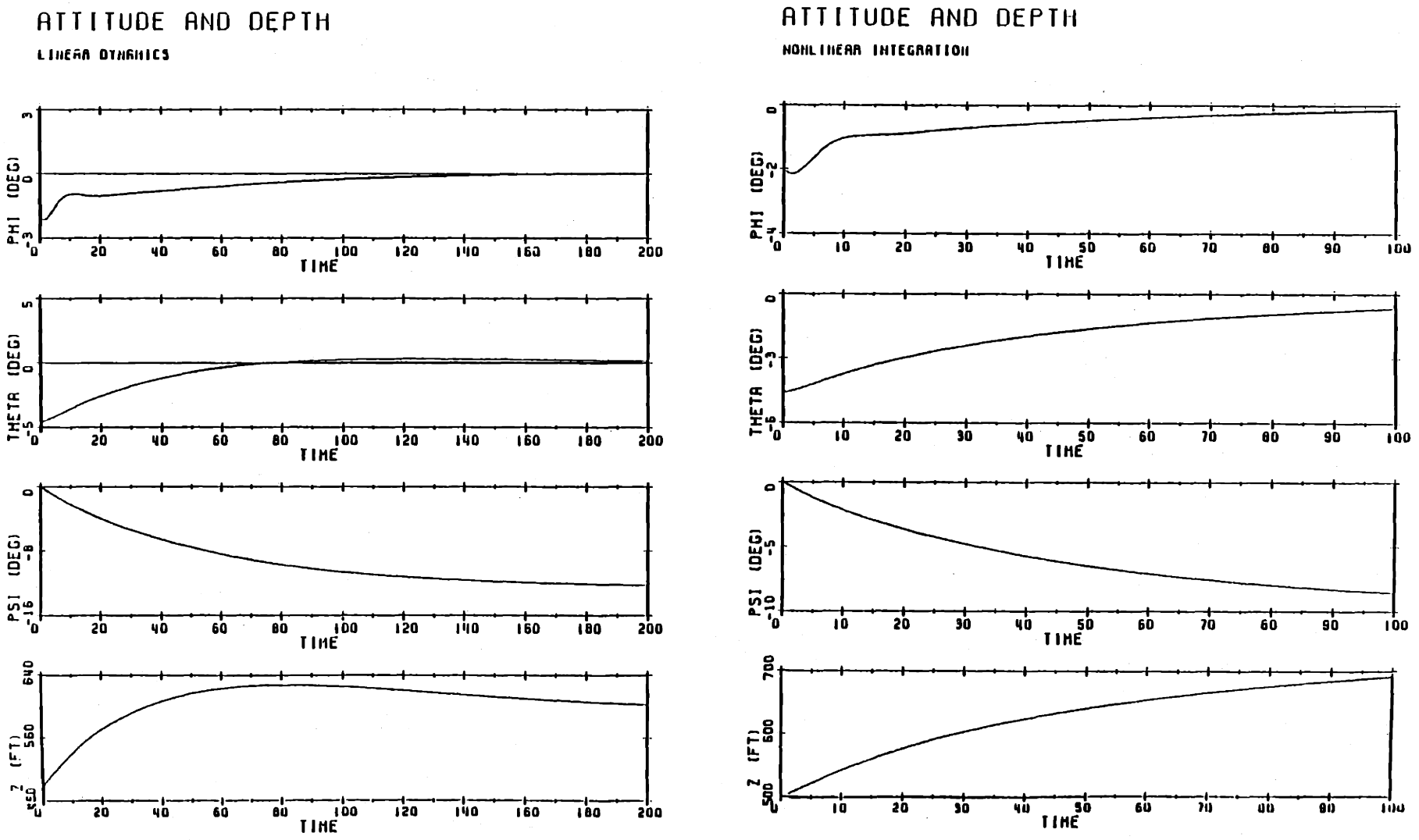

Figure 2.2(c) Comparison of Linear and Non-linear Dynamics for Model S30R0

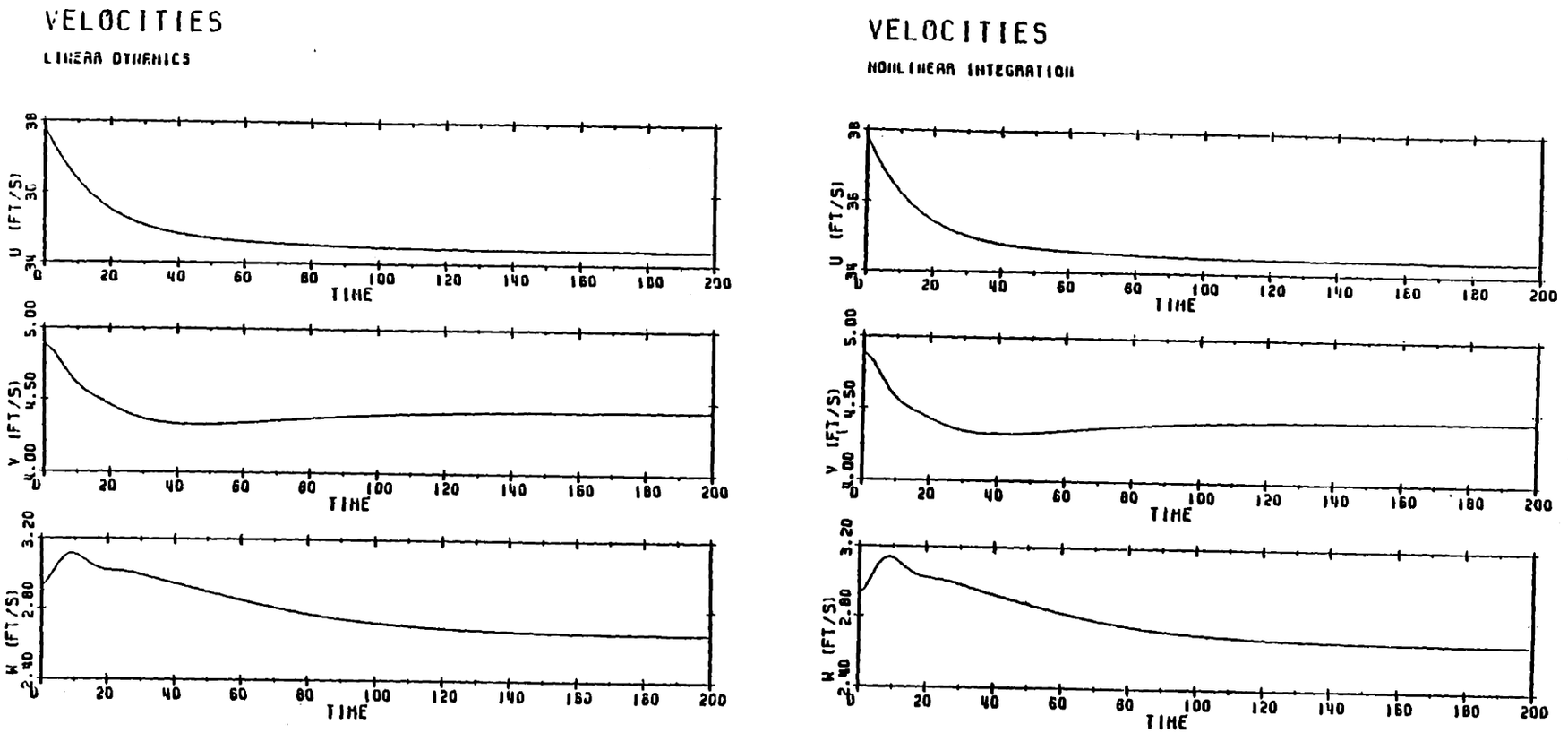

Figure 2.3(a) Comparison of Linear and Non-linear Dynamics for Model S30R15

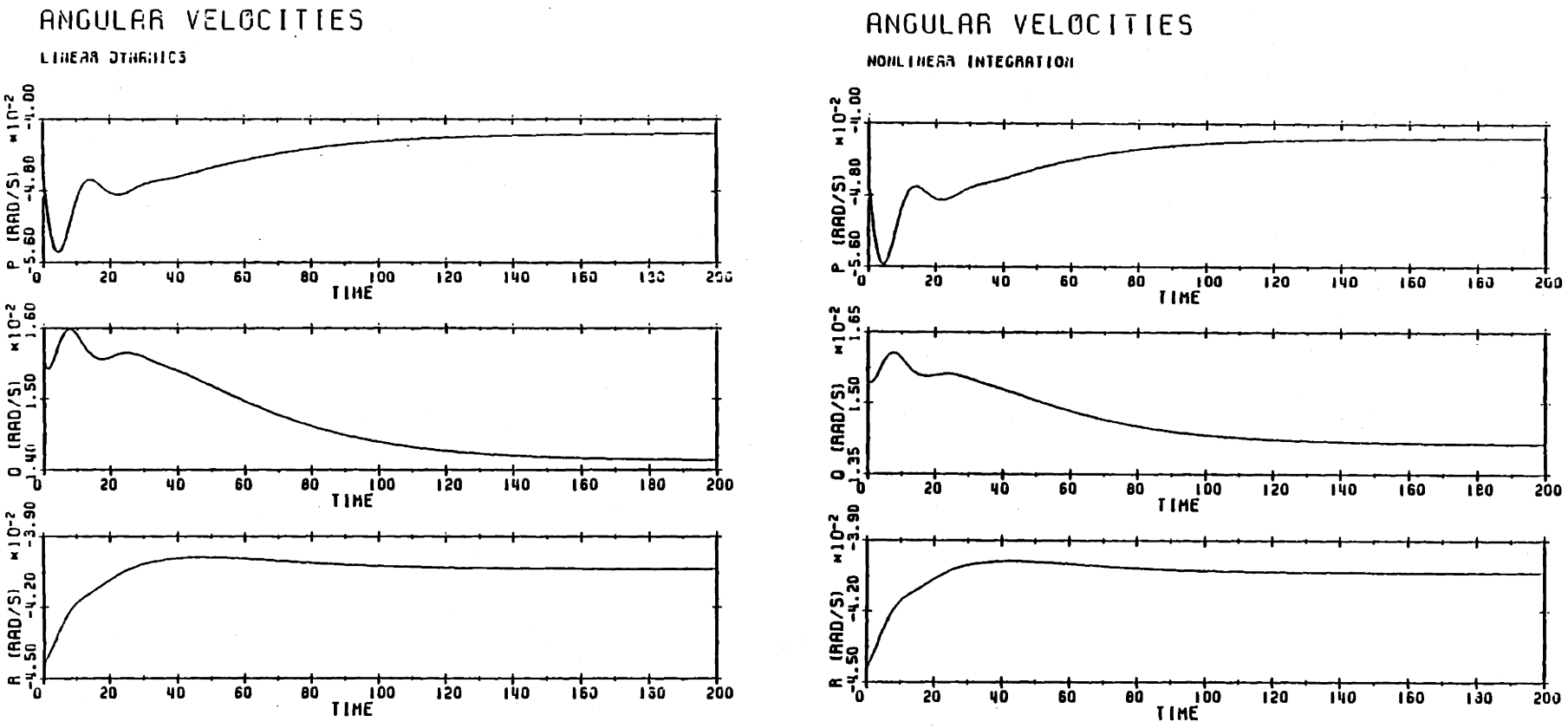

Figure 2.3(b) Comparison of Linear and Non-linear Dynamics for Model S30R15

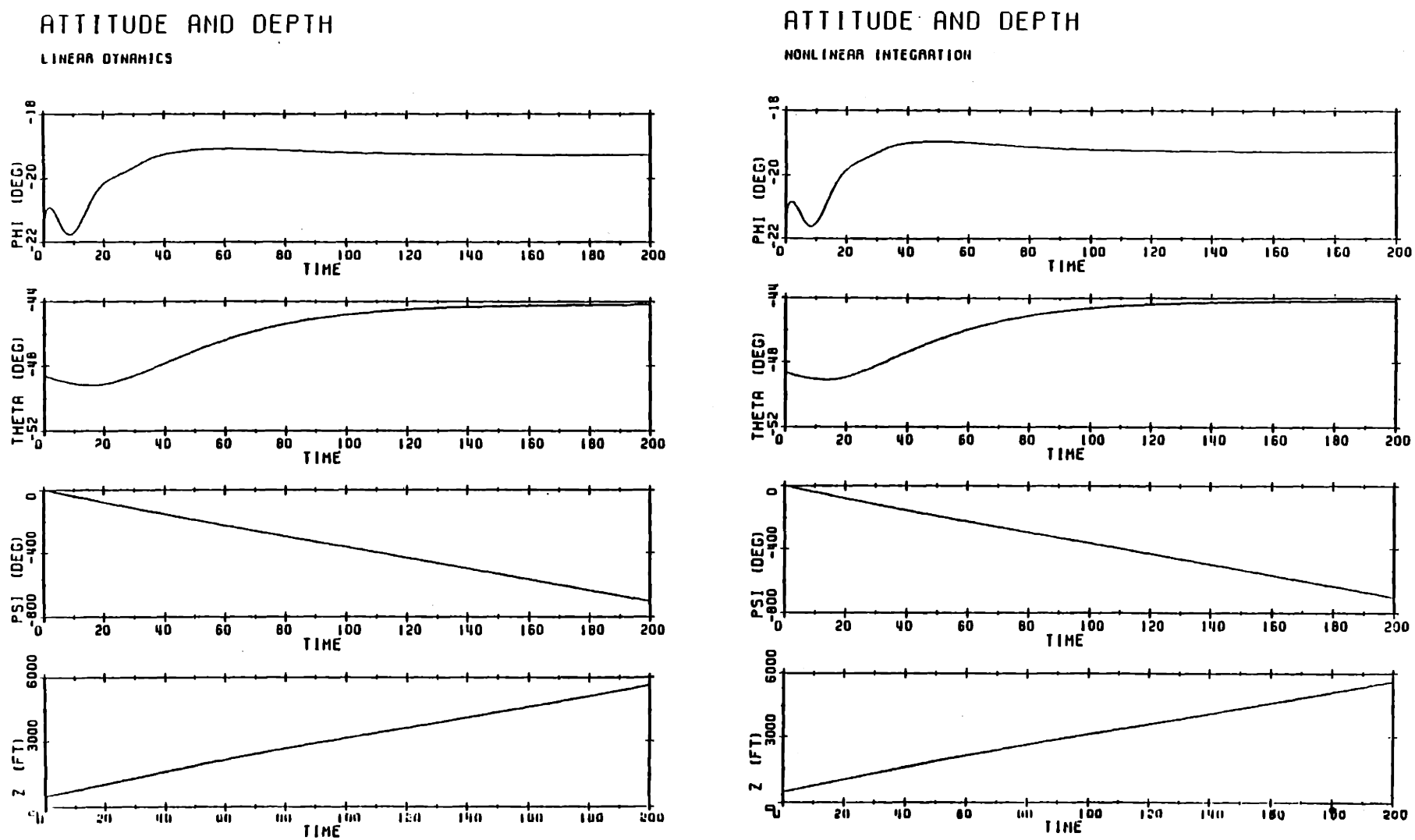

Figure 2.3(c) Comparison of Linear and Non-linear Dynamics for Model S30R15

where R indicates the dimension space of the system. Thus, the requirement is

$$p = m$$

and with four independent control surfaces available

$$p = 4.$$

2.5.2 Output Variable Selection:

An autopilot (position controller) is one option, where the position variables Ψ and z are used, or a rate controller could be designed, where the rate variables u, v, w, p, q, and r are used. The attitude variables θ and ϕ can be utilized in either design, depending on their importance. Additionally, a controller can be designed which is concerned with vertical or horizontal plane motion. A more challenging design, however, is one which controls the dynamics of the submarine simultaneously in both planes.

Since it is desired to control the submarine during maneuvering situations, a rate controller will be investigated. The four output variables selected are depth rate $\dot{z}$, yaw rate $\dot{\Psi}$, roll angle ϕ, and pitch angle θ.

Remember that depth rate can be constructed from the non-linear expression

$$\dot{z}(t) = -u \sin\theta + v \cos\theta \sin\phi + w \cos\theta \cos\phi \qquad (2.4)$$

and that yaw rate can be constructed from the non-linear expression

$$\dot{\psi}(t) = (r \cos\phi + q \sin\theta)/\cos\theta \qquad (2.5)$$

Using small angle approximations we obtain the expressions that

$$\dot{z}(t) = - u\theta + w$$

and

$$\dot{\psi}(t) = r.$$

With the output variables determined, and the $\underline{A}$ and $\underline{B}$ matrices calculated, the state space description of the submarine model is now complete and takes the form

$$\dot{\underline{x}}(t) = \underline{A}\,\underline{x}(t) + \underline{B}\,\underline{u}(t) \qquad (2.1)$$

$$\underline{y}(t) = \underline{C}\,\underline{x}(t), \qquad (2.2)$$

where the output vector $\underline{y}(t)$ is given by

$$\underline{y}(t) = [\ \phi(t) \quad \theta(t) \quad \dot{\psi}(t) \quad \dot{z}(t)\ ]^T. \qquad (2.3)$$

2.5.3 Control Variable Selection

As mentioned previously, there are four possible control variables if propeller RPS is held constant. These are δs_1, δs_2, δr, and δb. Figure 2.4 illustrates the control surface configurations used in this thesis.

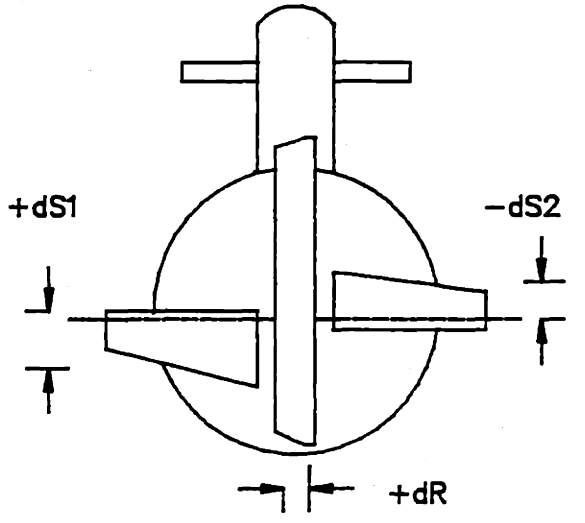

View From Stern
Showing Rudder and Differential Sterns

Figure 2.4 Submarine Control Surface Configurations

2.6 Summary

This chapter has introduced the submarine model used for this thesis. Additionally, the coordinate systems, definitions of the submarine states and control variables, and the process of developing a linear model were briefly described. Finally, the reasoning for selection of the output variables was presented.

Chapter Three will analyze the linearized models using the method of modal decomposition. The eigenstructure of the linearized models will also be presented.

CHAPTER THREE

ANALYSIS OF THE LINEAR MODEL

3.1 Introduction

In this chapter, the structure of the various models will be investigated.

In the previous chapter, a state space description of the submarine model was developed in the form of

$$\dot{\underline{x}}(t) = \underline{A}\,\underline{x}(t) + \underline{B}\,\underline{u}(t)$$

$$\underline{y}(t) = \underline{C}\underline{x}(t).$$

The state space description described results in a tenth order system. It will be shown that the order of the system can be reduced to an eighth order system because of the zero entries in the $\underline{A}$ and $\underline{B}$ matrices. This is desirable only if these states are not utilized in the control of the submarine.

The eigenstructure of the various models is analyzed using the method of modal analysis [17]. This method starts with a state equation in a nondiagonal form and uses matrix similarity transformations to arrive at the diagonalized form of the $\underline{A}$ matrix. The entries of the diagonalized $\underline{A}$ matrix are the poles of the open loop system. The advantage to using similarity transformations is that the linearized system is described in state space form as separately decoupled modes, thus yielding information as to the controllability and observability of the system.

This information, along with the pole-zero structure, will provide the basis and validity for the LQG/LTR design in the following chapters.

3.2 Reduction of the Model

Inspection of the **A** matrix for the linearized model (Appendix C1) show that the present value of the states Ψ and z can have no influence on any other state because the last two columns of the **A** matrix contains all zeros. This means the dynamic response of the submarine is not affected by either the heading angle or depth of the submarine. Again, note that this is for a deeply submerged submarine. For a submarine near the surface, heading and depth can have a significant impact on the dynamic response of the submarine due to wave action and hull suction forces.

Inspection of the **B** matrix (Appendix C1) for the model reveal zeros in the last four rows. This indicates that the control surfaces exert no direct influence on the derivatives of Ψ, θ, ϕ, or z.

Since the controller design is not concerned with any of these states, then they may be removed from the linear model. This is accomplished by deleting the rows and columns associated with those states, resulting in a reduced order system.

3.3 Scaling

Scaling is a method of weighting the physical units of a system so the numerical values of the variables make sense and become equally important. Scaling and its effects have recently been discussed by Kappos [20] and Boettcher [21]. Note that scaling does change the magnitude of the singular values, and as such, it impacts the design.

In this thesis, scaling is performed in two distinct steps. The first step requires transformations of the linearized $\underline{A}$, $\underline{B}$, and $\underline{C}$ matrices such that angular components of the matrices are expressed in units of degrees, feet, degrees/sec, and feet/second. If the unscaled system is defined by

$$\underline{A},\ \underline{B},\ \underline{C},\ \underline{y},\ \underline{u},\ \text{and}\ \underline{x},$$

and we define the scaled system as

$$\underline{A}',\ \underline{B}',\ \underline{C}',\ \underline{y}',\ \underline{u}',\ \text{and}\ \underline{x}',$$

then the tranformations can be described by

$$\underline{A}' = \underline{S}_x\ \underline{A}\ \underline{S}_x^{-1}$$
$$\underline{B}' = \underline{S}_x\ \underline{B}\ \underline{S}_u^{-1}$$
$$\underline{C}' = \underline{S}_y\ \underline{C}\ \underline{S}_x^{-1},$$

where $\underline{S}_x$, $\underline{S}_y$, and $\underline{S}_u$ are matrices chosen to provide the desired scaling. Details of the matrices used for the transformation from radians to degrees can be found in Appendix C2.

Now that the state space description of the model is in units that make physical sense, scaling is required to include weighting on the inputs and outputs. The weightings on the outputs are chosen to reflect the importance of the maximum allowable output state error. It is assumed that an error of one degree in pitch or roll is as significant as 0.1 degree/sec yaw rate or 0.1 ft/sec depth rate. This then determines the scaling matrix which will be applied at the output of the plant, $\tilde{\underline{S}}_y$, as

$$\tilde{\underline{S}}_y = \begin{bmatrix} .1 & & & \\ & .1 & & \\ & & 1 & \\ & & & 1 \end{bmatrix} .$$

Because the control surfaces have physical position limits, consideration must be given to weighting the inputs to the plant. The limitations on the control surfaces are shown below:

control	rate limit	position limit
δb	7°/sec	±20°
δr	4°/sec	±30°
$\delta s_1, \delta s_2$	7°/sec	±25°

Since the actuator dynamics are above the anticipated bandwidth of the compensator and plant, they will be considered as high frequency modelling errors, and will be neglected [10,11,12,13]. The position limits cannot be neglected however, because they are based on physical interference constraints, and on saturation of the control

surfaces. To model the control surface position limits, the input vector to the plant must be scaled by an appropriate matrix, $\tilde{\underline{S}}_u$, as

$$\tilde{\underline{S}}_u = \begin{bmatrix} 1 & & \\ & 0.667 & \\ & & 0.8 \\ & & & 0.8 \end{bmatrix}.$$

Appendix C3 lists the matrices used for weighting the inputs and outputs, and the final state space matrices for the linearized model are listed in Appendix C4. Figure 3.1 represents the block diagram of the plant transformed for units, and weightings on the inputs and outputs. This will hereafter be referred to as the linearized model.

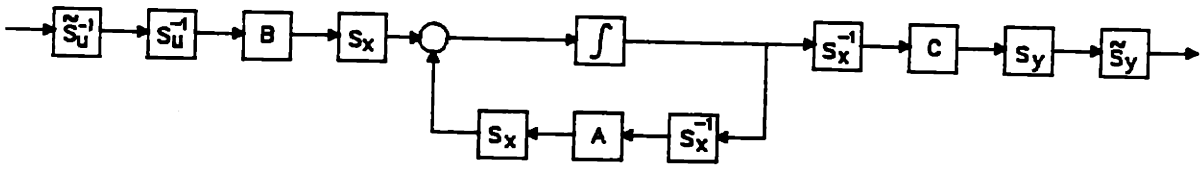

Figure 3.1 Block Diagram of Plant Transformed for Units, and Weightings of Inputs and Outputs.

3.4 Modal Analysis of the System

The natural modes of the linearized model are determined by diagonalizing the state space description of the system. For a linearized dynamic system which does not have direct coupling of the output and input,

$$\dot{\underline{x}}(t) = \underline{A}\,\underline{x}(t) + \underline{B}\,\underline{u}(t) \tag{3.1}$$

$$\underline{y}(t) = \underline{C}\,\underline{x}(t). \tag{3.2}$$

Performing a linear transformation from the state vector $\underline{x}(t)$ to a new state vector $\underline{z}(t)$ by means of an as yet unspecified constant, square, and invertible matrix $\underline{T}$ yields

$$\underline{x}(t) = \underline{T}\,\underline{z}(t). \tag{3.3}$$

Then we have

$$\underline{T}\,\dot{\underline{z}}(t) = \underline{A}\,\underline{T}\,\underline{z}(t) + \underline{B}\,\underline{u}(t) \tag{3.4}$$

$$\underline{y}(t) = \underline{C}\,\underline{T}\,\underline{z}(t). \tag{3.5}$$

Multiplying (3.4) by $\underline{T}^{-1}$, we have

$$\dot{\underline{z}}(t) = \underline{T}^{-1}\,\underline{A}\,\underline{T}\,\underline{z}(t) + \underline{T}^{-1}\,\underline{B}\,\underline{u}(t) \tag{3.6}$$

$$\underline{y}(t) = \underline{C}\,\underline{T}\,\underline{z}(t). \tag{3.7}$$

If $\underline{T}$ is such that the resulting $\underline{T}^{-1}\,\underline{A}\,\underline{T}$ matrix is diagonal, then the vector $\underline{z}(t)$ defines a new state space in which the eigenvalues of the diagonal matrix are equal to the diagonal elements. Now, define

$$\underline{\Lambda} = \underline{T}^{-1}\,\underline{A}\,\underline{T}. \tag{3.8}$$

The $\underline{T}$ matrix is called the modal matrix because of the decoupling of the modes that is accomplished when the state space vector is transformed. To find out the nature of the modal matrix, we premultiply both sides of (3.8) by $\underline{T}$ which yields

$$\underline{A}\,\underline{T} = \underline{T}\,\underline{\Lambda}. \qquad (3.9)$$

If we now designate each column of the modal matrix by v_i, where i represents the number of column vectors, then (3.9) can be expressed as

$$\underline{A}\,v_i = \underline{A} \begin{bmatrix} T_{1i} \\ T_{2i} \\ \cdot \\ \cdot \\ \cdot \\ T_{ni} \end{bmatrix}.$$

Thus we see that the columns of $\underline{T}$ are the eigenvectors of $\underline{A}$. Each column of the modal matrix describes the submarine motion along the coordinate axes of the state vector components u, v, w, p, q, r, Φ, and Θ for a particular mode. Since the dynamic response of the submarine consists of linear combinations of the decoupled modes, analyzing the columns of $\underline{T}$ can provide useful information regarding the dynamic response of the submarine.

The modal matrix columns are graphed in bar chart form by taking the absolute value of each element of the normalized column vectors. The bar charts for the linearized model, provided in Figure 3.2, have a vertical scale of 0 to 100% which reflect the relative magnitude of

the response, with the eigenvalue of the mode considered being displayed directly beneath the chart. Additionally, although the bar charts provide a convenient means to display the modes of the linearized system, the physical interpretation is fairly obscure. As such, interpretation of the modes is limited to the following observations:

1. All open loop poles are in the left hand plane.

2. Modes 1, 2, and 3 for the various models are dominated by the response of variables w, ϕ, and θ.

3. Modes 4 through 8 exhibit reductions in the response of the variables w, ϕ, and θ., with corresponding increase in the other variables.

4. Modes 5 and 6 represent an oscillatory mode dominated by the roll response.

The eigenvalues and modal matrices for the linearized model are presented in Appendix D1.

To form a complete analysis, the specifications for controllability and observability will be discussed in the following section.

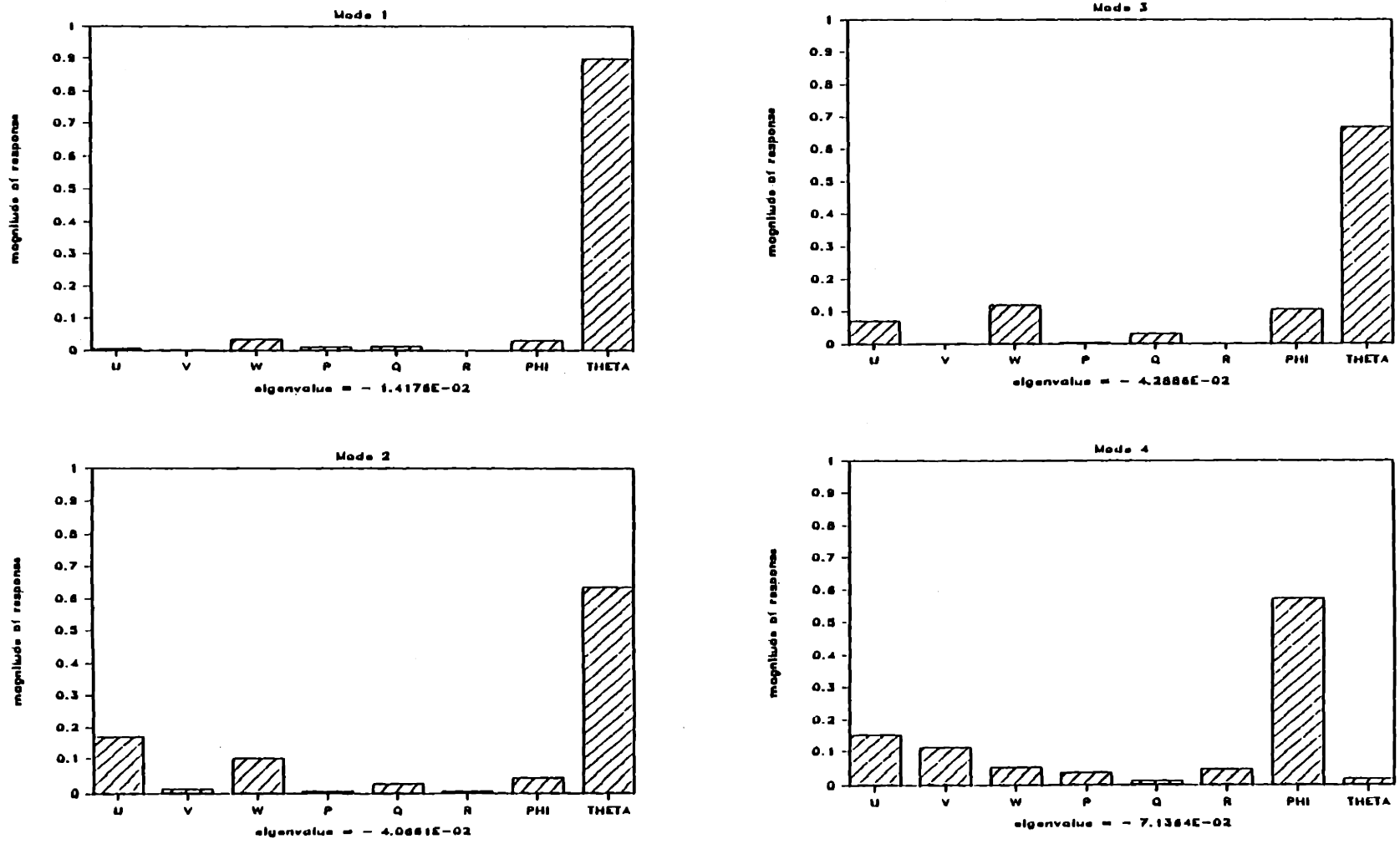

Figure 3.2(a) Modal Analysis for the Linearized Roll Control Model

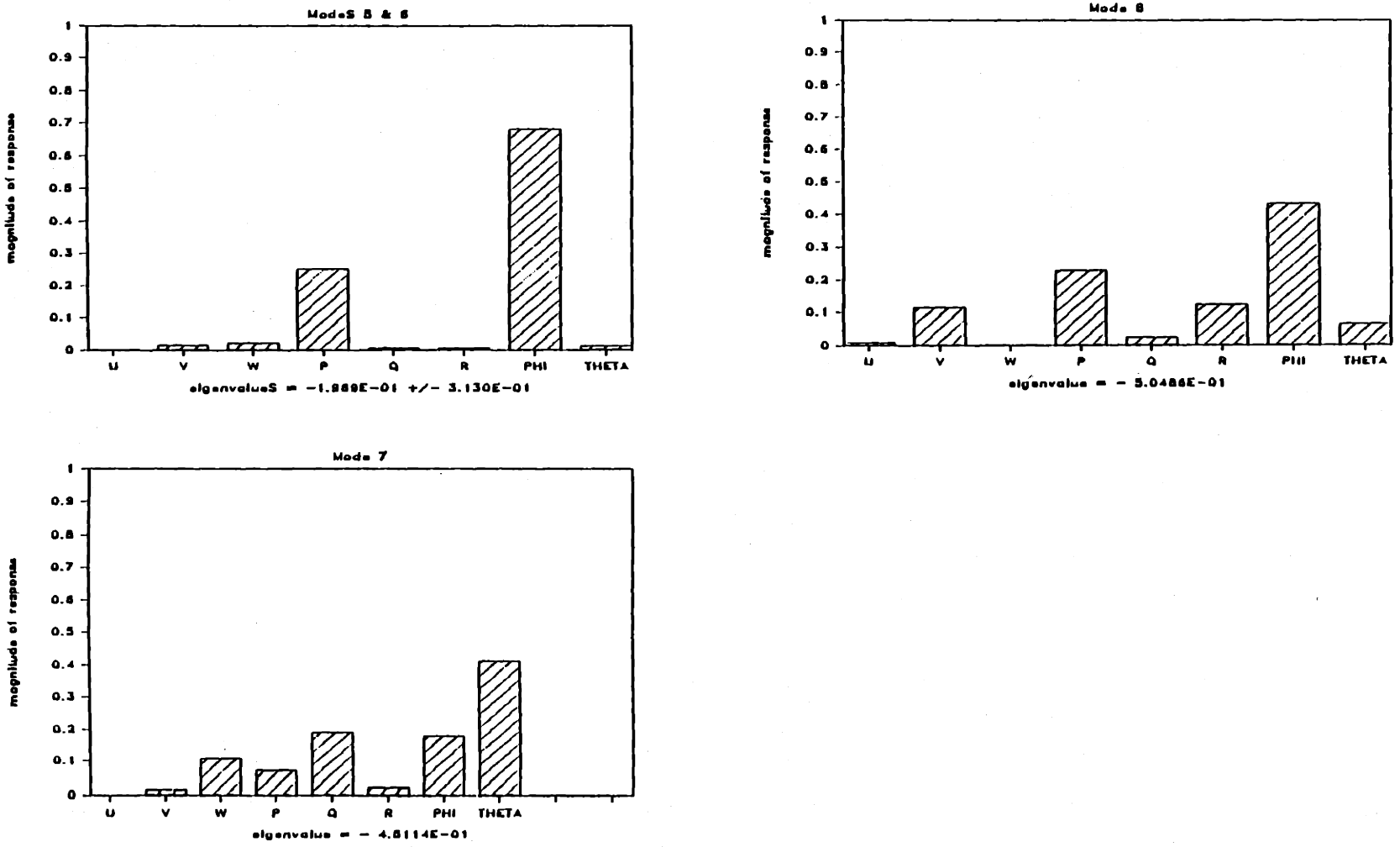

Figure 3.2(b) Modal Analysis for the Linearized Roll Control Model

3.5 Controllability and Observability

The eigenvalues and eigenvectors that were determined in the previous steps will be studied, and the conditions for controllability and observability of the linearized systems will be investigated. This step is vital in establishing the validity of the linearized model.

First, the linearized system must have no unstable modes which are not controllable. Second, the system must have no unstable modes which are not observable. If these conditions of controllability and observability are established, then the weaker conditions of stabilizability and detectability are assured.

The modal transformation leading to a diagonalized $\underline{A}$ matrix provides a fairly straightforward technique to determine satisfaction of controllability and observability requirements. Additionally, if the system does not meet those conditions, the weaker conditions of stabilizability and detectability can be determined.

Since the new state space representation of the linearized system (3.6) defines a state space in which the natural modes of the system are decoupled, the eigenvalues give the response characteristics of the system's modes. The eigenvectors are the link that relate these response characteristics to particular changes in the state of the system as measured by the state variables x_1, x_2, ..., x8. Thus, a particular row of the $\underline{T}^{-1}\ \underline{B}$ matrix links the input vector $\underline{u}$ to a particular mode of $\underline{z}$. Each element in the row

will then link a specific input to a mode. Consequently, a zero entry in the (i,j) position of the $\underline{T}^{-1}\ \underline{B}$ matrix would indicate the i^{th} mode cannot be controlled by the j^{th} input.

In a similar manner, the $\underline{C}\ \underline{T}$ matrix (3.7) indicates whether a particular mode is observable in the output.

In the previous section it was observed that, for the linearized model, the system response was dominated by the variables w, ϕ, and θ in the first two or three modes. In the remaining modes, it was evident that all the state variables are affected to some extent. Questions generally arise in Modal Analysis on the significance of the responses when the physical units are not the same. Because the scaling in section 3.3 accounted for the differences in units, and weightings on the magnitude of the system responses, the ability to compare the relative magnitudes of the system responses is valid.

Combined with the analysis of $\underline{T}^{-1}\ \underline{B}$, it is observed in Figure 3.3, that modes 4,7, and 8 appear to be least affected by the control inputs. For the other modes, it appears the control inputs exhibit strong influence on the submarine's response.

It appears then, that the modes which should be considered in the controllability issue are Modes 1,2,3,5, and 6. Referring back to the modal response charts for each model, the variables which show the most promise of controlling are w, θ, p, q, r, and ϕ.

It is desirable to select the output variables which can be referenced in the inertial reference frame instead of the body reference frame. Based on this desire, and the fact that it is also desirable to control heading rate in high speed maneuvers with a minimum excursion in depth, this analysis shows that the selection of $\dot{z}$, ϕ, θ, and $\dot{\psi}$, are reasonable output variables.

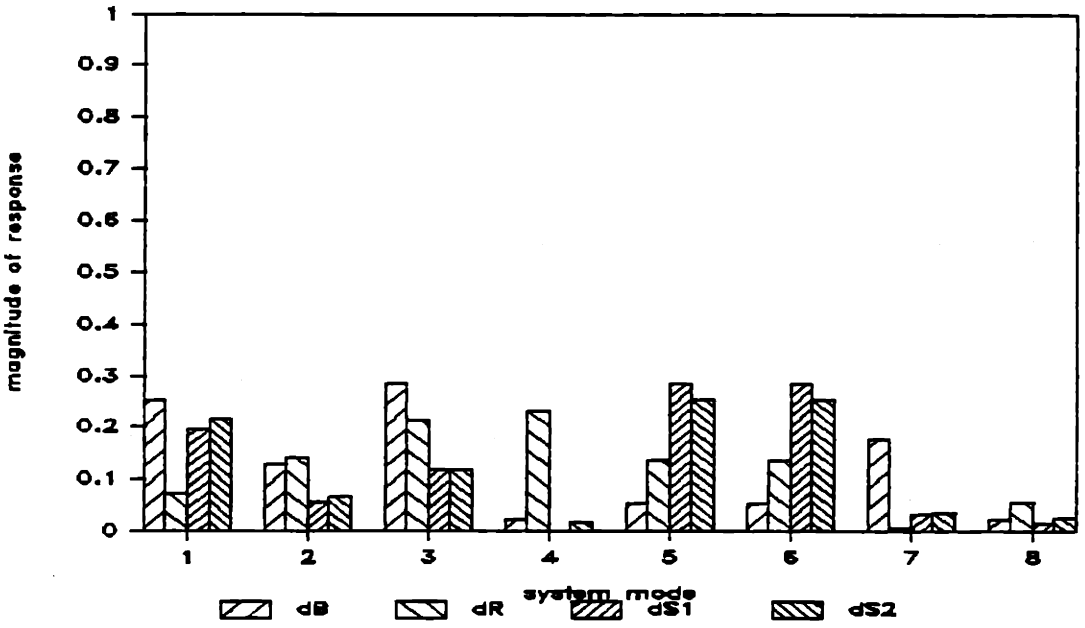

Figure 3.3 Controllability Analysis for the Linearized Roll Control Model.

3.6 Structure of the Poles, Zeros, and Singular Values

In section 3.1 it was observed that the poles of the open loop plant are the eigenvalues of the $\underline{A}$ matrix. The models investigated are all open loop stable because they all have left half plane poles.

The multivariable transmission zeros are listed in the Modal Analysis results in Appendix D1. The model presented is for a reduced order state space system in which the states z and Ψ were removed, as described in section 3.2. The output variables, $\dot{z}$ and $\dot{\Psi}$, for the $\underline{C}$ matrix are derived using the appropriate rows of the $\underline{A}$ matrix. If a transmission zero is in the right half plane, and if it is in the bandwidth of the system, it will impose severe limitations on the performance of the system [4,18,19]. If the non-minimum phase zero is above the system bandwidth, then its adverse effect should be greatly attenuated. None of the linear models studied have low frequency non-minimum phase zeros.

In the multivariable case, a plot of the transfer matrix singular values is analogous to the Bode plots for Single Input Single Output (SISO) systems [18]. The singular values of a matrix $\underline{M}$, $\sigma(\underline{M})$, are defined as:

$$\sigma_i(\underline{M}) = [\ \lambda_i(\underline{M}^H\underline{M})\ ]^{1/2} \qquad (3.9)$$

where: $\sigma_i = i^{th}$ singular value

$\lambda_i = i^{th}$ eigenvalue of $\underline{M}$

$\underline{M}^H$ = complex conjugate transpose of $\underline{M}$

In the MIMO case, substituting the plant transfer matrix, $\underline{G}(s)$, for $\underline{M}$, yields

$$\underline{G}(s) = \underline{C}_p[s\underline{I} - \underline{A}_p]^{-1}\underline{B}_p. \qquad (3.10)$$

Solution for $\underline{G}(s)$, with $s = j\omega$, on a computer yields the singular values of $\underline{G}(s)$ as a function of frequency. The singular value plot of the scaled open loop model is shown in Figure 3.4. The larger singular values of Figure 3.4 are dominated by $\dot{z}$ and $\dot{\Psi}$. The smaller singular values are dominated by θ and ϕ.

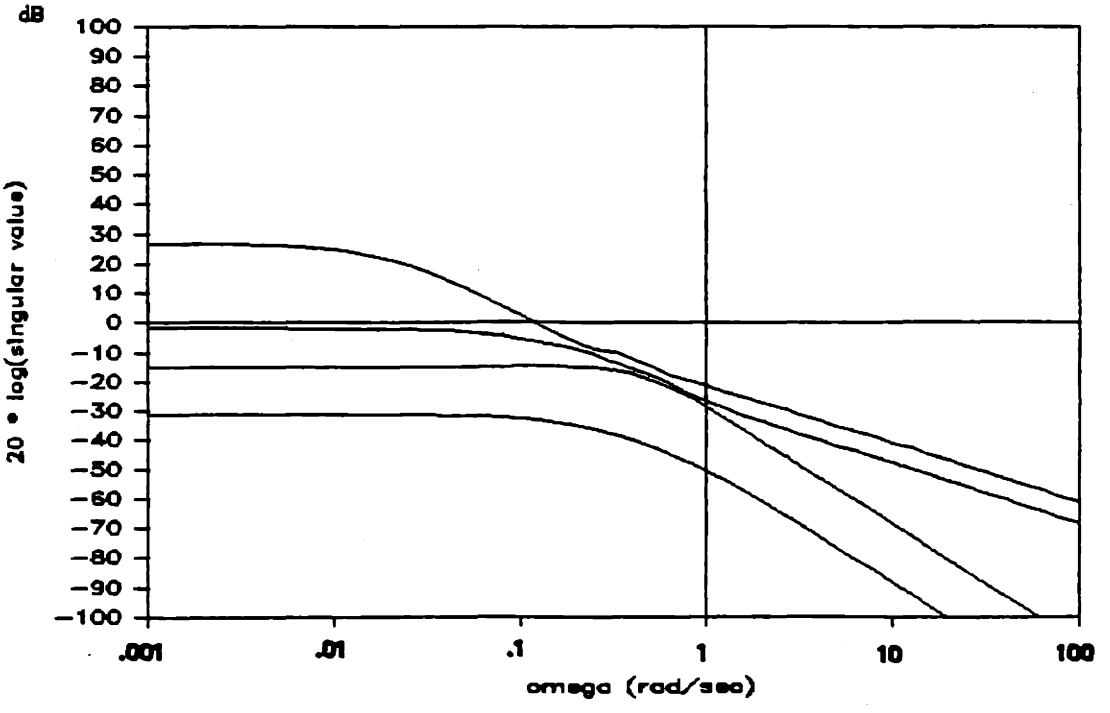

Figure 3.4 Singular Value Plot of the Scaled Linear Model

As an indication of the effect of the control surfaces on the outputs, the dc gains of the open loop transfer function

matrix are listed in Table 3.1 By reading across for each output variable, the relative effect of the control surfaces can be determined. The rudder angle is shown to strongly influence the roll angle, which is as expected. Pitch angle is most affected by the stern planes, and the rudder strongly influences yaw rate. Depth rate is strongly influenced by the stern planes, and slightly affected by the bow planes. The rudder strongly influences depth rate due to the roll angles, which influence the depth rate.

Table 3.1 Input to Output Coupling

	δb	δr	δs_1	δs_2
ϕ	-37.3	-5.1	-14.5	-16.9
θ	-13.2	0.2	3.4	5.3
$\dot{\psi}$	-45.1	-3.3	-30.5	-27.8
$\dot{z}$	4.1	18.6	21.8	23.7

Figure 3.5 represents singular value decomposition of the linearized model at dc. The bar charts represent the normalized left and right singular vectors where

$$\underline{G}(s) = \underline{C}[s\underline{I}-\underline{A}]^{-1}\underline{B}.$$

For $s = 0$,

$$\underline{G}(0) = -\underline{C}\underline{A}^{-1}\underline{B}, \text{ where}$$

$$\underline{G} = \underline{U}\underline{\Sigma}\underline{V}, \text{ and } \underline{y}(t) = \underline{G}\underline{u}(t).$$

Then $\underline{y}(t) = \underline{U}\underline{\Sigma}\underline{V}\underline{u}(t)$, and we can define $\underline{y}'(t) = \underline{\Sigma}\underline{u}'(t)$, where

$$\underline{y}'(t) = \underline{U}^{-1}\underline{y}(t) \text{ and } \underline{u}'(t) = \underline{V}\underline{u}(t).$$

Since $\underline{\Sigma}$ is a diagonal, square matrix, each element of $\underline{\Sigma}$ allows us to compare the left and right singular vectors to display the response of the output variables with respect to the input variables.

Referring to Figure 3.5(a), for σ_{11} we observe the stern planes contribute to both roll and yaw rate, and for σ_{22}, the bow planes contribute to pitch angle and depth rate. In Figure 3.5(b), for σ_{33}, we observe the stern planes and rudder contribute to depth rate and pitch angle, while, for σ_{44}, the rudder contributes primarily to roll angle and yaw rate.

3.7 Summary

This chapter concentrated on describing the technique of modal analysis and its ability to determine the eigenstructure and modal decomposition of the state space description of a linear model.

The use of modal analysis has allowed the formulation of the prerequisites necessary to pursue the LQG/LTR design methodology which will be discussed in the following chapter. These prerequisites are that the open loop linear model is detectable and stabilizable, and that the location of non-minimum phase zeros be known.

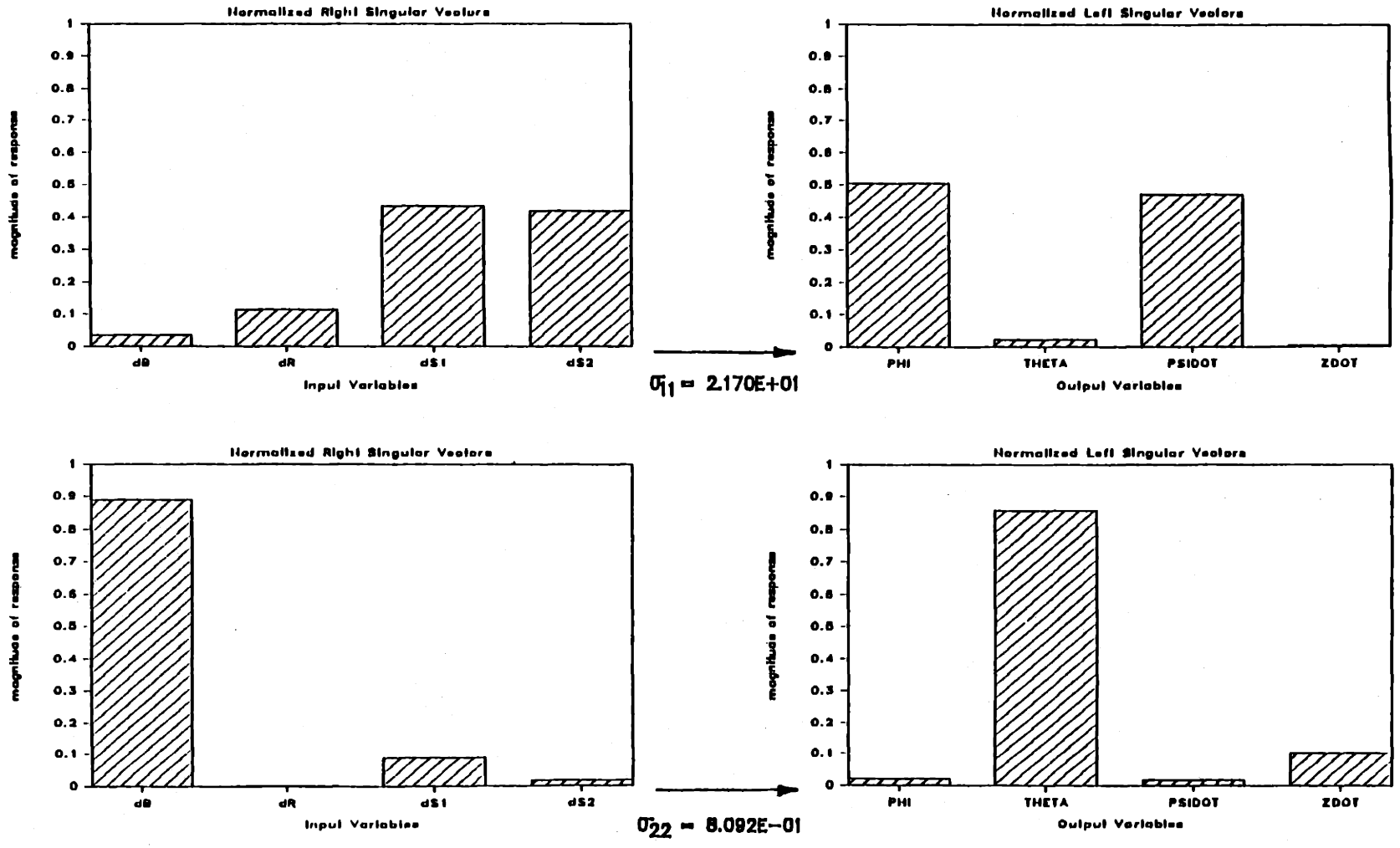

Figure 3.5(a) Singular Value Decomposition for the Scaled Linear Model at DC

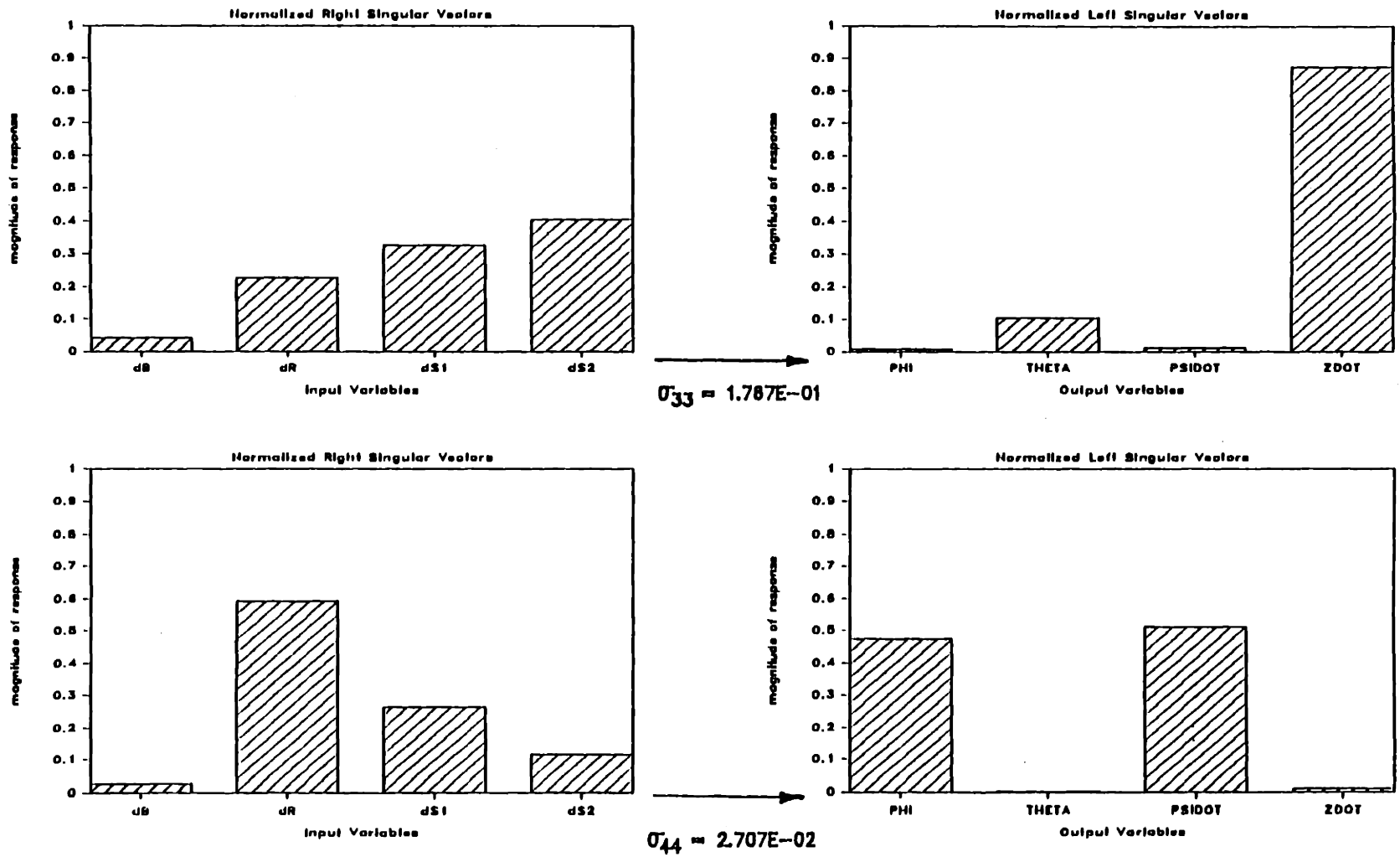

Figure 3.5(b) Singular Value Decomposition for the Scaled Linear Model at DC

CHAPTER FOUR

MULTIVARIABLE CONTROL SYSTEM DESIGN

4.1 Introduction

In this chapter, a controller is designed using the LQG/LTR design methodology. The singular value loop shaping approach is used to obtain desirable singular values of the system transfer function matrix to meet the specifications of performance and robustness to plant uncertainties and modelling errors.

The chapter begins with a description of the LQG/LTR design methodology, and specifications to which the controller will be designed.

Section 4 of the chapter is involved with the design of the controller, and its application with LQG/LTR. The last section of the chapter describes the closed loop system, which will be tested and analyzed in Chapter Five.

4.2 The LQG/LTR Design Methodology

The multivariable LQG/LTR design methodology consists of four major steps [18].

The first step is the development of a low frequency model of the nominal plant and determination of modelling uncertainties. For purposes of good command following and disturbance rejection, the frequency range of interest is at low frequencies (<10 rad/sec).

The modelling uncertainty in the nominal model due to sensor noise, unmodelled dynamics, and actuator dynamics, is assumed to be concentrated at high frequencies. Fixing the crossover frequency of the singular values of the loop transfer function matrix will determine the significance of the unmodelled dynamics, and the ability of the plant to meet command following specifications.

The actual linear time invariant plant and the nominal model at low frequencies are assumed to be identical, and determination of the modelling uncertainty will not be performed in this thesis. As a result, step one is limited to development of the linear model and determination of the maximum allowable crossover frequency.

The second step of the design process establishes the low frequency performance requirements. The state space block diagram of the compensated plant is shown in Figure 4.1.

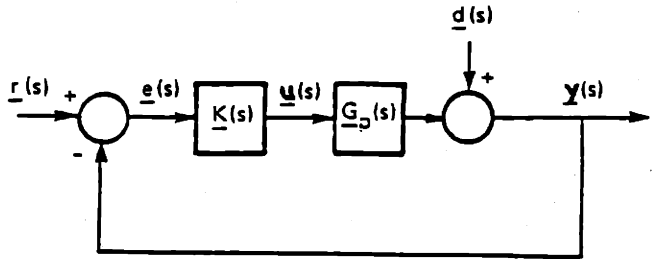

Figure 4.1 Block Diagram of a MIMO Compensated Plant

where:

$\underline{r}(s)$ = reference signal or command input vector

$\underline{e}(s)$ = error signal vector

$\underline{u}(s)$ = control vector to the plant

$\underline{y}(s)$ = output vector of the plant

$\underline{d}(s)$ = disturbance vector at the plant output

$\underline{K}(s)$ = compensator transfer function matrix

$\underline{G}(s)$ = augmented plant transfer matrix

The transfer matrix $\underline{G}(s)$ contains the nominal low frequency model $\underline{G}_p(s)$ and any augmenting dynamics $\underline{G}_a(s)$, and is defined the nominal design model. Thus

$$\underline{G}(s) = \underline{G}_p(s)\ \underline{G}_a(s). \tag{4.1}$$

To determine the requirements of $\underline{K}(s)$, the overall loop transfer function of the closed loop system is analyzed, where

$$\underline{y}(s) = [\underline{I} + \underline{G}(s)\underline{K}(s)]^{-1}\underline{d}(s) + [\underline{I} + \underline{G}(s)\underline{K}(s)]^{-1}\underline{G}(s)\underline{K}(s)\underline{r}(s).$$

For good command following, $\underline{y}(s) \approx \underline{r}(s)$, and for disturbance rejection, the effect of $\underline{d}(s)$ must be kept small. If the minimum singular value of $\underline{G}(s)\underline{K}(s)$ is large with respect to unity at frequencies below crossover, both of these requirements can be met. Likewise, for frequencies above crossover, the response of the outputs with respect to sensor noise can be minimized and stability-robustness enhanced if the maximum singular value of $\underline{G}(s)\underline{K}(s)$ is small with respect to unity.

Combining the above conditions, we essentially impose high and low frequency barriers on the singular value plots of $\underline{G}(s)\underline{K}(s)$, as shown in Figure 4.2.

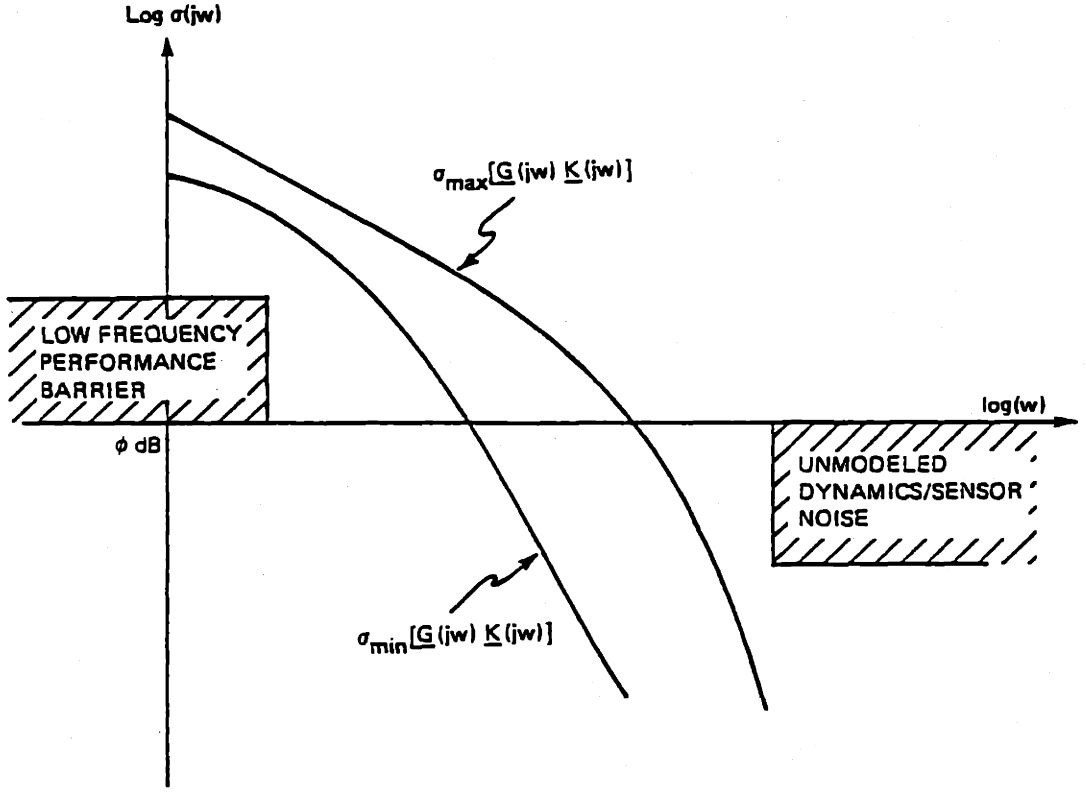

Figure 4.2 Plot of Desired Singular Value Shapes

The high frequency barrier imposes a robustness constraint on the compensator and the low frequency barrier imposes the command following and disturbance rejection requirements.

The third step of the design process is determining the compensator transfer function matrix, $\underline{K}(s)$, that will

provide the singular values of $\underline{G}(s)\underline{K}(s)$ shown above. This step of the process is appropriately termed "loop shaping".

The Kalman Filter methodology is first applied to the nominal design model. This produces a transfer matrix $\underline{G}_{KF}(s)$ that has the desired singular value loop shapes. A distinction is noted in this procedure however, because the KF theory is applied in a specific manner which is not to be confused with optimal state estimation.

Recall from Chapter 2, the nominal state space description

$$\dot{\underline{x}}(t) = \underline{A}\,\underline{x}(t) + \underline{B}\,\underline{u}(t) \qquad (4.2)$$

$$\underline{y}(t) = \underline{C}\,\underline{x}(t). \qquad (4.3)$$

This description is modified to reflect the process and measurement noise

$$\dot{\underline{x}}(t) = \underline{A}\,\underline{x}(t) + \underline{L}\,\underline{\xi}(t) \qquad (4.4)$$

$$\underline{y}(t) = \underline{C}\,\underline{x}(t) + \underline{\theta}(t), \qquad (4.5)$$

where:

$\underline{\xi}(t)$ = process white noise with $\underline{I}$ intensity matrix

$\underline{\theta}(t)$ = measurement white noise with $\mu\underline{I}$ intensity matrix.

The design parameters μ and $\underline{L}$ are used to produce the desired loop shapes of the transfer matrix $\underline{G}_{KF}(s)$ where

$$\underline{G}_{KF}(s) = \underline{C}[s\underline{I} - \underline{A}]^{-1}\underline{H} \qquad (4.6)$$

$$\underline{H} = (1/\sqrt{\mu})\underline{\Sigma}\underline{C}', \qquad (4.7)$$

and $\underline{\Sigma}$ is the solution to the Filter Algebraic Riccatti Equation (FARE)

$$0 = \underline{A}\underline{\Sigma} + \underline{\Sigma}\underline{A}' + \underline{L}\underline{L}' - (1/\sqrt{\mu})\underline{\Sigma}\underline{C}'\underline{C}\underline{\Sigma}. \tag{4.8}$$

For a specific value of μ, the transfer matrix $\underline{G}_{KF}(s)$ can be approximated quite readily. Since at high and low frequencies $s = j\omega$,

$$\underline{G}_{FOL}(s) = \underline{C}[s\underline{I} - \underline{A}]^{-1}\underline{L}, \text{ and} \tag{4.9}$$
$$\sigma_i[\underline{G}_{KF}(s)] \approx (1/\sqrt{\mu})\sigma_i[\underline{G}_{FOL}(s)],$$

then the $\underline{L}$ matrix can be chosen in a way to produce the desired loop shapes and μ can then be used to adjust the singular values up or down to meet the required crossover frequency specifications.

As long as $[\underline{A},\underline{L}]$ is stabilizable and $[\underline{A},\underline{C}]$ is detectable, then any choice of μ and $\underline{L}$ will provide the following guaranteed properties for $\underline{G}_{KF}(s)$:

1. closed loop stable
2. robust
$$\sigma_{min}[\underline{I} + \underline{G}_{KF}(s)] \geq 1$$
$$\sigma_{min}[\underline{I} + \underline{G}_{KF}^{-1}(s)] \geq 1/2$$
3. infinite upward gain margin
4. 6 dB downward gain margin
5. $\pm$ 60° phase margins

The fourth and final step of the design process involves the "recovery" of the loop shapes of $\underline{G}_{KF}(s)$ by the

compensated plant transfer matrix $\underline{G}(s)\underline{K}(s)$. This is done by solving the Control Algebraic Riccatti Equation (CARE)

$$0 = -\underline{K}\underline{A} - \underline{A}'\underline{K} - q\underline{C}'\underline{C} + \underline{K}\underline{B}\underline{B}'\underline{K}, \text{ for } q > 0, \qquad (4.10)$$

Using the design parameter q, and defining the control gain matrix

$$\underline{G} = \underline{B}'\underline{K}. \qquad (4.11)$$

For a valid solution of the CARE, three conditions are necessary:

1. $[\underline{A},\underline{B}]$ must be stabilizable,
2. $[\underline{A},\underline{C}]$ must be detectable, and
3. The nominal design plant must not have non-minimum phase zeros.

When calculated using the above procedure, the Filter gain matrix $\underline{H}$ and the Control gain matrix $\underline{G}$ define a special type of compensator known as a "Model Based Compensator" (MBC), designated as $\underline{K}_{MBC}(s)$. This compensator differs from other LQG/LTR compensators only in the manner in which $\underline{G}$ and $\underline{H}$ are calculated. The state space description of the MBC is

$$\dot{\underline{z}}(t) = (\underline{A} - \underline{B}\underline{G} - \underline{H}\underline{C})\ \underline{z}(t) - \underline{H}\ \underline{e}(t) \qquad (4.12)$$

$$\underline{u}(t) = -\ \underline{G}\ \underline{z}(t), \qquad (4.13)$$

and is shown pictorially in Figure 4.3.

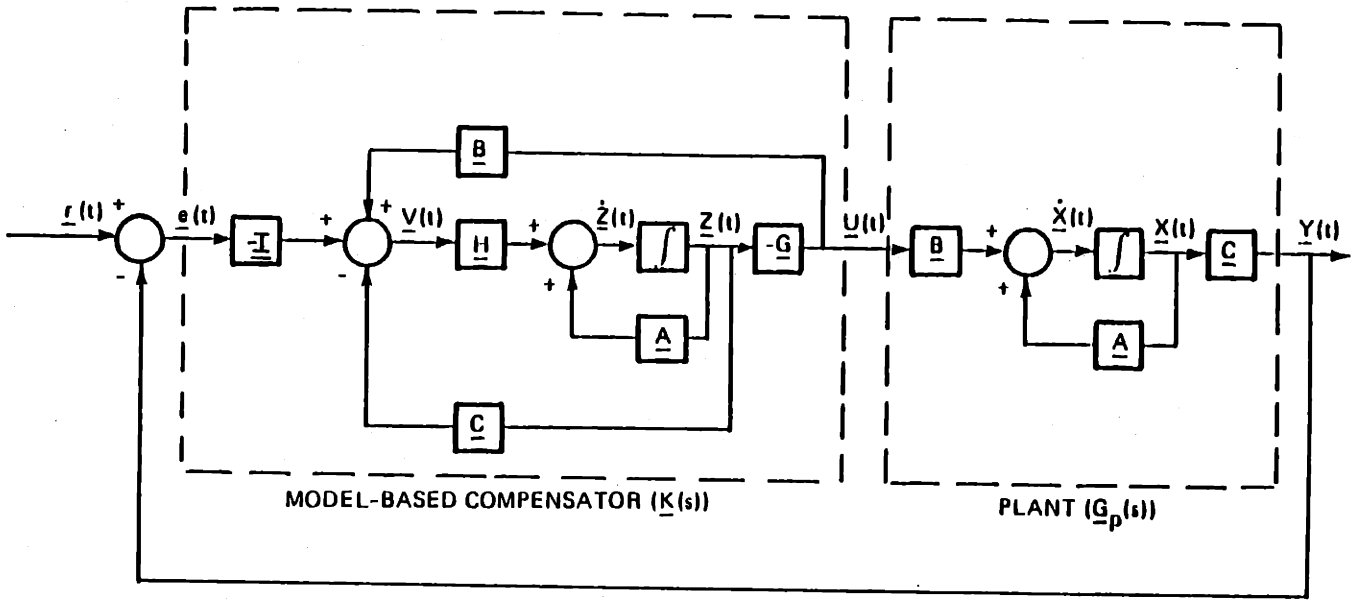

Figure 4.3 Model-Based Compensator in a feedback configuration.

Providing the plant is minimum phase [2], the singular values of $\underline{G}(s)\underline{K}_{MBC}(s)$ converge to the singular values of $\underline{G}_{KF}(s)$ as the design parameter $q \rightarrow \infty$. Above crossover frequencies, additional rolloff is produced by the recovery phase, which further enhances the high frequency robustness characteristics. As a result, the loop shape of $\underline{G}_{KF}(s)$ is recovered, and the resulting controller will have the desired performance characteristics.

4.3 Controller Specifications

Performance specifications outlined in this thesis are not all encompassing and do not necessarily reflect established Navy specifications for submarine control systems. The performance requirements are mainly driven by the intuitive engineering approach to obtain good command following, good system response, robustness, and disturbance rejection. These performance requirements will be met through loop shaping techniques.

Two performance requirements are imposed on the controller design. First, the steady state error to step commands and step disturbances is to be zero. Second, the maximum crossover frequency is limited by the ability of the submarine to respond and by the rate at which the compensator deflects the control surfaces.

The zero steady state requirement is met by placing integrators in each of the four input channels. Since the error signal appears at the input to the plant, this is

where the integrators will be placed. In this manner, the integrators will then become part of the compensator which is before the plant in the feedback loop. Note that the use of integral control in the input channels will not prevent the specification for maximum crossover frequency from being met.

The maximum crossover frequency of the compensator determines the rapidity of the control surface deflections based on the error signals which are generated by the difference between the reference commands and the measured outputs. Various models were analyzed during this research to determine the effects of the maximum crossover frequency. As the maximum crossover frequency was varied from 0.1 rad/sec to 1.0 rad/sec, two major observations were made. The first observation was that for high crossover frequencies the dynamic response of the submarine reacted more quickly and improved. The second observation was that the control surface deflections occurred more rapidly, which contributed to the improved dynamic response of the submarine. Since actuator dynamics are not directly modelled in this thesis, the maximum crossover frequency was selected based on control surface deflections which approximate actuator dynamics as listed in section 3.3.

Although not explicitly stated as a performance specification, from the performance aspect, it is desirable to have all singular values cross over at about the same frequency. Also, on the high frequency side, the controller

must be capable of rejecting noise and be robust to high frequency modelling errors. Noise sources generally originate from the environment, or from the sensor itself. Sensor noise typically occurs at a higher frequency than the system bandwidth and should not affect the dynamics of the ship since ship eigenvalues will typically lie in the lower frequency band.

4.4 Controller Design

4.4.1 Augmentation of the Model Dynamics

Augmenting the dynamics of the submarine control system normally serves a dual purpose. One is to model the actuator dynamics to make the model as accurate as possible and to achieve desirable rolloff at crossover for robustness. The other is to include integrators to cause the compensator to permit the submarine to achieve zero steady state error to step inputs and disturbances (i.e., good command following). The actuator dynamics are above the maximum expected crossover frequency, and thus are neglected [11,12,13]. This is perfectly valid as long as the rolloff above crossover is fast enough and satisfies the robustness criteria.

A block diagram of the augmented model appears in Figure 4.4. It is seen that the integrators are placed in the control channels. The mathematics of the augmented states will be manipulated in such a way as to provide a means to achieve the desired loop shapes of $\underline{G}_{FOL}(s)$.

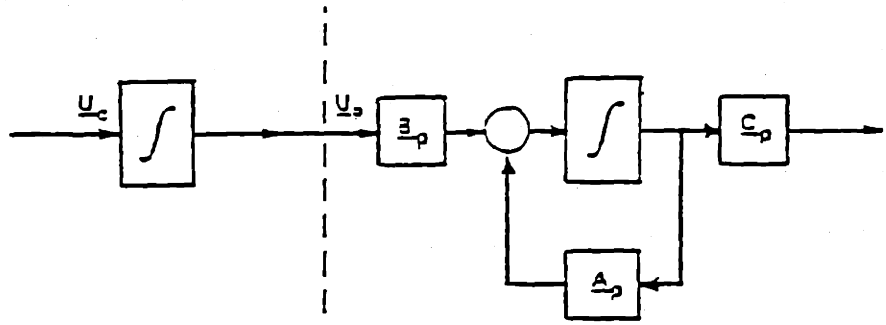

Figure 4.4 Integrators placed in the control channel of plant.

We define the augmentation dynamics by $\underline{G}_a(s)$, whose state space description is

$$\dot{\underline{u}}_p(t) = \underline{u}_c(t) \quad ; \quad \underline{G}_a(s) = \underline{I}/s$$

where each matrix is [4 x 4]. The augmenting dynamics are introduced to the 8^{th} order system using state space multiplication, producing a 12^{th} order system. Note that the physical input to the plant is labelled $\underline{u}_p(s)$ to distinguish it from the output of the compensator $\underline{u}_c(s)$. Although the augmentation dynamics $\underline{G}_a(s)$ will eventually be lumped with the compensator, they are kept separate until the LQG/LTR procedure is complete. Figure 4.5 shows a comparison of the unaugmented and augmented model. As shown, the integrators at the input produce a high dc gain increase at 0.001 rad/sec.

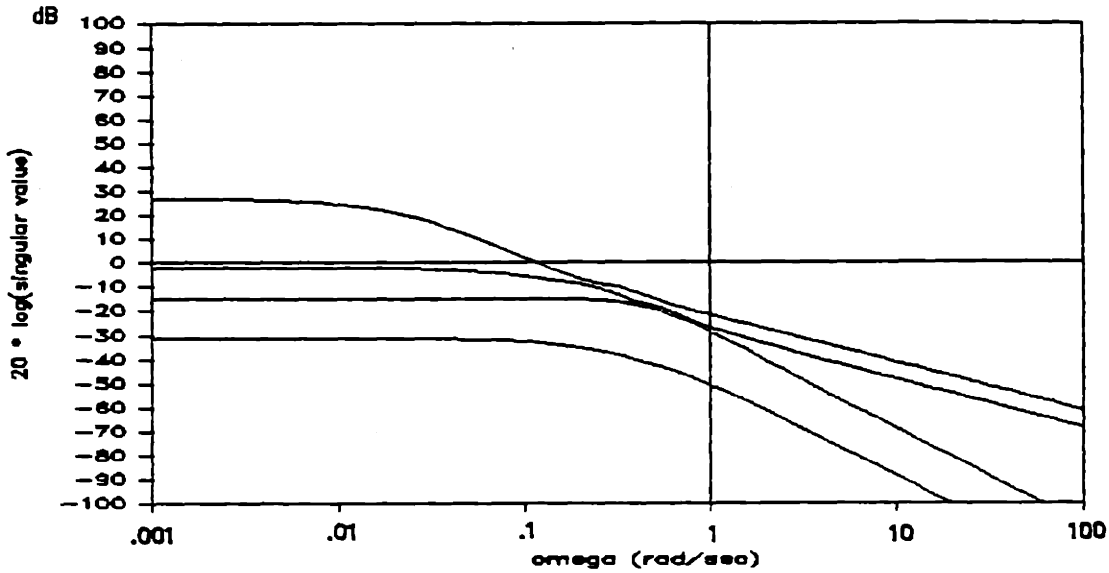

(a) Unaugmented Plant

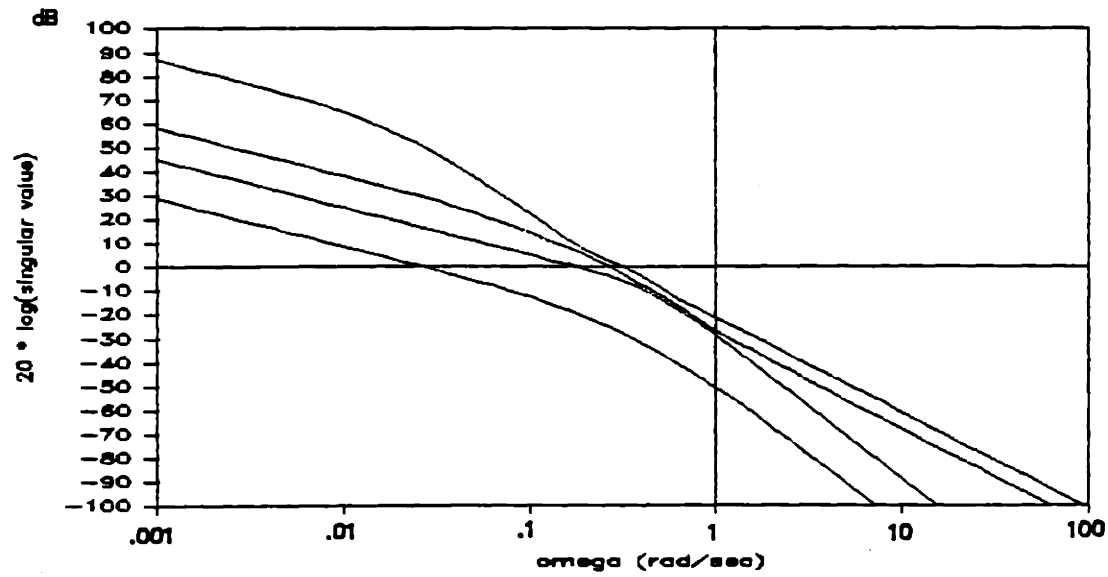

(b) Plant augmented with integral control

Figure 4.5 Comparison of Open Loop Singular Values with and without augmenting dynamics

4.4.2 Kalman Filter Loop Design

In section 4.2, it was stated that at high and low frequencies the singular values of the Kalman filter transfer function matrix are approximated by the singular values of $(1/\sqrt{\mu})\underline{G}_{FOL}(s)$. For each choice of $\underline{L}$, $\underline{G}_{FOL}(s)$ is easily calculated using available software.

To meet the loop shaping requirements displayed in Figure 4.2, the maximum and minimum singular values of $\underline{G}_{KF}(s)$ should be identical at high and low frequencies, and as close as possible at crossover. The choice of the design parameter $\underline{L}$ will thus be based on this philosophy.

Recall from section 4.2 that $\underline{G}(s) = \underline{G}_p(s)\underline{G}_a(s)$, and define $\underline{G}(s) = \underline{C}[s\underline{I} - \underline{A}]^{-1}\underline{B}$, where

$$\underline{A} = \begin{bmatrix} \underline{0} & \underline{0} \\ \underline{B}_p & \underline{A}_p \end{bmatrix} \qquad \underline{C} = [\underline{0} \quad \underline{C}_p],$$

and

$$s\underline{I}-\underline{A} = \begin{bmatrix} s\underline{I} & \underline{0} \\ -\underline{B}_p & s\underline{I}-\underline{A}_p \end{bmatrix}, \quad [s\underline{I}-\underline{A}]^{-1} = \begin{bmatrix} \underline{I}/s & \underline{0} \\ [s\underline{I}-\underline{A}_p]^{-1}\underline{B}_p/s & [s\underline{I}-\underline{A}_p]^{-1} \end{bmatrix}.$$

At low frequencies, $s\underline{I}-\underline{A}_p \approx -\underline{A}_p$ and $[s\underline{I}-\underline{A}_p]^{-1} \approx -\underline{A}_p^{-1}$. Since $\underline{A}_p$ has distinct and non-zero eigenvalues, $\underline{A}_p^{-1}$ exists. We now partition the $\underline{L}$ matrix into $\underline{L}_1$ and $\underline{L}_2$, where $\underline{L}_1$ will be selected for low frequency matching, and $\underline{L}_2$ will be selected for high frequency matching.

Forming $\underline{G}_{FOL}(s)$ for low frequencies,

$$\underline{G}_{FOL}(s) = \underline{C}[s\underline{I}-\underline{A}]^{-1}\underline{L}$$

$$\underline{G}_{FOL}(s) \approx [\underline{0} \quad \underline{C}_p] \begin{bmatrix} \underline{I}/s & \underline{0} \\ -\underline{A}_p^{-1}\underline{B}_p/s & -\underline{A}_p^{-1} \end{bmatrix} \begin{bmatrix} \underline{L}_1 \\ \underline{L}_2 \end{bmatrix}$$

$$\approx - \underline{C}_p\underline{A}_p^{-1}\underline{B}_p\underline{L}_1/s - \underline{C}_p\underline{A}_p^{-1}\underline{L}_2. \qquad (4.14)$$

It is now seen that the singular values can be matched at low frequencies if we select the matrix $\underline{L}_1$ as follows:

$$\underline{L}_1 = -[\underline{C}_p\underline{A}_p^{-1}\underline{B}_p]^{-1}. \qquad (4.15)$$

At high frequencies, $s\underline{I}-\underline{A}_p \approx s\underline{I}$, and $[s\underline{I}-\underline{A}_p]^{-1} \approx \underline{I}/s$. Forming $\underline{G}_{FOL}(s)$ for high frequencies,

$$\underline{G}_{FOL}(s) = [\underline{0} \quad \underline{C}_p] \begin{bmatrix} \underline{I}/s & \underline{0} \\ \underline{B}_p/s^2 & \underline{I}/s \end{bmatrix} \begin{bmatrix} \underline{L}_1 \\ \underline{L}_2 \end{bmatrix}$$

$$\approx \underline{C}_p\underline{B}_p\underline{L}_1/s^2 + \underline{C}_p\underline{L}_2/s.$$

The singular values can now be matched at high frequencies if we select $\underline{L}_2$ as follows:

$$\underline{L}_2 = \underline{C}_p'(\underline{C}_p\underline{C}_p')^{-1}, \qquad (4.16)$$

since as $s \to \infty$, $1/s > 1/s^2$, and the second term dominates the maximum singular values.

The above method for constructing the $\underline{L}$ matrix provides the designer with a guarantee of identical behavior of the Kalman filter loop singular values at both high and low

frequencies. However, this method does not provide an opportunity to directly control the shape of the singular values at crossover.

Once the $\underline{L}$ matrix is determined, the parameter μ is used to move the singular value plots up or down to obtain the desired crossover frequency. Then we can solve the FARE and calculate $\underline{G}_{KF}(s)$. The final value of μ used for the model during the Kalman filter design process is 4. The Kalman filter gain matrices are included in Appendix E.

Figure 4.6 is a plot of the singular values of the Kalman filter transfer matrix $\underline{G}_{FOL}(s)$ for the $\underline{L}$ matrix as defined in equations 4.15 and 4.16, and for $\mu = 4.0$. Although the singular values match at high and low frequencies, some differences exist at crossover.

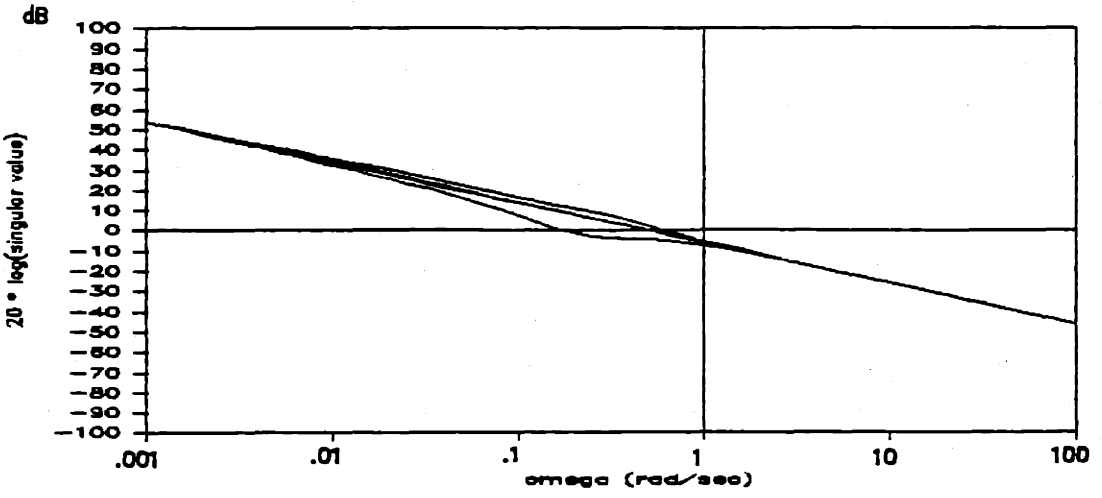

Figure 4.6 Singular Values of $\underline{G}_{FOL}(s)$

If the dynamic response of the model is not satisfactory, it is necessary to investigate the elements of the transfer function matrix $\underline{G}_{FOL}(s)$ in an attempt to control the separation of the singular values at crossover. The purpose is to achieve a scaling matrix for $\underline{C}_p$ which will result in a tight crossover pattern of the singular values.

4.4.3 Application of LQG/LTR

As stated in the overview of the LQG/LTR design procedure, once the Kalman filter design is complete, the remainder of the design process is quite straightforward.

It is now necessary to choose the design parameter q, and solve the CARE to obtain the $\underline{K}$ matrix. Then, we determine the Control gain matrix

$$\underline{G} = \underline{B}'\underline{K}.$$

Recall that for this recovery method to work well, the submarine model must not have low frequency transmission zeros. A value of $q = 1000$ was used for the model, producing the Control gain matrices in Appendix E1.

The entire design sequence is summarized in Figure 4.7, which are the singular value plots of $\underline{G}_{FOL}(s)$, $\underline{G}_{KF}(s)$, and $\underline{G}(s)\underline{K}(s)$. The minimum and maximum crossover frequencies are 0.2 rad/sec and 0.5 rad/sec, respectively.

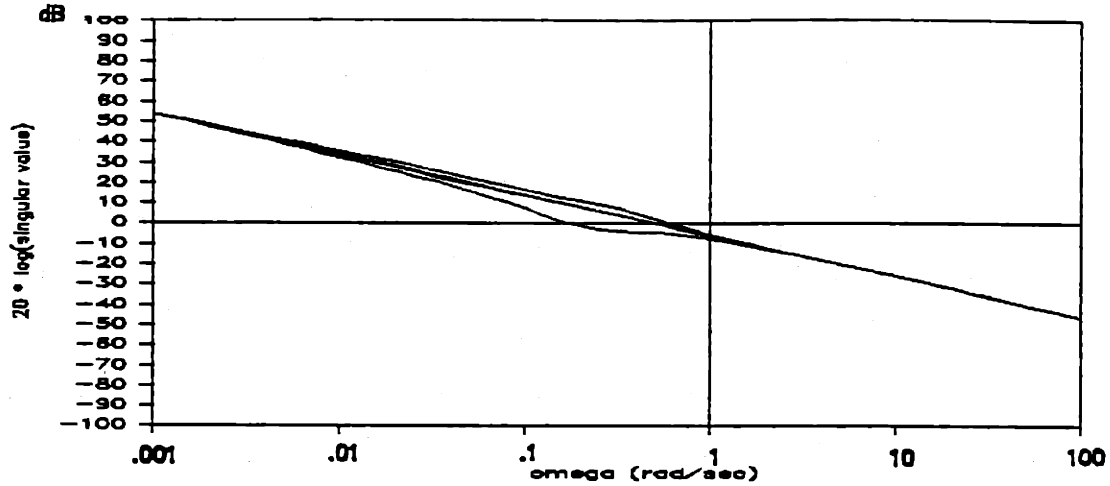

(a) Kalman Filter Open Loop, $\underline{G}_{FOL}$

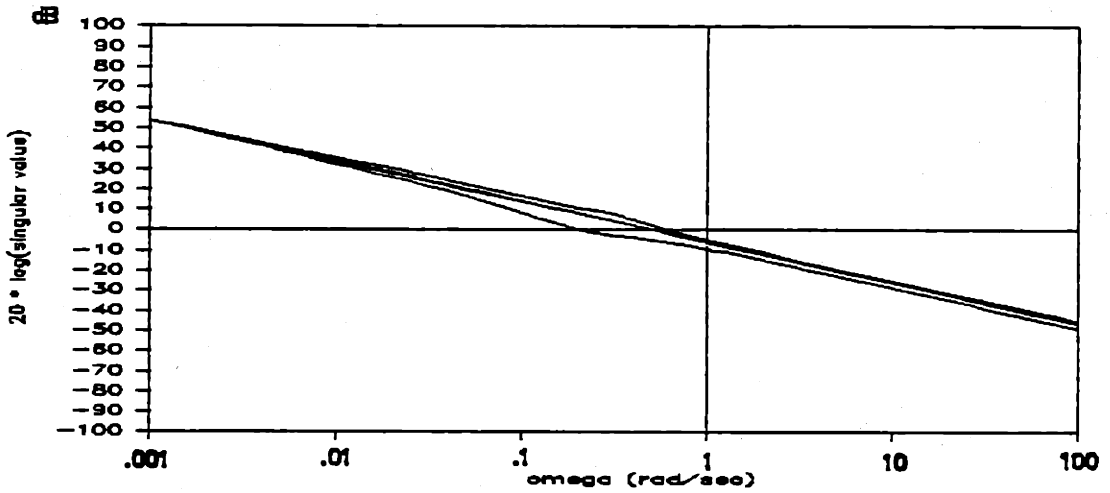

(b) Kalman Filter Loop, $\underline{G}_{KF}$

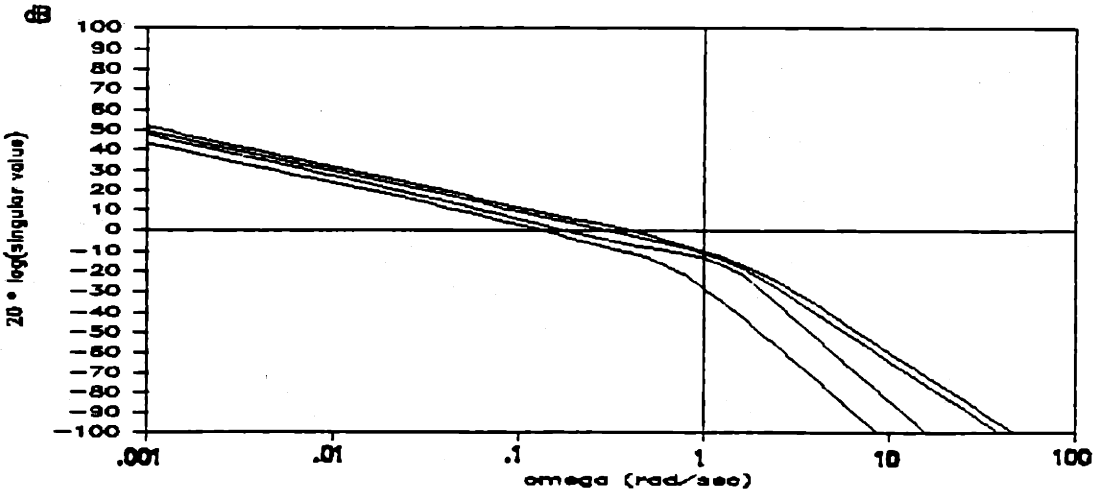

(c) Recovered Open Loop Transfer Function, $\underline{G}(s)\underline{K}(s)$ with q = 1000

Figure 4.7 Summary of the LQG/LTR Design Sequence

4.5 The Closed Loop System

The closed loop system can be written in state space form as

$$\begin{bmatrix} \dot{\underline{x}}(t) \\ \dot{\underline{z}}(t) \end{bmatrix} = \begin{bmatrix} \underline{A} & -\underline{B}\underline{G} \\ \underline{H}\underline{C} & \underline{A}-\underline{B}\underline{G}-\underline{H}\underline{C} \end{bmatrix} \begin{bmatrix} \underline{x}(t) \\ \underline{z}(t) \end{bmatrix} + \begin{bmatrix} \underline{0} \\ -\underline{H}\underline{C} \end{bmatrix} \underline{r}(t)$$

$$\underline{y}(t) = \begin{bmatrix} \underline{C} & \underline{0} \end{bmatrix} \begin{bmatrix} \underline{x}(t) \\ \underline{z}(t) \end{bmatrix} ,$$

where:

$\underline{x}(t)$ = the state of the nominal design model, and

$\underline{z}(t)$ = the state of the compensator.

The poles and zeros for the closed loop system are contained in Appendix E1. Since all the poles are in the left half plane, the system is in fact stable.

Referring to the overall loop transfer function of the closed loop system (section 4.2), from command input to output, then the singular values of the closed loop plant should be approximately 0 dB from dc up to the crossover frequency, and then rolloff at frequencies above crossover. This is shown in Figure 4.8, which is a singular value plot of the closed loop system.

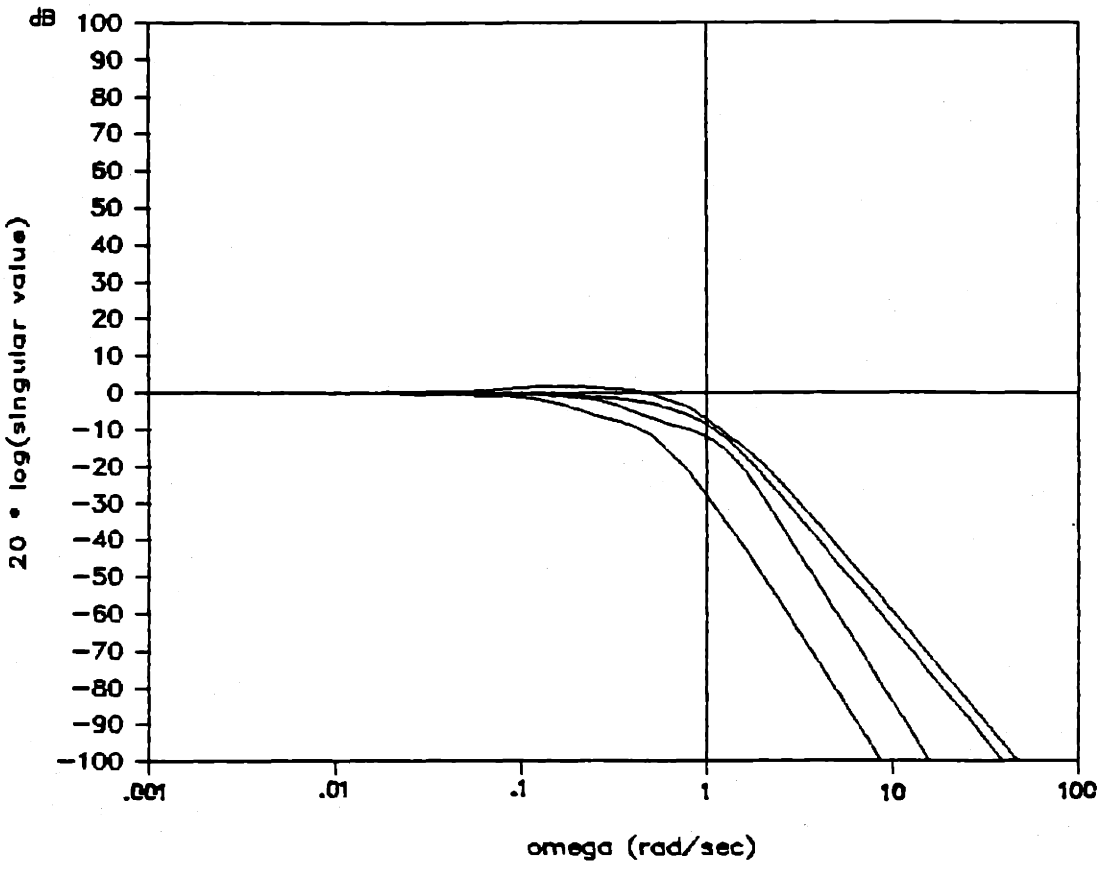

Figure 4.8 Singular Values of the Closed Loop

The singular values of the compensator are shown in Figure 4.9. Here we observe the lead-lag characteristics of the compensator over the frequency range of interest. Note the large amplifications at frequencies below crossover. The large spread in the singular values indicates certain directions are being amplified more than others.

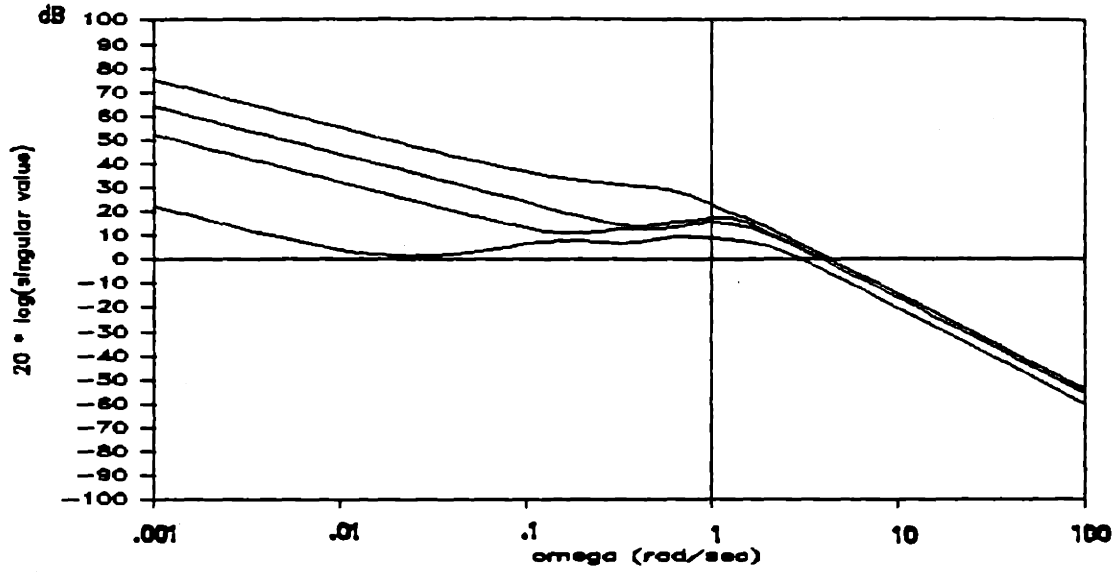

Figure 4.9 Compensator Singular Values

Figure 4.10 represents the singular values for the loop transfer function broken at the plant input instead of the plant output. Referring back to Figure 4.1, we see that the plots represent the net amplification from reference commands $\underline{r}(s)$ to the controls $\underline{u}_p(s)$, where

$$\underline{u}_p(s) = [\underline{I} + \underline{K}(s)\underline{G}(s)]^{-1}\underline{K}(s)\ \underline{r}(s) \ .$$

The figure shows that there are certain directions where amplification is required more than in others.

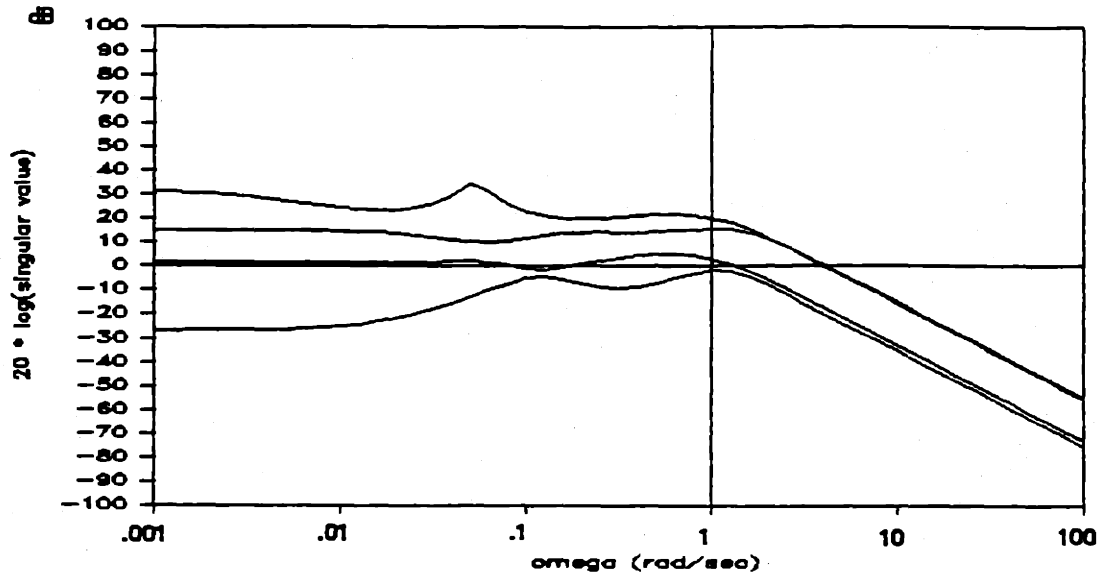

Figure 4.10 Singular Values for the Transfer Function broken at the Plant Input

4.6 Summary of LQG/LTR Design Sequence for Model without Roll Control

Figure 4.11 displays a summary of the LQG/LTR design sequence for a model which does not have active roll control. The entire design sequence is illustrated from the singular values of the original 3-input 3-output plant, through the loop transfer recovery process. For completeness, the singular value plot of the closed loop is also presented.

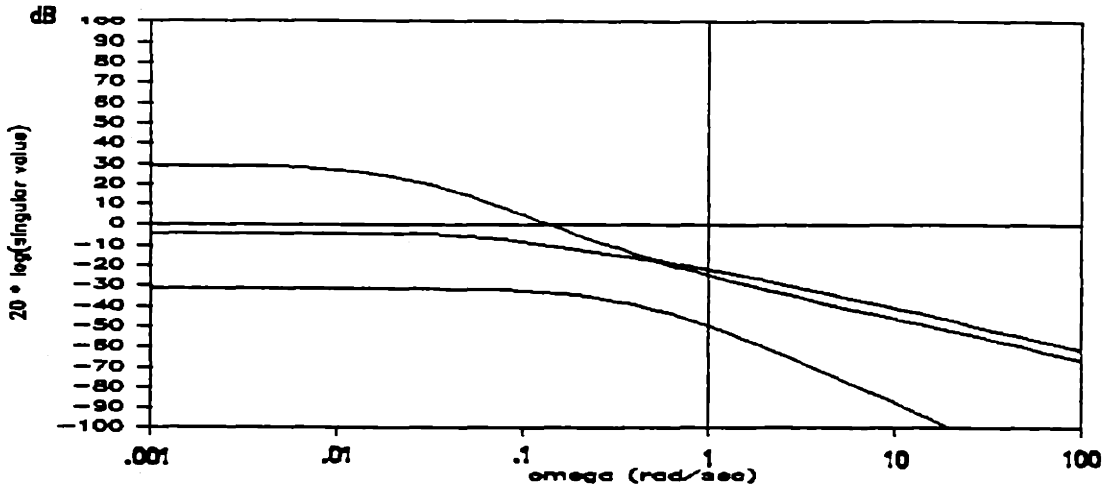

(a) Open Loop Plant

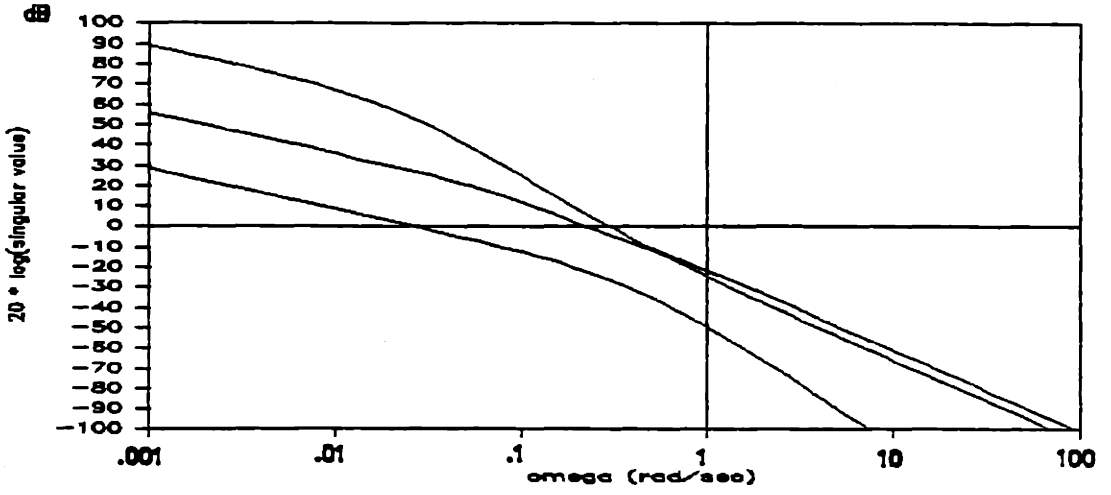

(b) Augmented Open Loop Plant

(c) Kalman Filter Open Loop, G_{FOL}

Figure 4.11 Summary of the LQG/LTR Design Sequence for Model without Roll Control

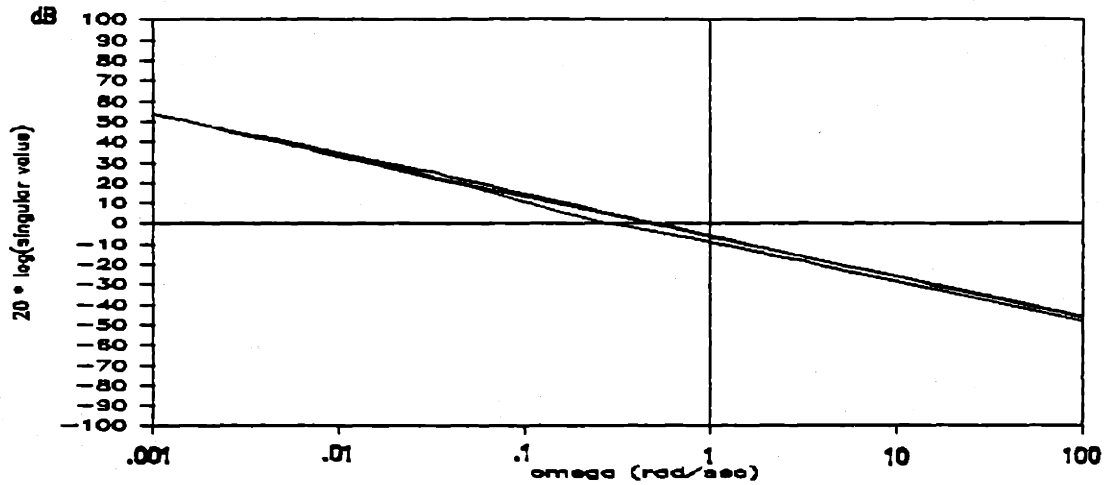

(d) Kalman Filter Loop, $\underline{G}_{KF}$

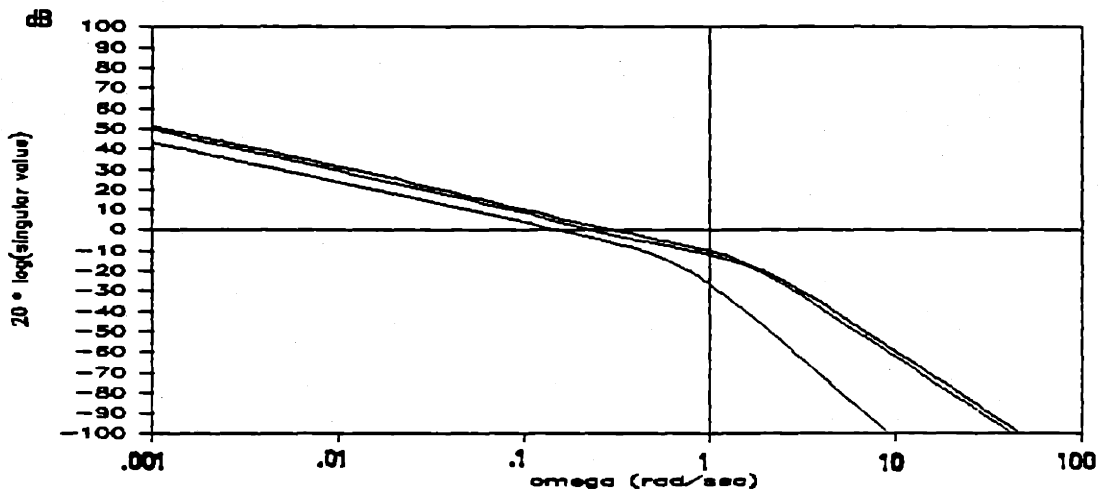

(e) Recovered Open Loop Transfer Function, $\underline{G}(s)\underline{K}(s)$

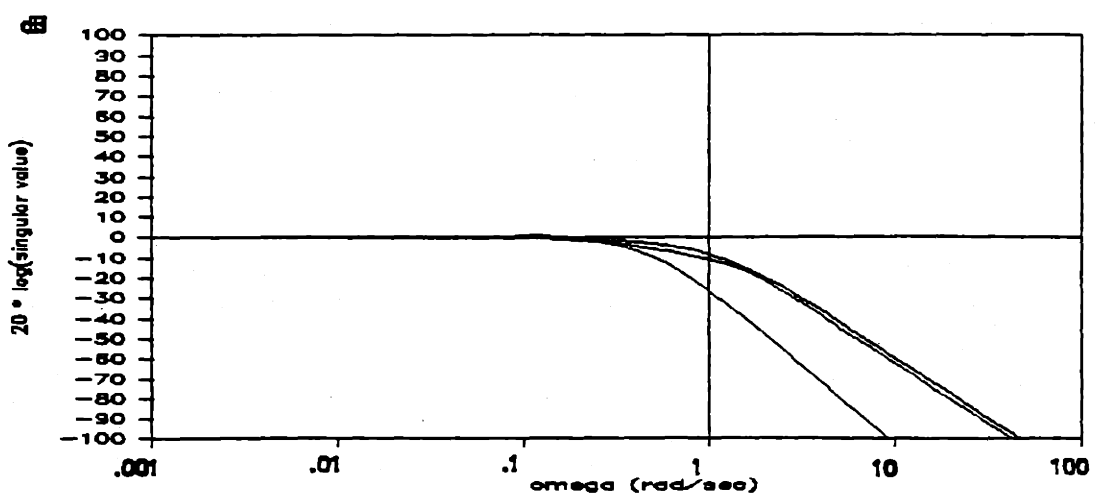

(f) Singular Values of the Closed Loop

Figure 4.11 Summary of the LQG/LTR Design Sequence for Model without Roll Control

4.7 Summary

This chapter demonstrated the application of the LQG/LTR control system design methodology. Specifications for the controller design were also presented, and then the methodology was applied to the design of a submarine control system.

Compensator designs were studied for various crossover frequencies, and then a compensator was selected which provided system response characteristics which were desirable, and which deflected the control surfaces in a reasonable manner.

Additionally, summary plots of the design sequence for a control system design without active roll control capability was also provided.

Figure 4.12 represents the final closed loop design on which Chapter Five is based.

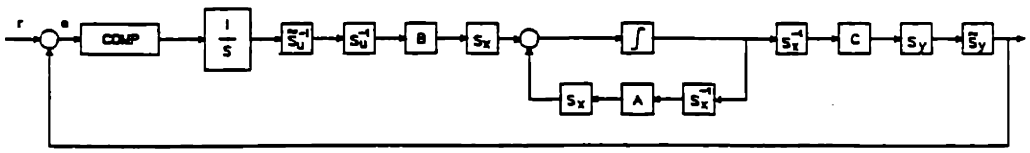

Figure 4.12 Block Diagram of the Closed Loop System

CHAPTER FIVE

EVALUATION OF THE MODEL BASED COMPENSATOR

5.1 Introduction

In this chapter, the performance of the controller design is evaluated. The controller is tested using both the linear and non-linear submarine simulations to determine how closely the performance specifications are met, and to test for instabilities in the design.

The 4-input, 4-output design is also compared to a 3-input, 3-output design that does not have the capability of active roll control. The comparisons provide a measure of performance improvements for the submarine when active roll control using the differential stern planes are employed.

5.2 Implementation of the Compensator

To implement the compensator on the computer facility at Draper, programming changes were necessary in two subroutines which are needed by the submarine simulation program. Subroutines OUTPTS and MBDCMP were modified to reflect scaling for consistent units from radians to degrees. Additionally, to maintain a properly scaled error vector to the compensator, it was necessary to apply appropriate scaling matrices to the $\underline{B}$ and $\underline{C}$ matrices of the MBC. These matrices reflect the weightings which were applied to the input and output vectors of the open loop model during the compensator designs of Chapter Four.

Once complete, the linear plant dynamics, upon which the compensator was designed, were replaced with the submarine simulation program to evaluate the performance of the compensator. This implies then, that the error vector, $\underline{e}(t)$, at the input to the Model Based Compensator is always the true difference between the commanded input and the output variables.

Figure 5.1 displays how the MBC feedback configuration for this design is modified by scaling. The block identified as COMP is now the MBC with the augmenting dynamics as discussed in the previous chapter. Describing the MBC with $\underline{A}$, $\underline{B}$, and $\underline{C}$ matrices (as shown in section 4.5) we now include the scaling matrices $\tilde{\underline{S}}_u^{-1}$ and $\tilde{\underline{S}}_y$ into the compensator, and define the resulting compensator as the compensator provided to the computer simulation at Draper.

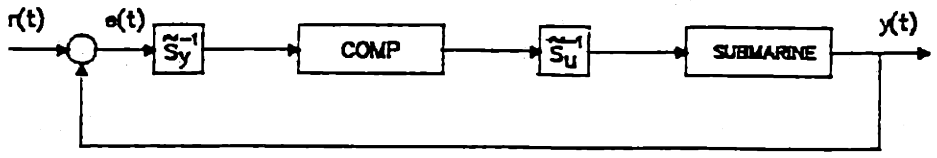

Figure 5.1 Modifications of the MBC Feedback Design for Weightings on Inputs and Outputs

5.3 Testing of the Compensator Design

The LQG/LTR compensator design was tested by providing the computer simulation at Draper with a data file

the computer simulation at Draper with a data file containing time sequenced command inputs and then integrating either the linear or non-linear equations of motion. Transient and steady state maneuvers were performed to validate the resulting designs. To provide comparisons for the various models, however, only the steady state maneuvers will be displayed in this thesis.

The evaluations of the Model Based Compensators are performed by first comparing the linear and non-linear simulations of the roll control model. The evaluations are completed by comparing a second MBC, designed without roll control capability, to the MBC designed with roll control capability.

5.4 Comparison of the Linear and Non-linear Simulations

Use of the LQG/LTR design methodology allows us to analyze the linear and non-linear applications of the design to ascertain whether the design is valid. Discounting effects due to non-linearities, the resulting linear simulation provides a prediction of initial derivatives, natural frequencies, and damping effects which can be expected in the non-linear simulation.

Figure 5.2 represents a comparison of the linear (LQG/LTR) and non-linear responses of the submarine simulation for a commanded 1.5° pitch angle. In the linear model, we observe that the forward velocity is essentially constant, while in the non-linear model we observe a

decrease of approximately 0.5 knots in the ship's forward velocity. Because the linear model neglects the non-linear dynamics of the submarine, we see a roll angle develop for the linear model which causes a heading change and depth excursion which is much more significant than in the non-linear response.

Comparing the control surface deflections, we see that the linear model requires slightly more deflection to obtain the desired response, which indicates that, in the linear case, the control surfaces are less effective. The fact that the linear model indicates less control surface authority explains the fact that the controller error signal does not disappear until much later than in the non-linear simulation.

For completeness, the outputs are also provided. Note that the outputs essentially exhibit the mirror image of the controller error, but additionally provide indication of the true output in the variable commanded for the maneuver, in this case, pitch angle θ.

The purpose of this comparison was to establish the validity of both the compensator design, and the computer software used for the simulations. This was particularly important because of the modifications made to the computer subroutines for scaling and selection of output variables. The simulations performed in the next section use only the non-linear computer models.

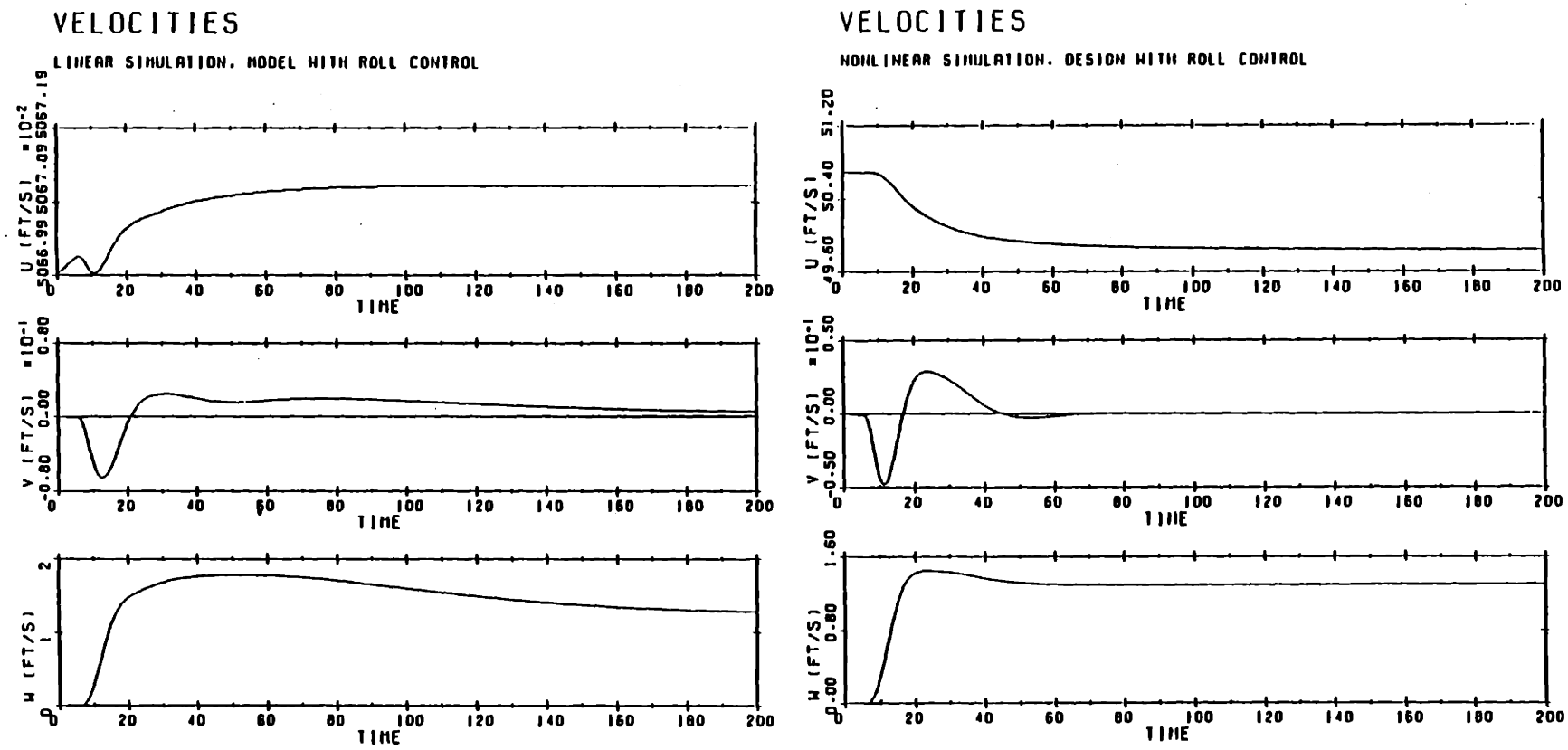

Figure 5.2(a) Comparison of the Linear and Non-linear Response of the Roll Control Model for a 1.5 degree pitch angle

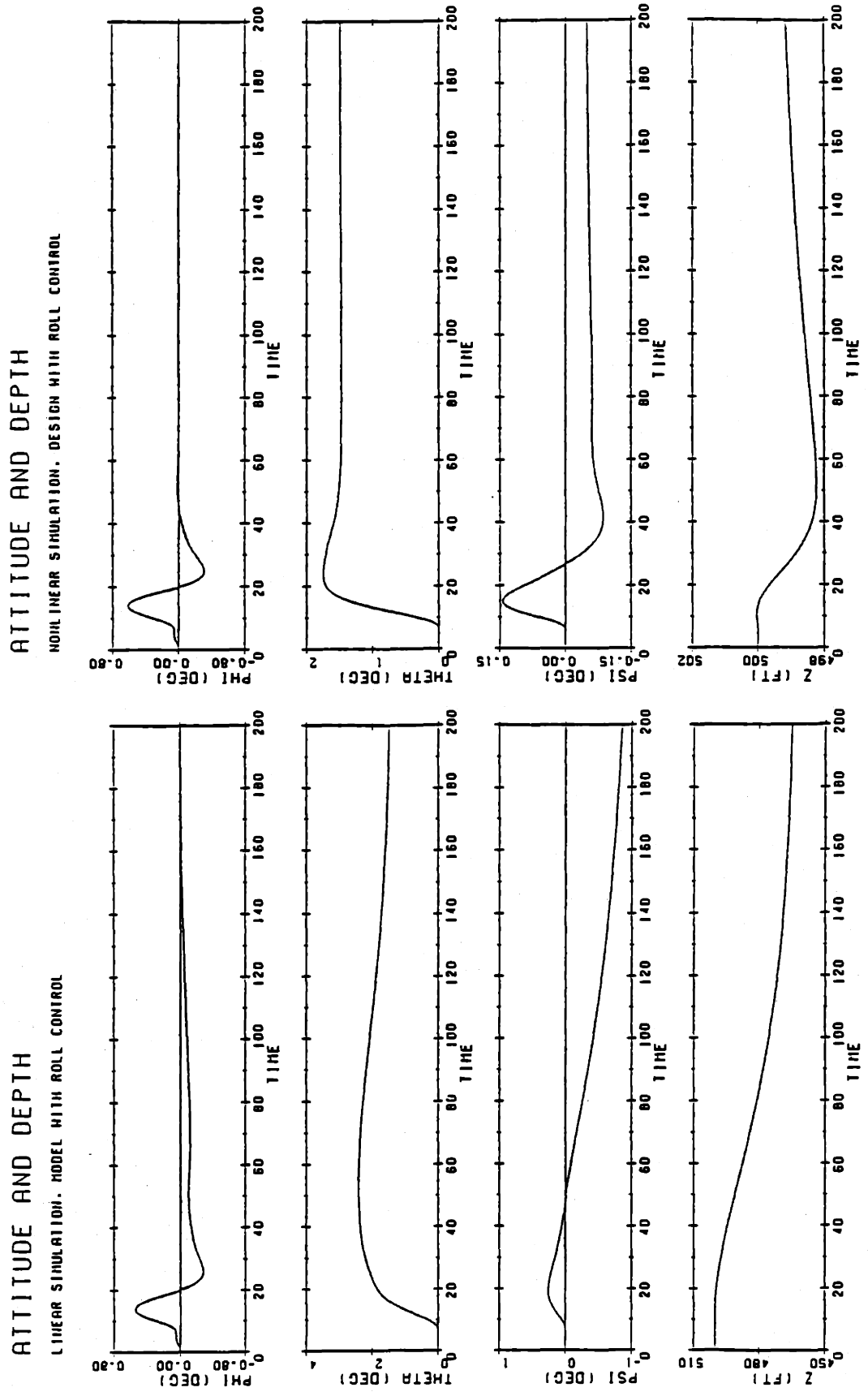

Figure 5.2(b) Comparison of the Linear and Non-linear Response of the Roll Control Model for a 1.5 degree pitch angle

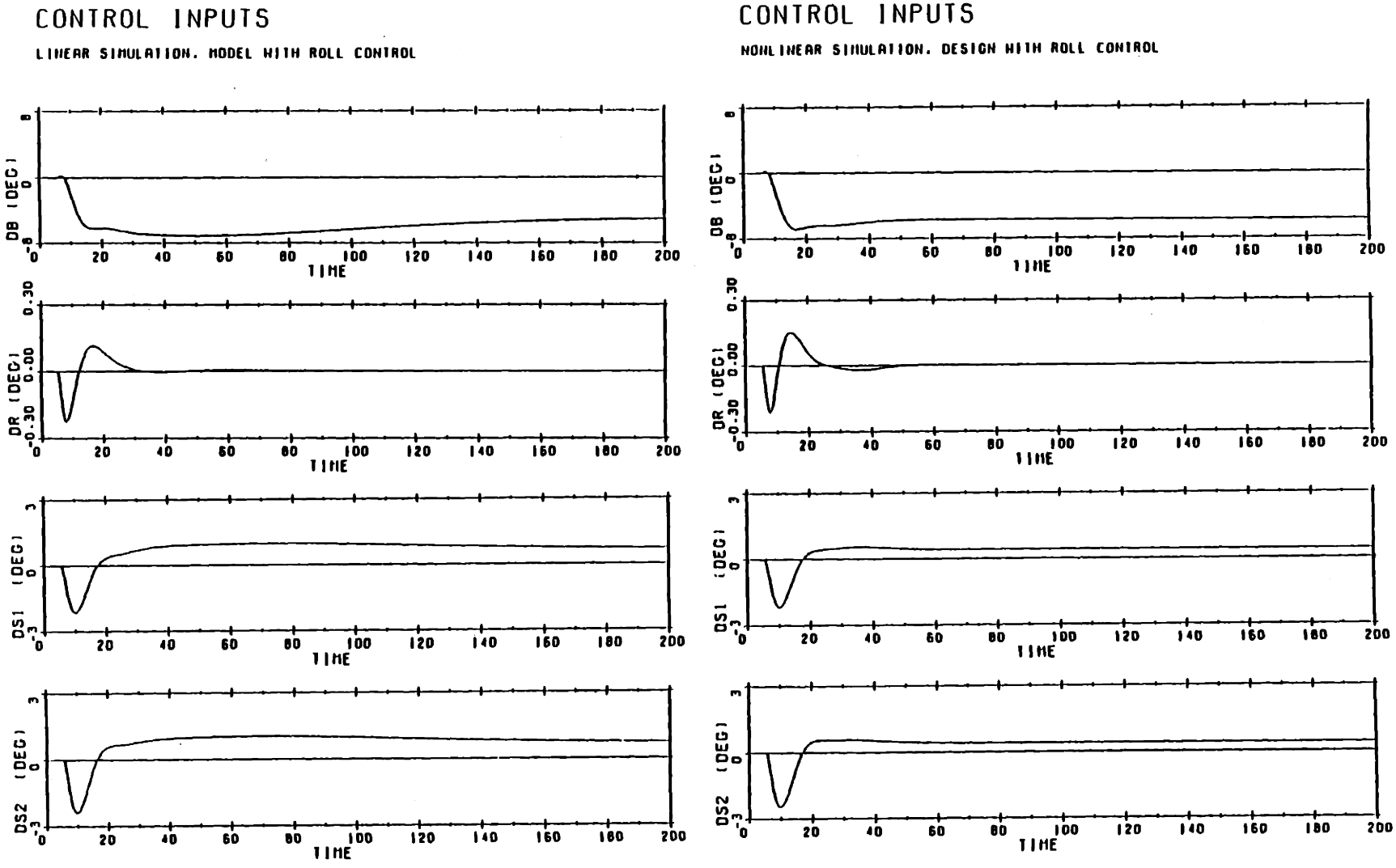

Figure 5.2(c) Comparison of the Linear and Non-linear Response of the Roll Control Model for a 1.5 degree pitch angle

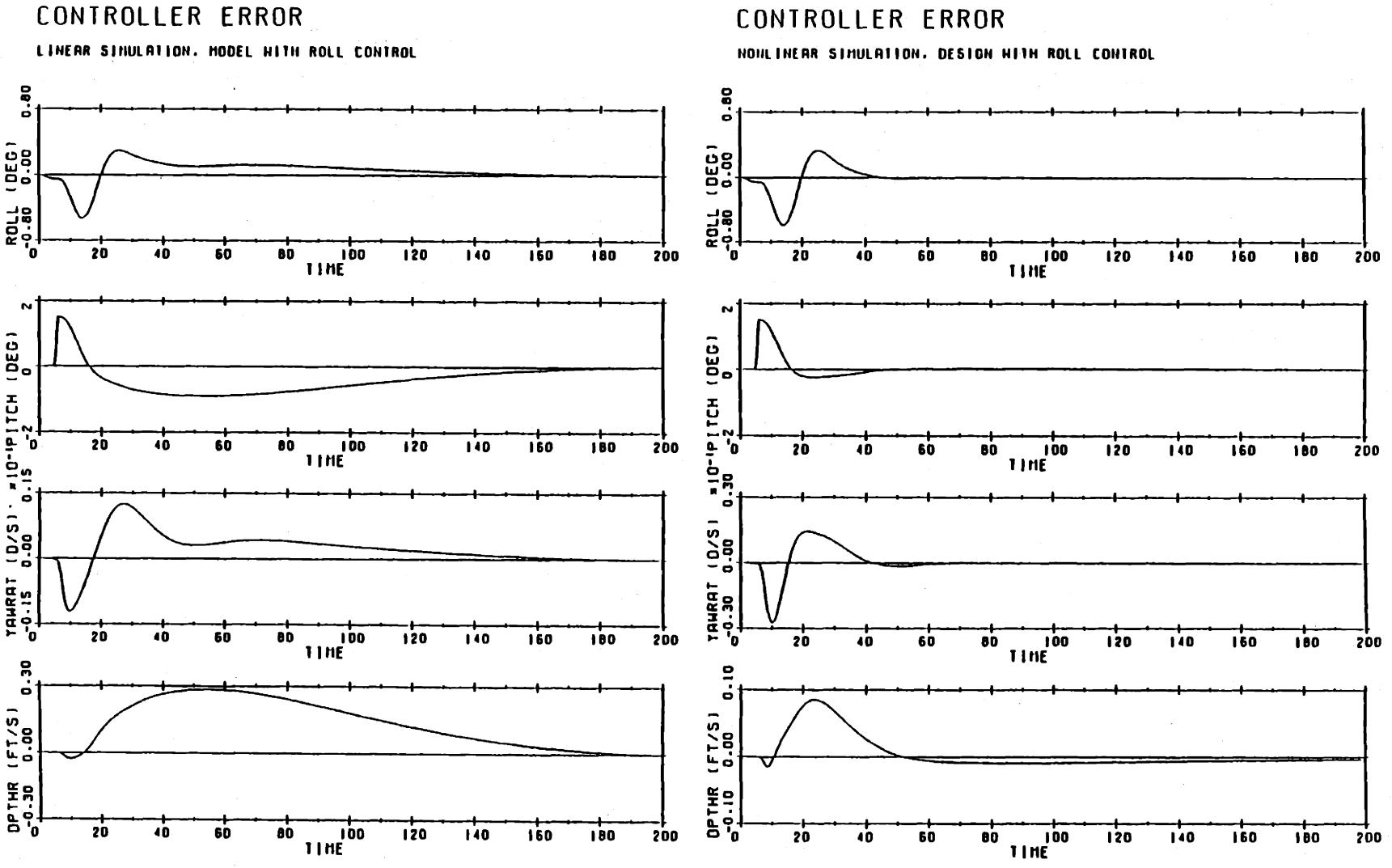

Figure 5.2(d) Comparison of the Linear and Non-linear Response of the Roll Control Model for a 1.5 degree pitch angle

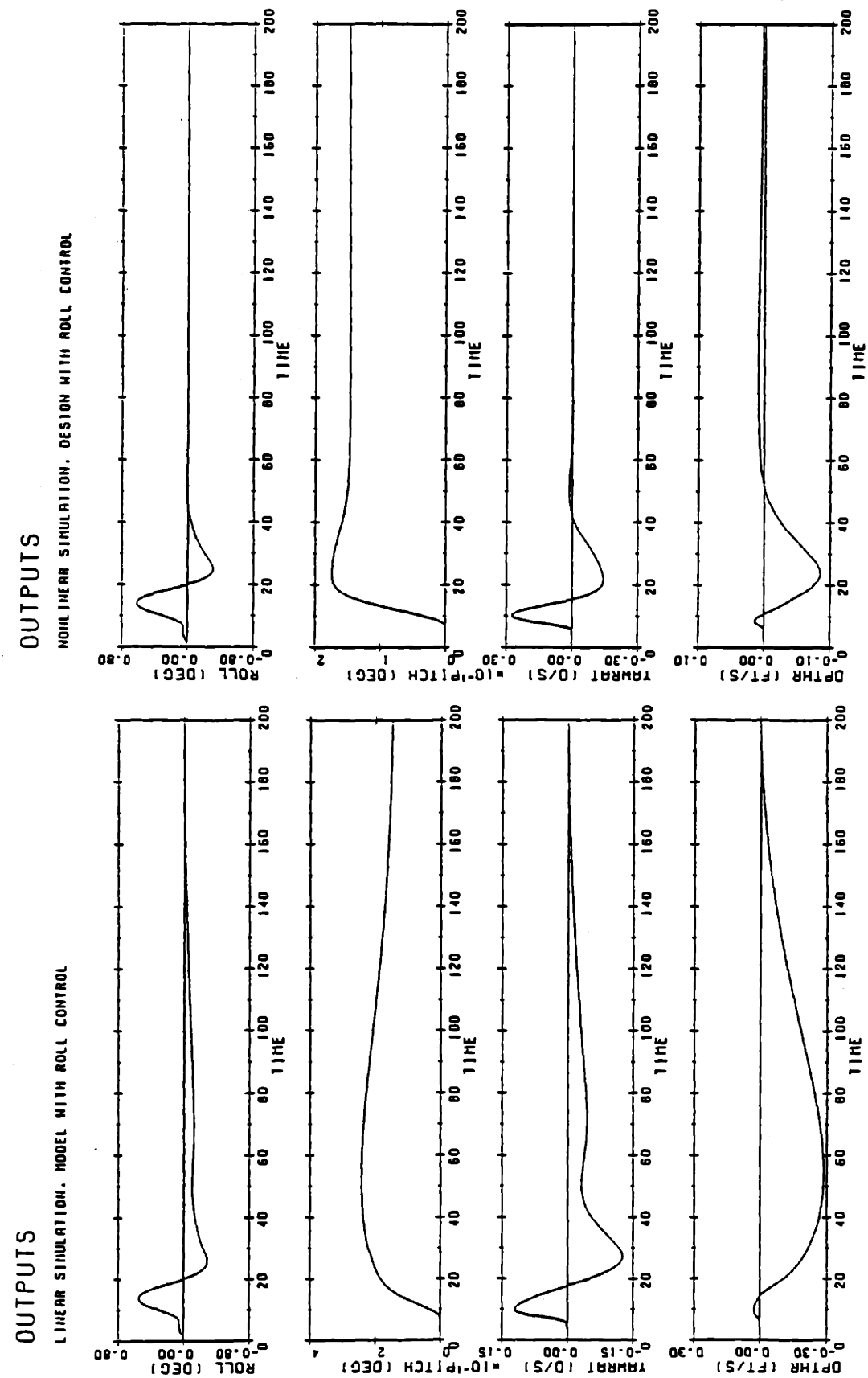

Figure 5.2(e) Comparison of the Linear and Non-linear Response of the Roll Control Model for a 1.5 degree pitch angle

5.5 Roll vs Non-roll Control Model

Having established the validity of the compensator design and the compensator software, it is now necessary to demonstrate the performance characteristics of the roll control model as compared to a comparably designed compensator without roll control capability.

Using the criteria presented in Chapter Four, a Model Based Compensator was designed which does not have roll control capability. The elimination of roll angle, Φ, as a state of the output vector resulted in an input vector $\underline{u}(t)$, where

$$\underline{u}(t) = \begin{bmatrix} \delta b \\ \delta r \\ \delta s \end{bmatrix} \quad \text{and} \quad \delta s = \delta s_1 + \delta s_2 \ .$$

Information regarding the state space descriptions of the model without roll control capability is provided in Appendix C4. Modal analysis results are provided in Appendix D2, and properties of the closed loop system are provided in Appendix E2.

To allow comparisons between the two models that provide useful information, the same design parameters were used for both models. The output vector for this model is $\underline{y}(t)$, where

$$\underline{y}(t) = [\ \underline{\theta}(t) \quad \dot{\underline{\Psi}}(t) \quad \dot{\underline{z}}(t)\ ]^T \ .$$

Comparisons are made for four simulations. The first two simulations are for heading changes by commanding a step

input of 1 deg/second, and 2 deg/second, respectively. The intent of these two simulations is to display the submarine trajectory when a steady turning rate is commanded. A larger commanded heading rate should accelerate the nonlinear characteristics of the system. The third comparison is for a combined maneuver in which step commands of 1 degree of pitch, 0.5 feet/second of depth rate, and 1 degree/second of heading change are provided to the compensators. The fourth simulation is less detailed than the three preceding ones, however, the commanded turning rate is 3 degrees/second, and provides additional insight into the differences in the two compensators.

In all four simulations the commands are applied as step inputs at t = 5 seconds. Additionally, in the simulations for the design without roll control, the stern plane deflections δs_1 and δs_2 are shown separately to further illustrate the stern plane deflections in the design with roll control.

5.5.1 Mild Turning Maneuver

Figure 5.3 displays the results of commanding a mild turning maneuver of 1 deg/sec. For this turning rate, the ship experiences a decrease in forward velocity of 6%.

Looking first at the design with roll control, we observe that the submarine initially rolls outward, then snap rolls into the turn at t = 12 seconds. The maximum inward roll angle is 2° at t = 22 seconds. The ship has a

maximum downward pitch angle of -1°. The ship loses 8 feet in depth during the entire maneuver. It is observed the stern planes deflect differentially to compensate for the roll moment, with a steady state difference of 6°. Note the use of bow planes to minimize the depth rate. Once depth rate error has been eliminated, the bow planes return to their neutral position.

To obtain the commanded turning rate, the rudder initially deflects 5°. As the error in yaw rate decreases, the rudder steadies at slightly less than 2° deflection.

Looking now at the model without roll control, it is immediately observed that the ship experiences a snap roll of 10°, with roll angle steadying out at 8°. Due to the roll angle, and the effect of the rudder, the ship experiences a downward pitch angle of approximately 2°, which causes the ship to experience a depth loss of almost 65 feet. Because the roll angle is contributing to the depth rate, the bow planes are deflected 7°, with stern plane deflections of -1°. The combination of stern planes and bow planes are minimizing the depth excursion. Note, however, that since roll angle strongly influences pitch and depth rate, that these two terms are not being damped as readily as they were in the roll control model.

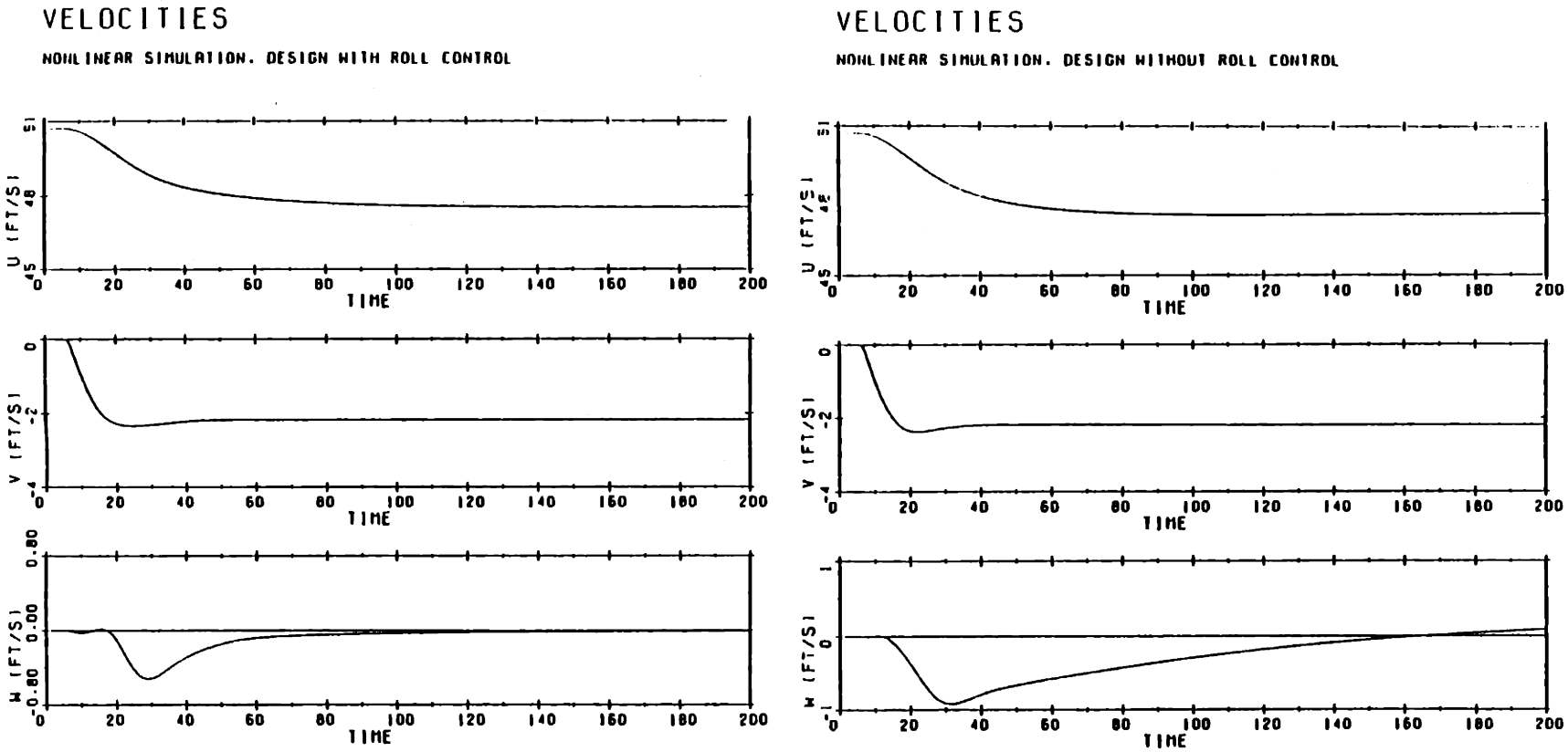

Figure 5.3(a) Comparison of the Non-linear Response of Models with and without Roll Control for a Mild Turn

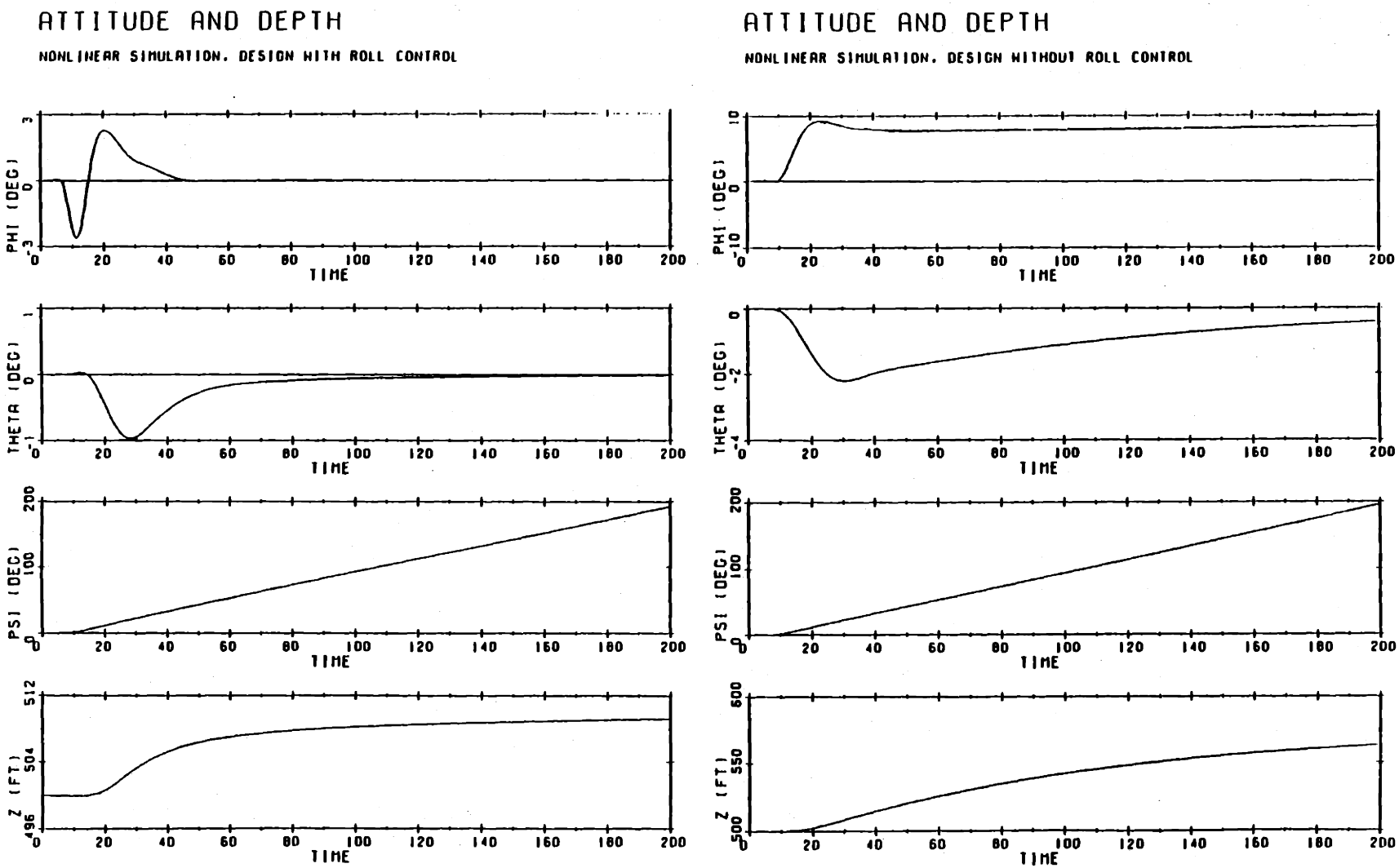

Figure 5.3(b) Comparison of the Non--linear Response of Models with and without Roll Control for a Mild Turn

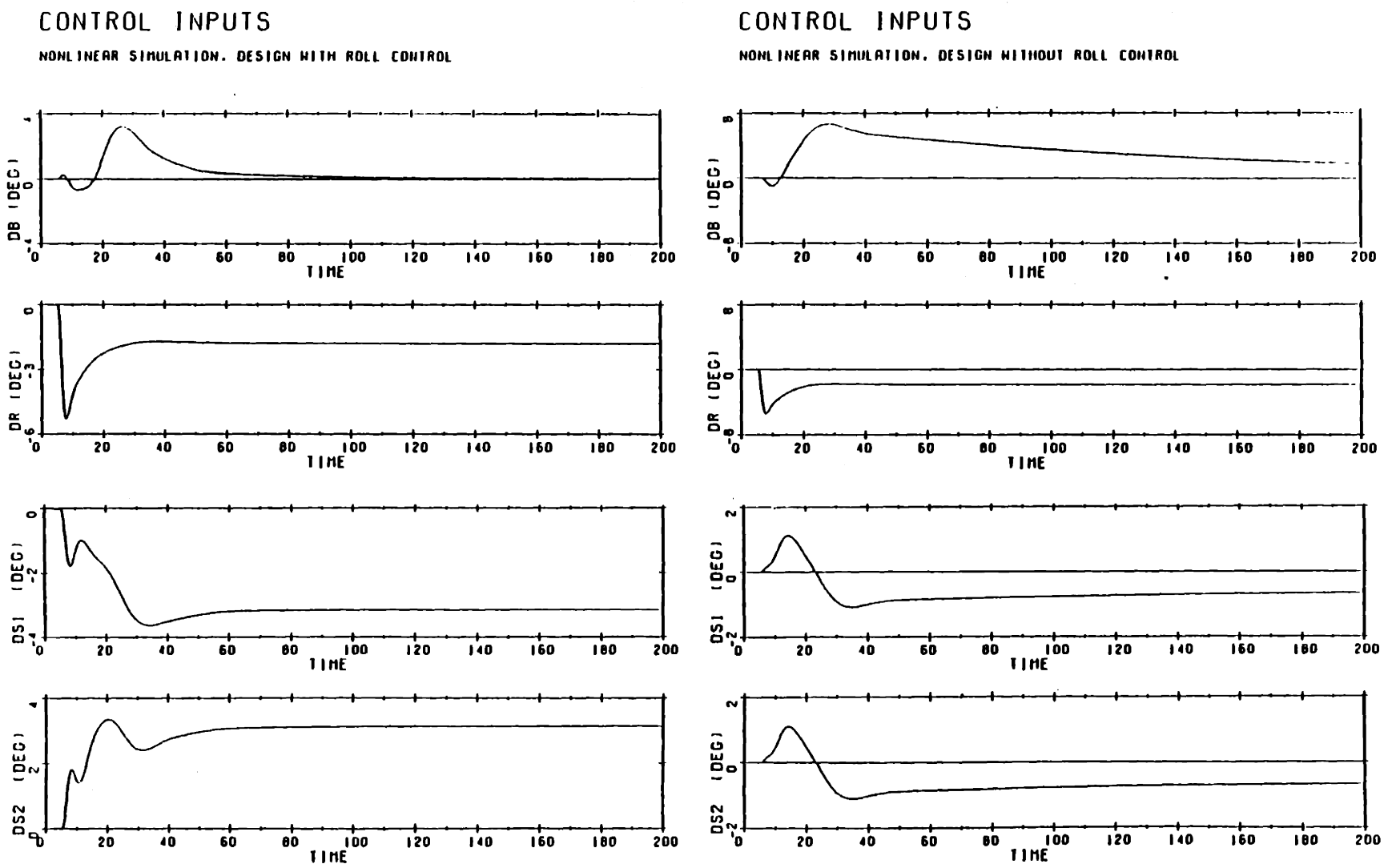

Figure 5.3(c) Comparison of the Non-linear Response of Models with and without Roll Control for a Mild Turn

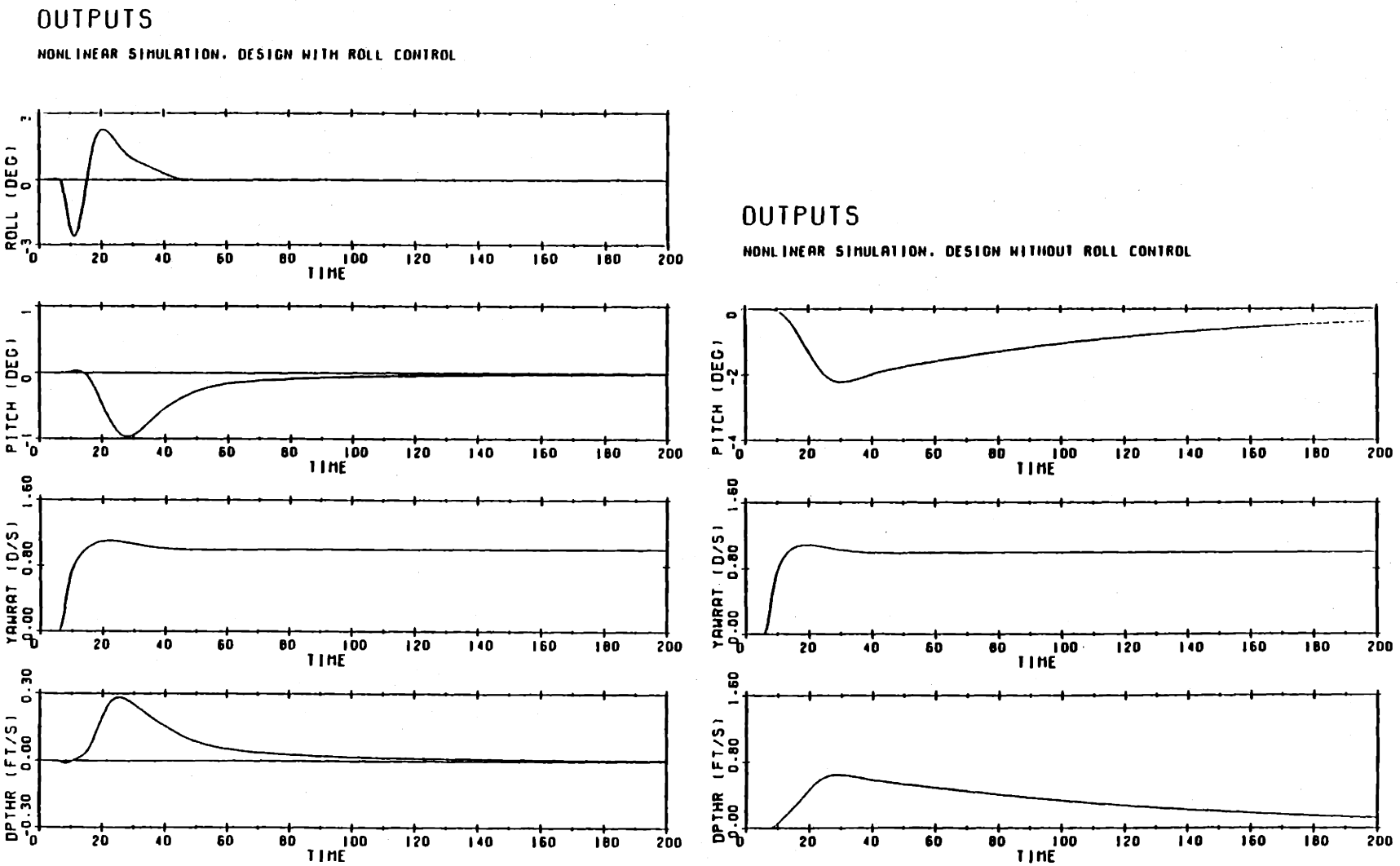

Figure 5.3(d) Comparison of the Non-linear Response of Models with and without Roll Control for a Mild Turn

5.5.2 Moderate Turning Maneuver

This simulation is for a commanded yaw rate of 2 deg/sec. Referring to Figure 5.4, we observe a 25% decrease in forward velocity. The model with roll control experiences an outward roll of 6°, then snap rolls inward to 3°. By t = 30 seconds, the roll angle is essentially zero. The ship initially pitches upward due to the outward roll and rudder deflection. When the snap roll occurs, the pitch angle achieves an angle of -2°, but steadies out at -1.3° at t = 55 seconds. This negative pitch angle contributes to the constant depth rate of 0.4 ft/sec. The significant loss of speed contributes to the lack of ability of the control surfaces to minimize vertical plane errors. For this simulation, the stern planes a deflecting a difference of 12° to compensate for the roll moment in the turn. To minimize depth rate, we see the bow planes are deflecting 3°, and to maintain the turn, the rudder is deflecting almost 8°.

Comparing the model without roll control, we observe the ship snap rolls inward 15°, then comes to a steady roll angle of 12°. Because of the large roll angle, the ship pitches down 6° initially, with pitch angle coming to -2.5° at t= 200 seconds. The depth loss in the turn is 225 feet. The bow planes almost saturate initially, deflecting to 18° to counteract the depth rate. At t = 200 seconds, the bow planes are deflected 9° (or three times the deflection in the roll control model). The rudder is deflected

approximately 8°, which is similar in the roll control model. Additionally, the stern planes are deflected to minimize the depth rate, whereas, in the roll control model, they were deflected only to minimize roll angle because the bow planes were better able to minimize depth rate.

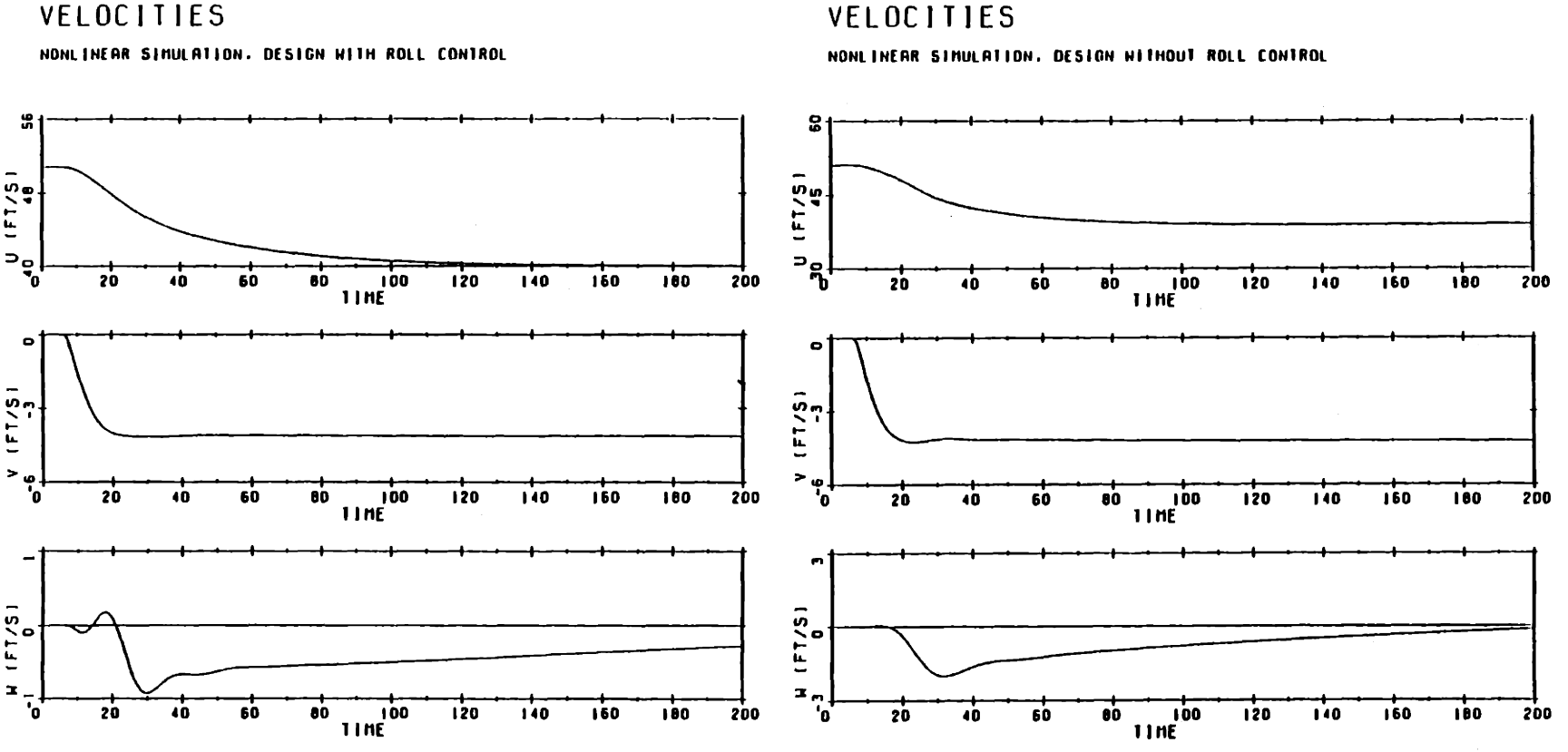

Figure 5.4(a) Comparison of the Non-linear Response of Models with and without Roll Control for a Moderate Turn

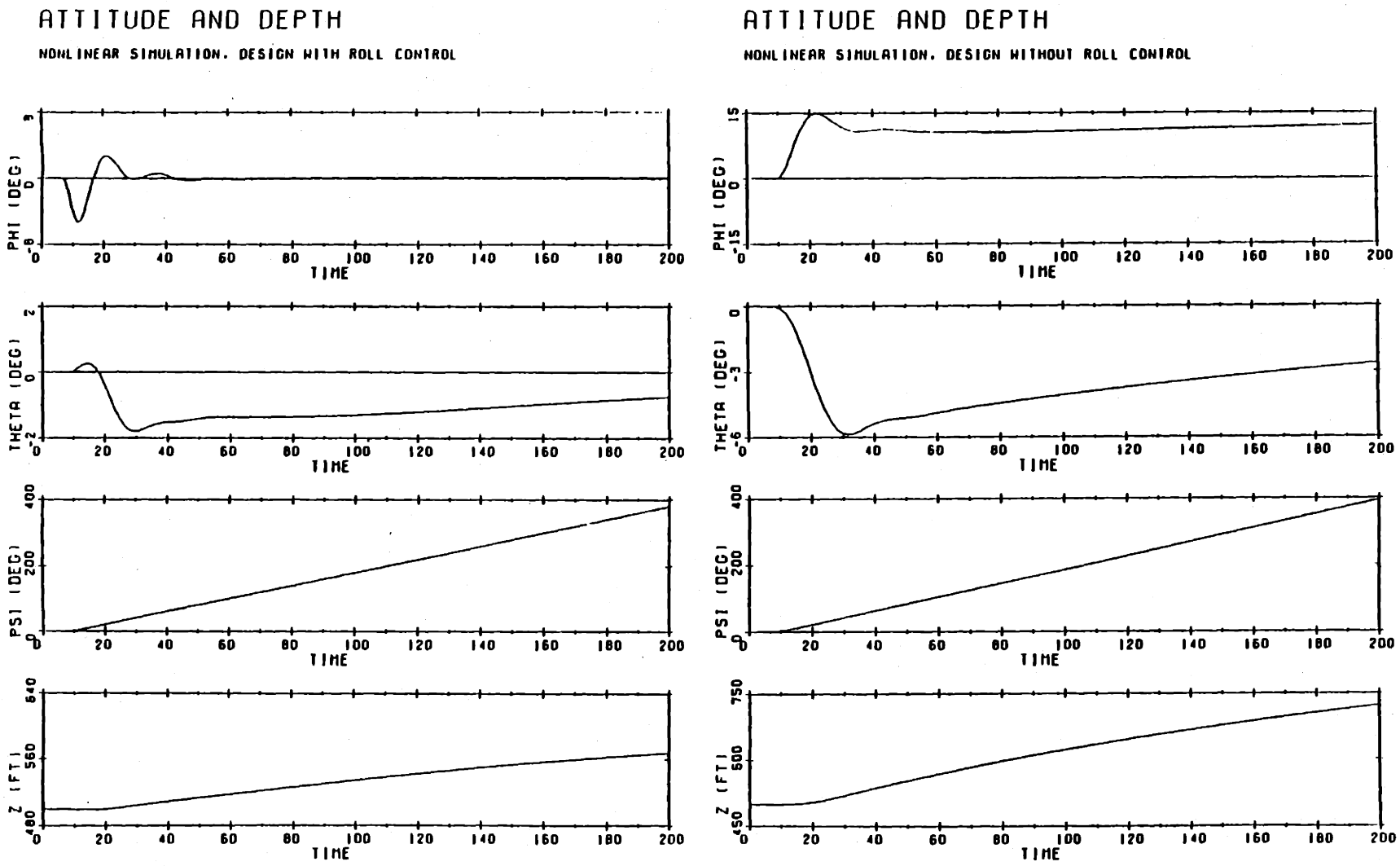

Figure 5.4(b) Comparison of the Non-linear Response of Models with and without Roll Control for a Moderate Turn

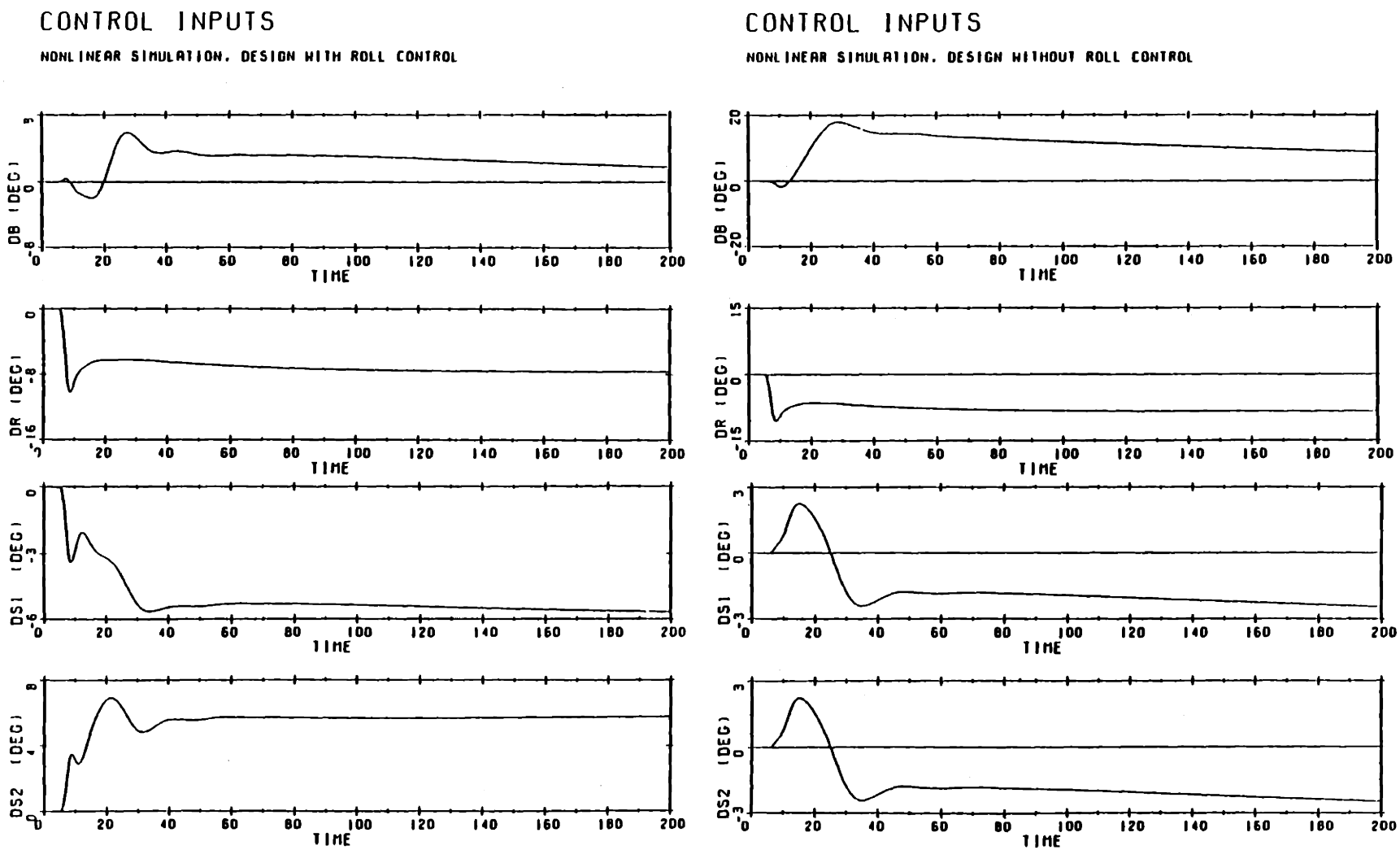

Figure 5.4(c) Comparison of the Non-linear Response of Models with and without Roll Control for a Moderate Turn

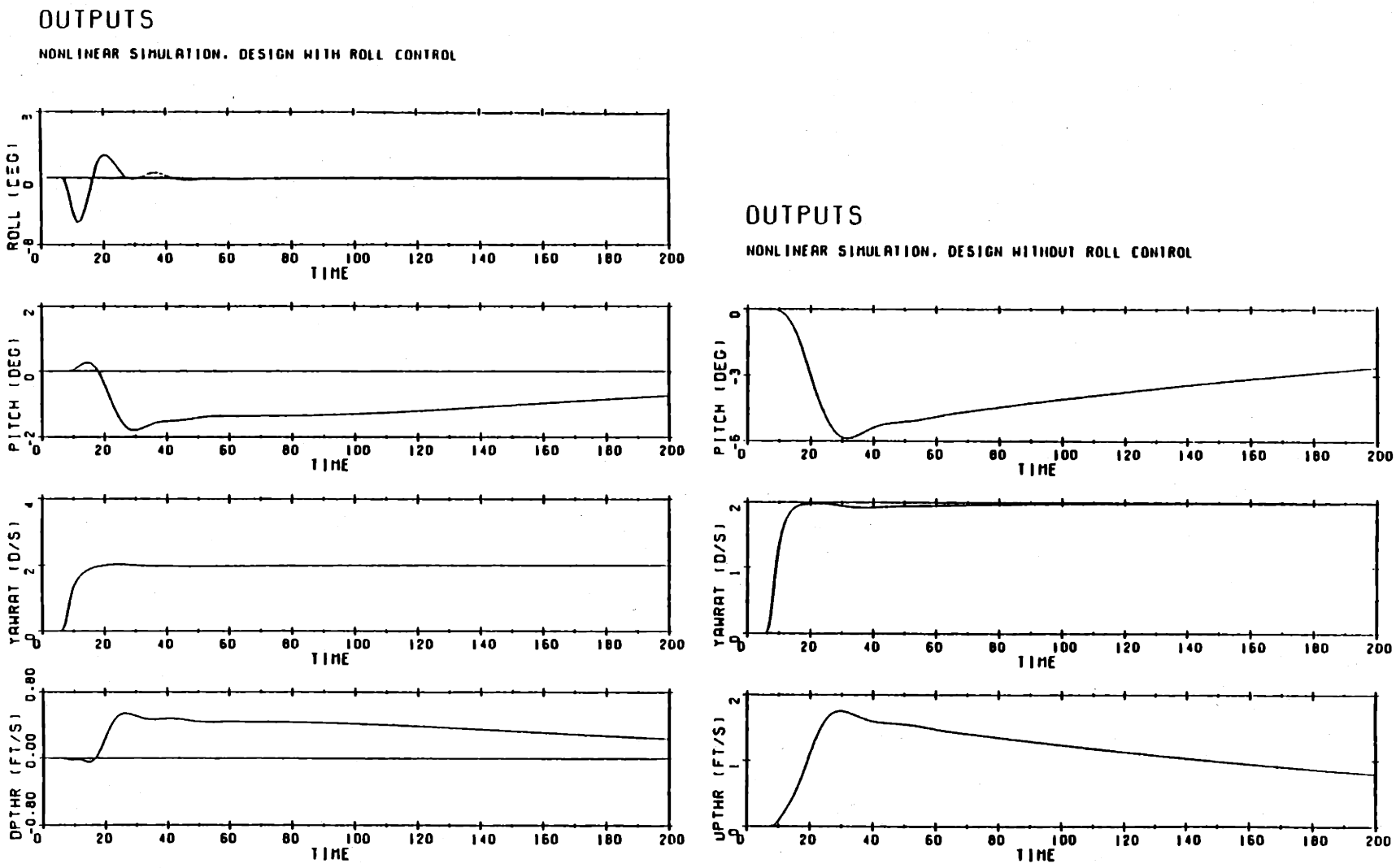

Figure 5.4(d) Comparison of the Non-linear Response of Models with and without Roll Control for a Moderate Turn

5.5.3 Combined Maneuver

This maneuver is for step input commands of -0.5 ft/sec in depth rate, 1 deg/sec in yaw rate, and 1 degree in pitch. Referring to Figure 5.5, we observe a 6% decrease in the forward velocity.

Looking first at the model with roll control, it is observed that the errors in roll angle and yaw rate are damped by t = 40 seconds. The errors in pitch and depth rate, however, are not damped until t = 140 seconds. By t = 200 seconds, the ship has experienced a depth rise of 80 feet. Again, the stern planes are deflected differentially to counteract the roll moment, with a steady differential deflection of 6°. The bow planes are deflected at -1.5° to maintain the commanded depth rate, and the rudder is deflected -2° to maintain the commanded yaw rate.

Comparing the design without roll control, it is observed that the ship experiences a snap roll of 10°. This roll angle causes a pitch angle of -2° which results in a large pitch error. In fact, at t = 200 seconds, there is still an error in pitch of 0.5°, or 50% of the commanded pitch angle. This also causes a -0.35 ft/sec depth rate instead of the commanded -.5 ft/sec. The net result of these errors is displayed in the depth of the ship. The depth rise in this design is 25 feet, instead of 80 feet, as in the model with roll control. Note here, that a depth rise is commanded.

The steady state stern planes angle is -0.75°, which indicates the stern planes are being used to obtain the ordered pitch angle. Because the depth rate is a result of the combination of pitch angle and ship's speed, we observe the bow planes are being used to obtain the ordered depth rate. In the roll control model, the ship obtained the ordered pitch angle rather quickly, thus, the bow planes are deflected in the opposite direction to limit the depth rate to -0.5 ft/sec.

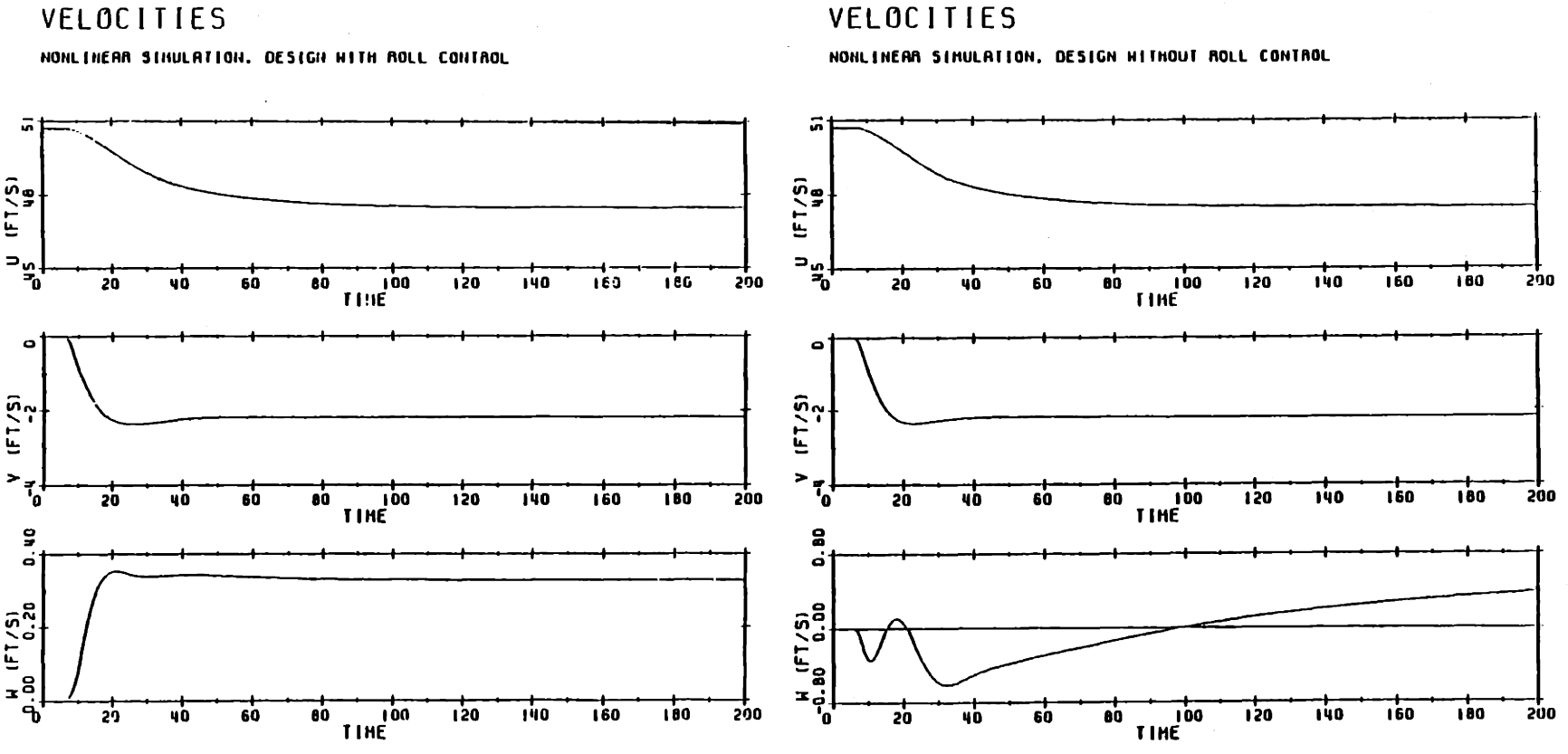

Figure 5.5(a) Comparison of the Non--linear Response of Models with and without Roll Control for a Combined Maneuver

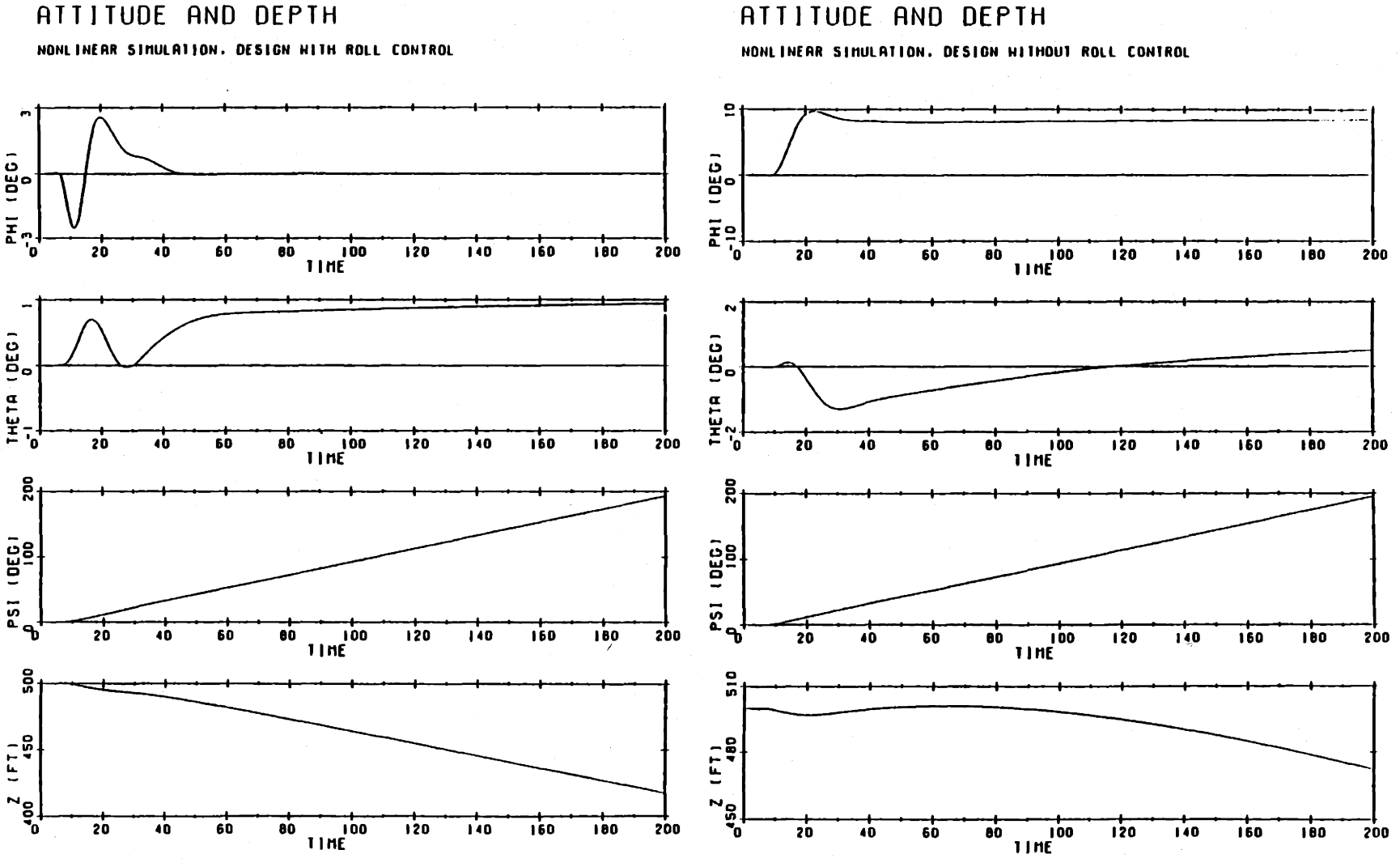

Figure 5.5(b) Comparison of the Non-linear Response of Models with and without Roll Control for a Combined Maneuver

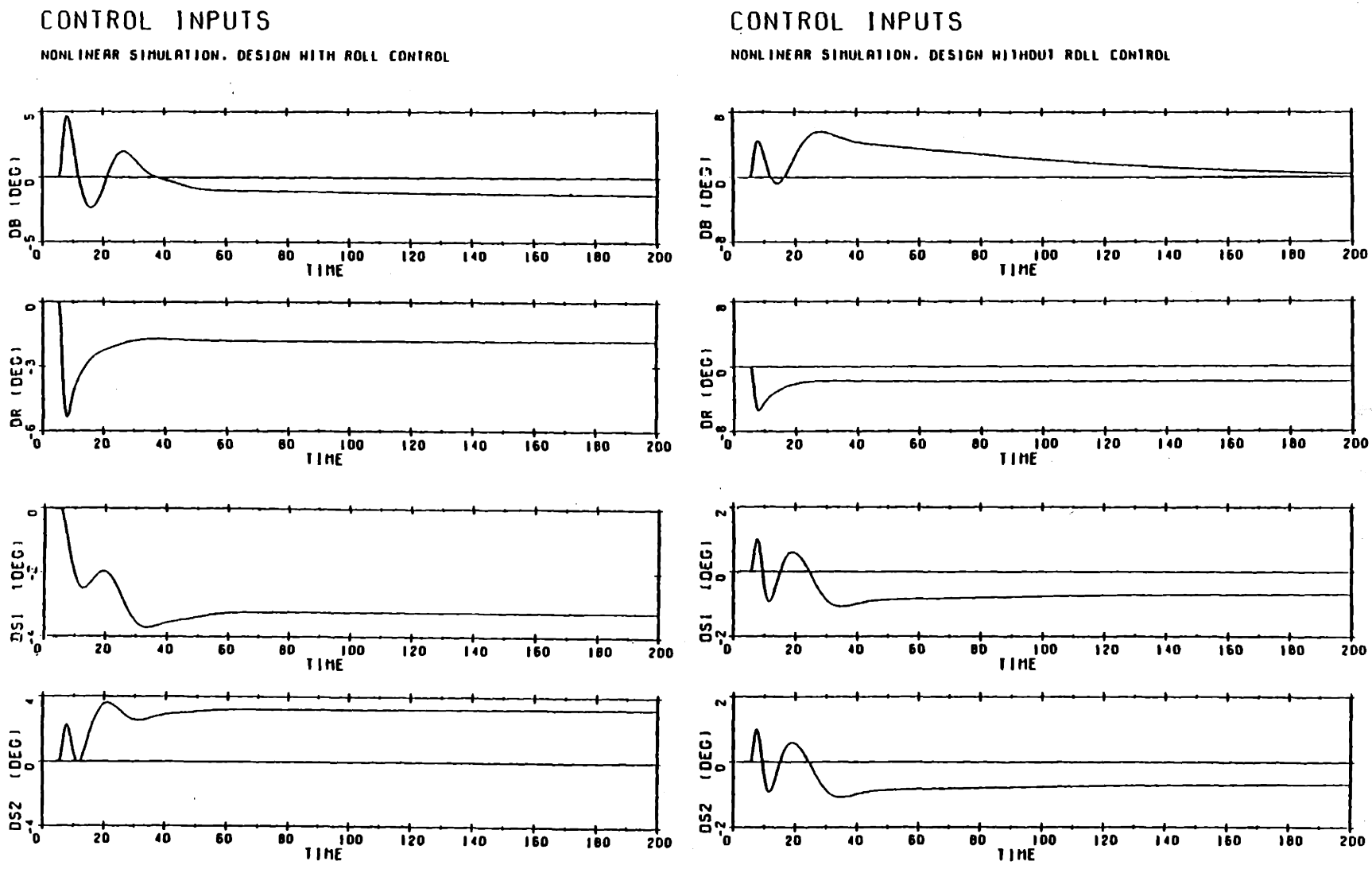

Figure 5.5(c) Comparison of the Non-linear Response of Models with and without Roll Control for a Combined Maneuver

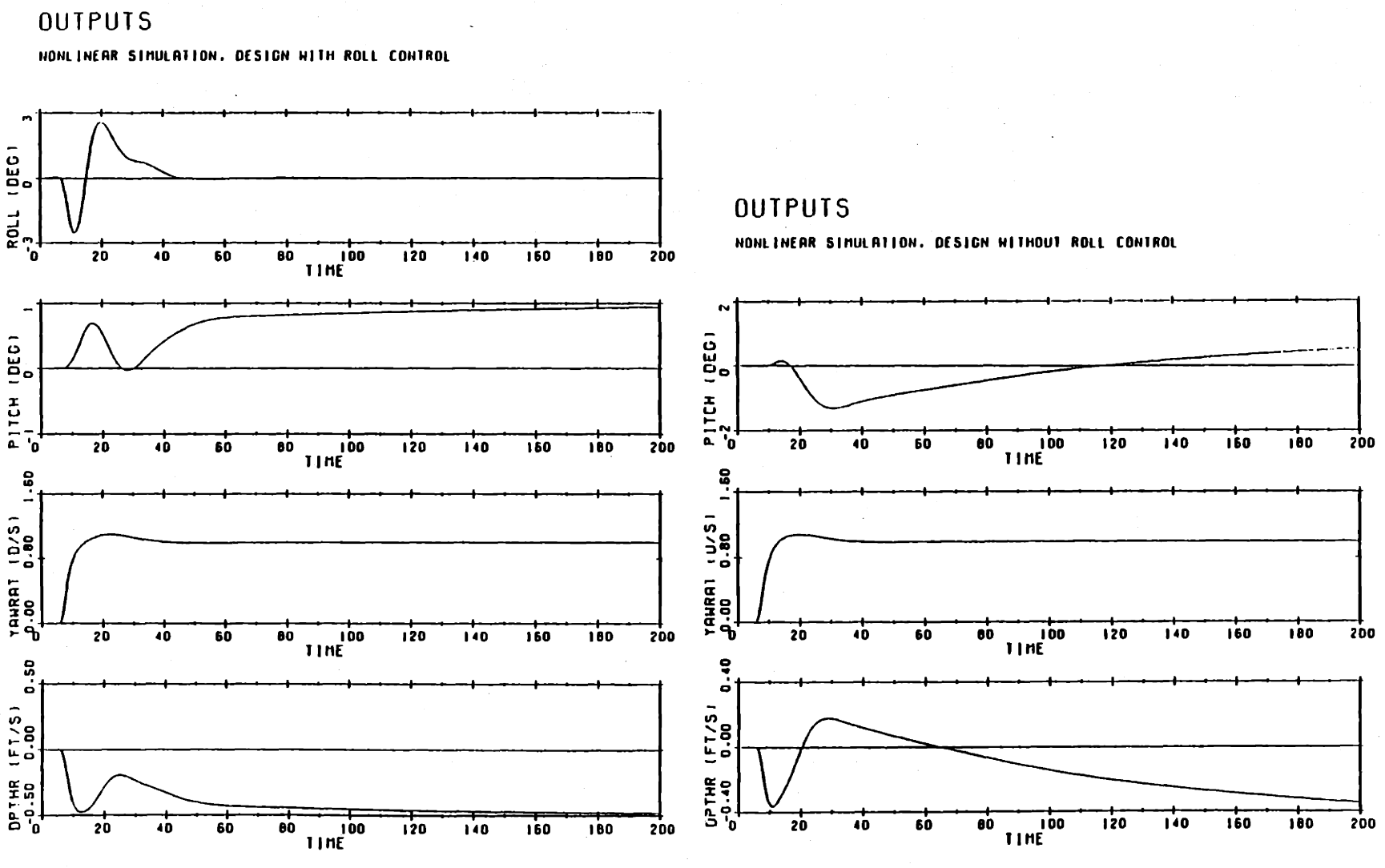

Figure 5.5(d) Comparison of the Non-linear Response of Models with and without Roll Control for a Combined Maneuver

5.5.4 Hard Turning Maneuver

This maneuver is for a commanded yaw rate of 3 deg/sec, and is provided to display the effects of control surface saturation. Referring to Figure 5.6, we observe a drop in ship's speed of almost 45%. Looking at the model with roll control, it is observed that the ship initially rolls outward approximately 8°, then snaps inward at t = 14 seconds. The maximum downward pitch angle reaches 4° at t = 160 seconds, and starts to reduce by the end of the run. The depth loss in this case is 184 ft. The stern planes again deflect differentially to counteract the roll moment, but now, we observe the port stern planes are deflected at -3.9° at t =200 seconds whereas the starboard stern planes are deflected at 7.8°. This indicates that the stern planes, although deflecting differentially for roll control, are also being deflected for control of pitch angle. The bow planes are deflected at 6.25° in an attempt to minimize depth rate. To maintain the ordered yaw rate, the rudder is deflected -27° at the end of the run.

Comparing the model without roll control, we observe that the ship snap rolls inboard 19°, and pitch angle approaches -12°. The stern planes deflect to limit the pitch angle, and the bow planes deflect to limit depth rate. The bow planes, however, saturate in this run at t = 22 seconds. Up to this point, the ship's depth was maintained fairly well. As soon as the bow planes saturate, the depth rate increases, causing the ship to lose depth. This causes

the stern planes to deflect in the opposite direction in an attempt to minimize pitch angle and depth rate. At t = 25 seconds, the pitch angle steadies, and starts to come off. At t = 108 seconds, the depth rate goes negative, and it is observed the bow planes come out of saturation. By t = 200 seconds, we observe that the roll angle has been reduced to 8°, maximum negative pitch angle is 7°, depth rate is significantly reduced, and none of the control surfaces are saturated. Depth at the end of the run is 820 feet, which equates to a depth loss of 320 feet, as compared to the roll control model's depth loss of 184 feet.

The purpose of this run was to demonstrate how different the submarine's trajectory is when the control surfaces saturate.

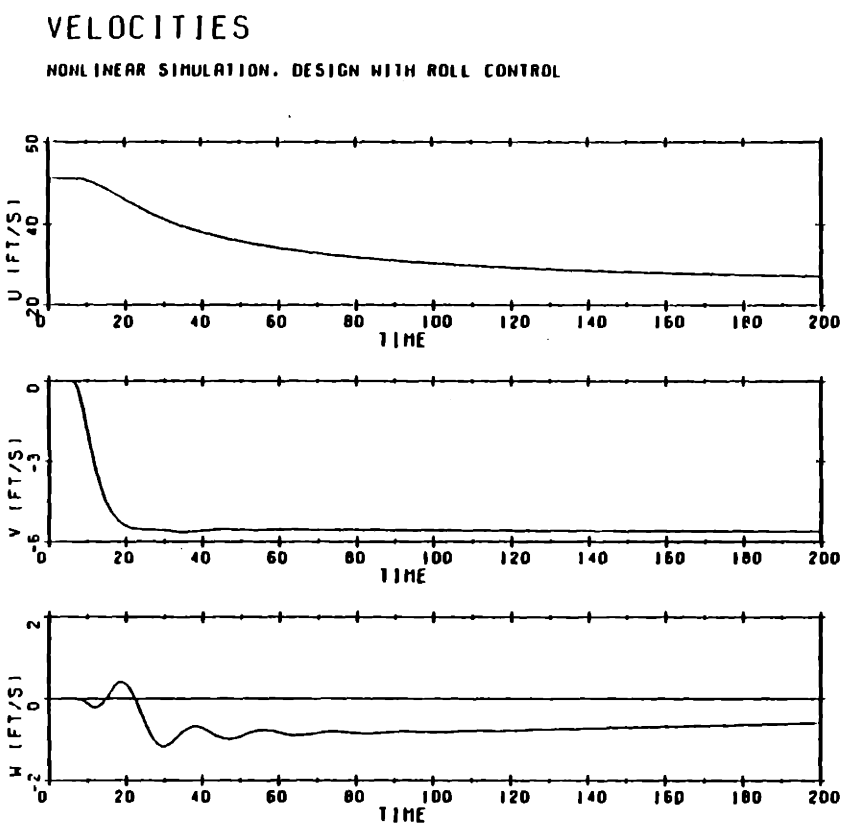

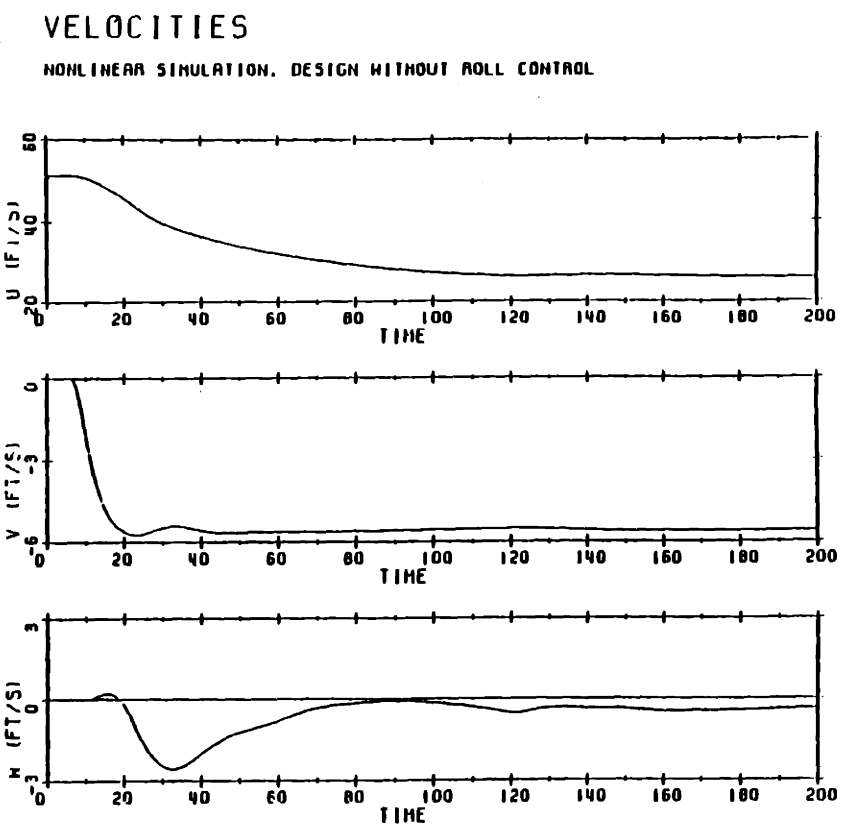

Figure 5.6(a) Comparison of the Non-linear Response of Models with and without Roll Control for a Hard Turn

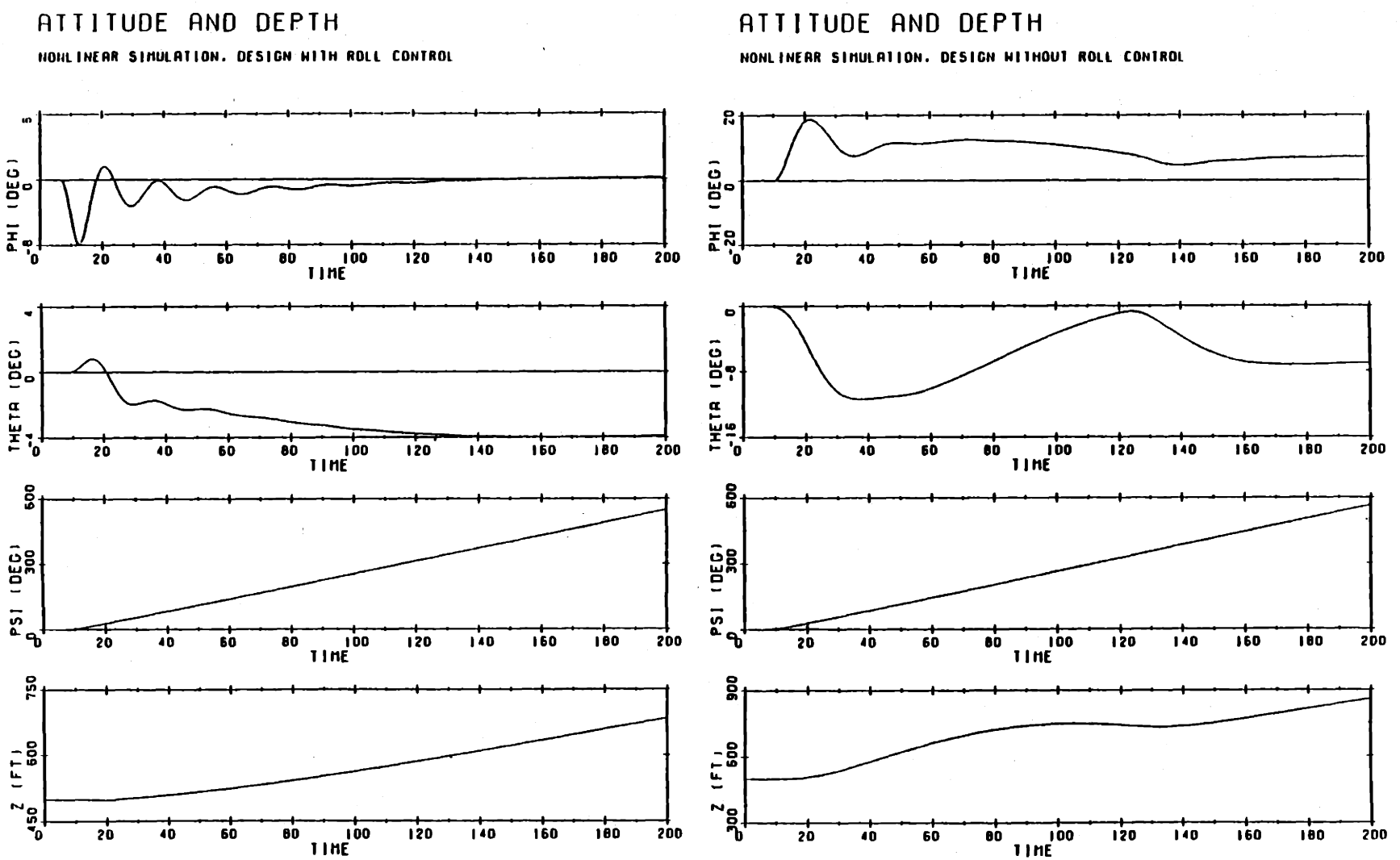

Figure 5.6(b) Comparison of the Non-linear Response of Models with and without Roll Control for a Hard Turn

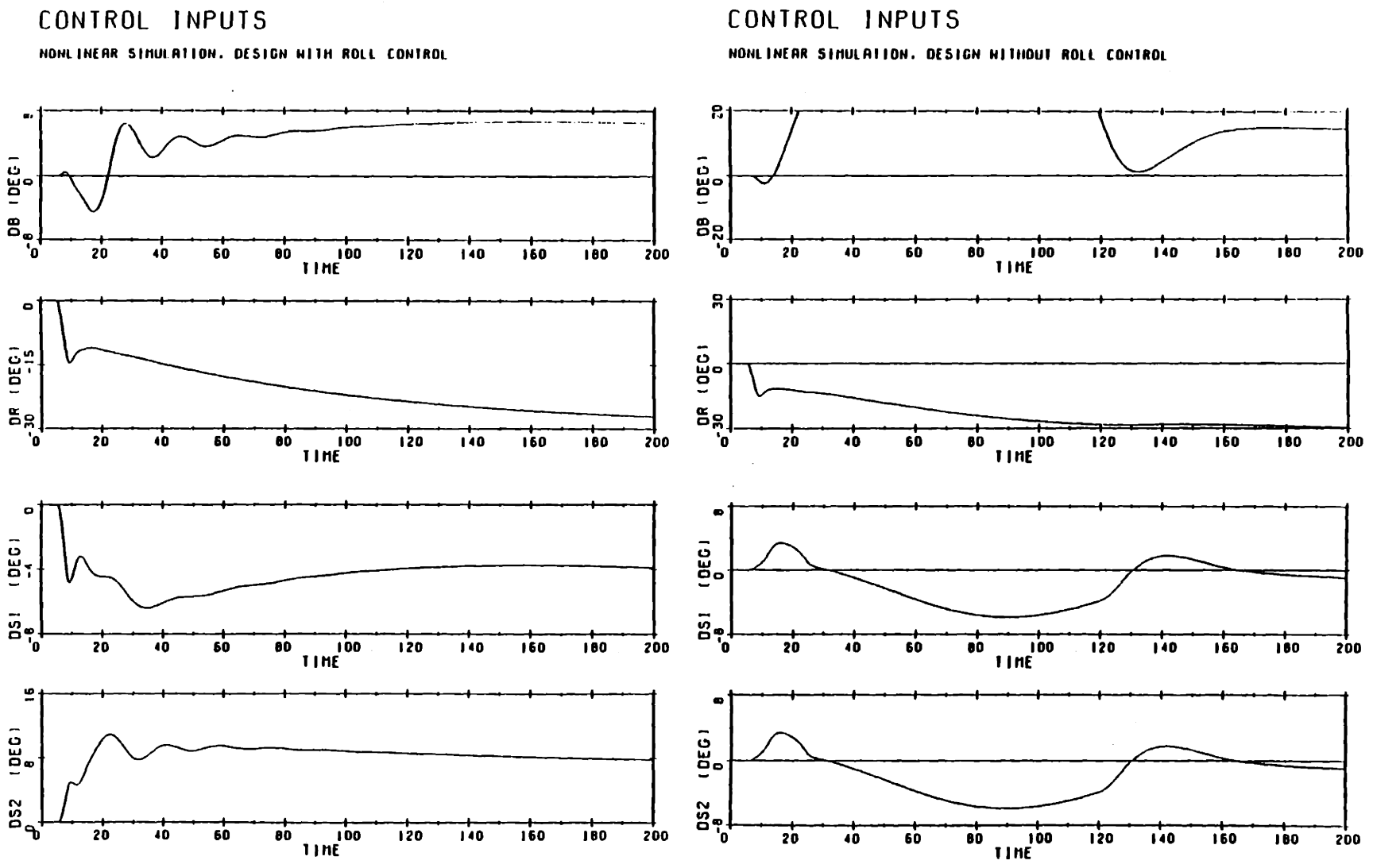

Figure 5.6(c) Comparison of the Non-linear Response of Models with and without Roll Control for a Hard Turn

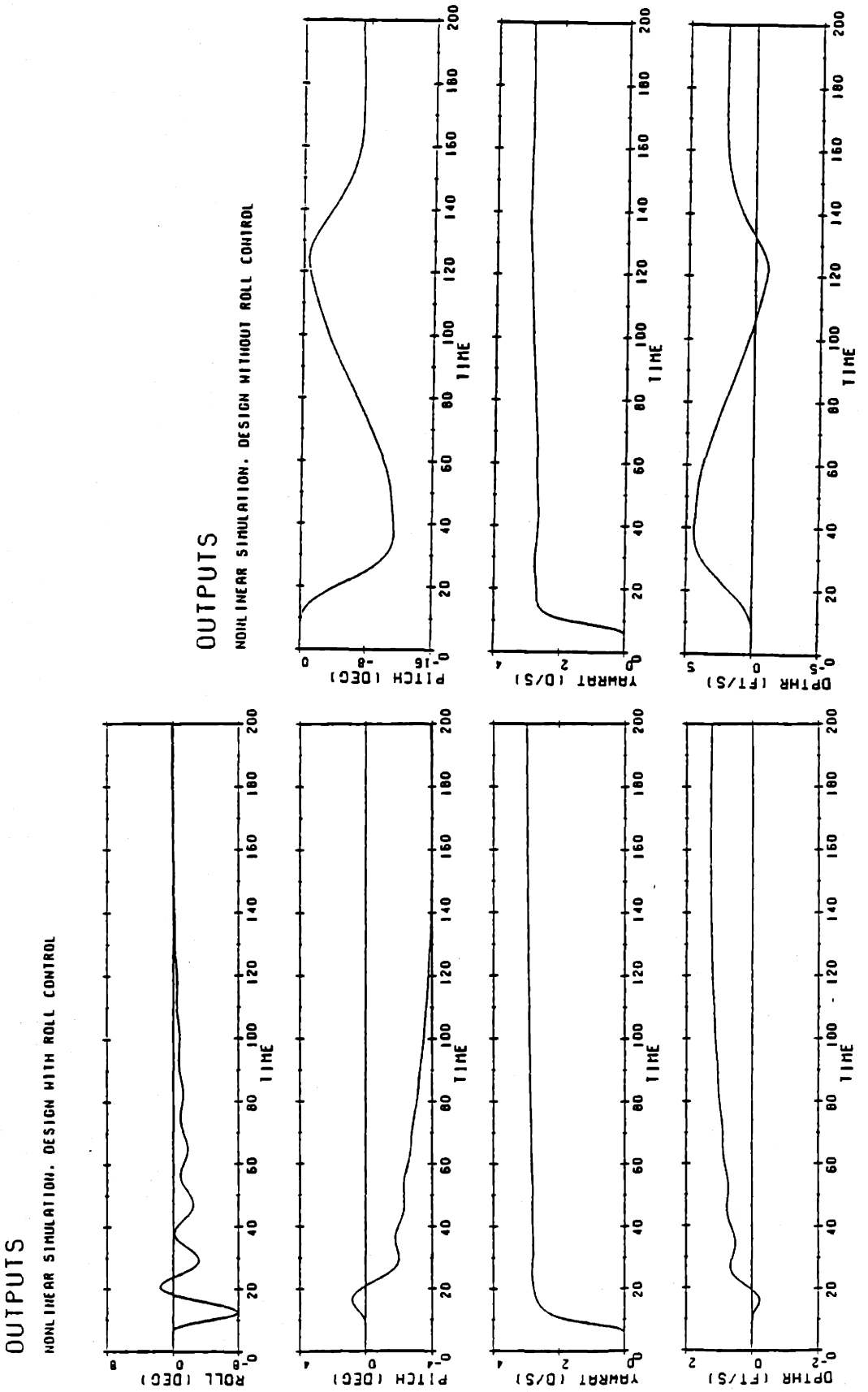

Figure 5.6(d) Comparison of the Non-linear Response of Models with and without Roll Control for a Hard Turn

5.6 Summary

This chapter has presented the implementation of the MBC designed in Chapter Four, and evaluation of the closed loop model. The linear and non-linear simulations were performed to demonstrate how the predictions for the Kalman filter loop of the linear can be used to validate the compensator's use on the non-linear model.

A second compensator, designed without roll control capability was presented, and then used to display the advantages of employing differential stern planes control on full scale submarines.

CHAPTER SIX

SUMMARY, CONCLUSIONS, AND DIRECTIONS FOR FUTURE RESEARCH

6.1 Summary

This thesis has presented a multivariable control design example for a submarine using active roll control capability.

The vehicle model was based on the NSRDC 2510 equations including vortex shedding and crossflow drag terms. These equations were linearized to generate linear models of the submarine which were then analyzed and verified.

The resulting models were reduced to eight order systems, scaled, and then subjected to modal analysis, which allowed the formulation of the prerequisites necessary to pursue the LQG/LTR design methodology.

Model Based Compensators with and without roll control capability were designed for the time and frequency domains. Specifications for the controller designs were presented, then, the methodology was applied to the design of submarine control systems. Compensators were designed and studied for various crossover frequencies, and a compensator was selected which provided desirable closed loop system response characteristics.

The selected compensator was evaluated by comparing the linear and non-linear dynamic simulations and determining how closely the performance specifications were met, and also, whether instabilities existed in the design. The MBC

was then compared with an equivalent compensator which did not have roll control capability.

6.2 Conclusions

Multivariable control system design using the LQG/LTR methodology has been successfully utilized to design a submarine control system with roll control capability.

It has been demonstrated that modal analysis and decomposition of the singular values of the plant can be used effectively in control system design. Modal analysis allows us to investigate the structure of the linear model and consider the ability to control and observe selected state variables. Singular value decomposition, once understood, can be used in a similar manner as Bode plots, and provides a convenient way to describe and ensure the performance requirements for the design.

The purpose of, and techniques used to scale the open loop plant were discussed in rigorous detail because the scaling strongly affects the singular value decomposition of the open loop plant, and the resulting compensator design.

The purpose of this thesis was to demonstrate the advantages of roll control on a full scale submarine. A limited number of simulations were performed, and the performance of the submarine with roll control is much improved over the design without roll control. The control system was designed for a submarine at 30 knots, and we observed the control system did fairly well, even for a

45% decrease in forward velocity of the ship. Additionally, the control system was designed using the inertial reference frame rather than the body reference frame of the ship. Use of the fixed inertial coordinate system provided better control of the submarine in maneuvering situations than for previous designs which used the body reference frame.

At this point it is important to stress the following observations:

- The performance characteristics of the submarine with active roll control are enhanced considerably over the design without roll control. The simulations demonstrated considerable depth improvement, and less control surface deflections and saturation in severe maneuvers, as demonstrated in Figure 5.6.

- This thesis demonstrates a technique to simulate performance characteristics of "paper" control systems for trade-off studies for specified performance criteria.

- One model cannot be used to globally control a submarine. Although the compensator performed well with large variations from the nominal operating point, reduced effectiveness of the control surfaces was observed.

- The fact that only small perturbations can be applied in validation of the design is not a limitation of the control design methodology. It is, however, a limitation of the linear model.

- Results of this thesis could be improved upon by including actuator dynamics, then selecting the compensator bandwidth and control gains to provide the best desirable ship response characteristics.

- To demonstrate the flexibility a controls engineer has when using multivariable control, the bow/fairwater planes were included in this thesis. Use of the bow/fairwater planes at 30 knots may not be considered practical due to flow noise and disturbances, and structural limitations.

6.3 Directions for Future Research

This thesis provides many of the building blocks necessary to refine the use of differential stern planes. Including actuator dynamics is an extension that needs to be completed. Additionally, limited designs were conducted which investigated the effects of compensator bandwidth and control gains. Much more work needs to be performed in this area.

Another area which needs additional research is in the use of propulsion as a dynamic control variable. If propeller rpm is allowed to vary, the control system design could effect maneuvers while minimizing speed loss in a turn (within propulsion constraints).

Finally, an area which is rather significant, and in which serious efforts have to be directed is in the area of casualty situations. This thesis has only looked at controlled maneuvers, in which the control system performs it's function completely. Failures of the control system during submerged operations must be fully investigated, understood, and designed into the compensator.

REFERENCES

1. Athans, M. "The Role and Use of the Stoichastic Linear-Quadratic-Gaussian Problem in Control System Design", IEEE Transactions on Automatic Control, Vol. AC-16, No. 6 (December, 1971): pp 529-552.

2. Athans, M. Multivariable Control Systems, Course Lecture Notes, MIT, Spring 1984.

3. Brogan, W. L. Modern Control Theory, New York, Quantum Publishers, Inc., 1974.

4. Doyle, J. C. and Stein, G. "Multivariable Feedback Design: Concepts for a Classical/Modern Synthesis", IEEE Transactions on Automatic Control, Vol. AC-26, No. 1 (February, 1981): pp 4-16.

5. Gertler, M. and Hagan, G. R. "Standard Equations of Motion for Submarine Simulation", Naval Ship Research and Development Report 2510, June 1967.

6. Kuo, B.C. Automatic Control Systems, Englewood Cliffs, N.J., Prentice Hall, Inc., 1982.

7. Kwakernaack, H. and Sivan, R. Linear Optimal Control Systems, New York, Wiley, 1972.

8. Ogata, K. Modern Control Engineering, Englewood Cliffs, N.J., Prentice Hall, Inc., 1972.

9. Triantafyllou, M. S., Bodson, M. and Athans, M. "Real Time Estimation of Ships Motion Using Kalman Filtering Techniques", IEEE Journal of Ocean Engineering, Vol. OE-8, No. 1 (January, 1983), pp 9-20.

10. Lively, K. A. "Multivariable Control System Design for a Submarine", Engineers Thesis, MIT, 1984.

11. Dreher, L. J. "Robust Rate Control System Designs for a Submersible", Engineers Thesis, MIT, 1984.

12. Milliken, L. G. "Multivariable Control of an Underwater Vehicle", Engineers Thesis, MIT, 1984.

13. Harris, K. A. "Automatic Control of a Submersible", Masters Thesis, MIT, 1984.

14. Bonnice, B. and Valavani, L. "Submarine Configuration and Control", CSDL Memo SUB 1-1083, 1983.

15. Bonnice, B. CONSTRPS Fortran and Executive Command Computer Programs, CSDL, May, 1984.

16. Abkowitz, M. Stability and Motion Control of Ocean Vehicles, MIT Press, Cambridge, MA., 1969.

17. Takahashi, Robins, and Auslander Control, Addison-Wesley, 1970, pp 65-86.

18. Athans, M. Multivariable Control System Design using the LQG/LTR Methodology, 6.232 Lecture Notes, MIT, Spring 1984.

19. Stein, G. "LQG-Based Multivariable Design: Frequency Domain Interpretation", AGARD, NATO, 1981.

20. Kappos, E. "Robust Multivarable Control for the F-100 Engine", Engineer's Thesis, MIT, 1983.

21. Boettcher, K. "Analysis of Multivarable Control Systems with Structural Uncertainty", Internal Report, MIT, 1983.

APPENDIX A

Detailed Definition of the Submarine Problem

Any submarine must meet certain minimum standards of controllability. Its course keeping and depth keeping stability must be adequate for transportation at the maximum speed and at a low but useful speed. While many surface ships and many submarines are directionally unstable to a small degree, requiring constant attention to steer an acceptable straight course, the consequences of a mistake or a temporary interruption of rudder or diving plane activity in a high speed submarine make it imprudent to accept even slight instability. For this reason, definite control-fixed stability is required.

Slow speed operation of a combatant submarine is often required. Because of the pendulum-like hydrostatic stability of the submarine, as the submarine moves very slowly through the water, the hydrodynamic effects of stern plane deflection are too small to change the submarine hull angle-of-attack by an amount large enough to develop rise or dive forces on the hull. The net vertical force on the submarine that results is due mostly to the force of the stern plane itself, which is always in the direction opposite to the conventional rise or dive command. This phenomenon is often referred to as "stern plane reversal". This particular effect can be controlled by proper design and building of the ship such that the vertical distance between the location of the center of buoyancy and the center of gravity of the ship are within prescribed max/min limits.

At or near zero ship speed, control of the ship's attitude and depth using forces generated by flow over the hull and control surfaces is not possible. Control of depth can be obtained by changing the weight of the submarine using the trim system.

In the absence of external force disturbances, such as are encountered near the surface under a seaway, hovering by application of small weight and/or buoyancy changes has become a common experience for submariners. Quiet seas, skill, experience, and an opportunity to improve the trim while slowing to hovering speeds are all necessary. Lacking any of these factors, and given a need to hover, one immediately recognizes a need for some form of properly engineered hovering system.

Each submarine must operate a portion of its service life on the surface, which generates a different set of steering parameters and requirements. Adequate surfaced steering with slight directional unstability is feasible, so that specific values of directional stability on the surface are not necessary or even useful. Some degree of steering

control while backing is also necessary when docking or for in-port maneuvering.

The attributes of combatant service that affect controllability and performance requirements range from those associated with stealth to those associated with maximum speed violent maneuvers. Violent maneuvers, involving full acceleration, possible course reversals, and severe depth changes could be necessary. The prescribed Submerged Operating Envelope (SOE) should be the same for peacetime and wartime operations. The maximum exploitation of speed, depth, and maneuvering capabilities will be a necessity to prepare for potential engagements or casualty environments that may be experienced over the lifetime of the submarine.

Underlying all combatant submarine attributes, and in many cases, dominating them, are the requirements to operate quietly. Mandatory noise requirements and even more stringent desirable goals are generally imposed on all systems; one of the most significant contributors to the overall noise characteristics are operations of the control surfaces, thus, the ship control system must now be optimized to minimize this noise source.

The fact that the submarine is a "dirigible" in space, within the bounds of the surface, the bottom, and collapse depth, mandates that its handling properties be described as a set of horizontal and vertical plane properties. The consequences of error in the vertical plane that can be imagined are dramatically different from those in the horizontal plane. Groundings and collisions due to horizontal plane error, no matter how distressing to the ship(s) involved, do not have the sense of finality that sinkings have. For this reason, the highest priority attention is given to vertical plane maneuvering properties and vertical plane consequences of horizontal plane maneuvers. The remaining mobility characteristics, course and speed, are ranked in priority in that order.

With depth factors as the first priority, the criteria for judging the quality of vertical plane maneuvers will be based upon reliability and precision of control at constant ordered depth, and upon the ease of making ordered depth changes.

In the horizontal plane, it is rare that a specific minimum value of turning diameter would be critical for a submarine. A much more useful turning quality to impose is the time to change heading by a given amount (for example 30°, 180°, etc.), with minimum depth keeping disruption and maximum speed remaining when the turn is completed. This is a property which can be perceived by the operators. Evasive maneuvers are very likely to involve large changes in

speed, course, and depth. The performance of the submarine during large changes should provide the most freedom to the operator. It must be possible, with confidence in the safety of the maneuver, to order simultaneous speed, course, and depth changes in any combination. This requirement leads to the addition of a parameter describing the required control authority in the vertical plane to the time to reach the heading change requirement within a specified time period. The depth change limitation associated with turns must be met using only a portion of the available depth control authority. The remaining depth control authority that is not used in a flat turn could be used to enforce a simultaneous depth change.

APPENDIX B

Summary of the SUBMODEL Program

The SUBMODEL program was written to perform any of the following tasks:

1) Integrate the nonlinear equations of motion of a submarine.

2) Search for a local equilibrium point in the nonlinear equations of motion. (A local equilibrium point is the point where the derivatives of the state variables chosen are zero.)

3) Calculate the linearized dynamics about a particular nominal point.

4) Integrate the linearized equations of motion.

This description of the SUBMODEL program consists of three sections. Section 2 describes briefly the equations of motion that are implemented in the program. Section 3 describes the program.

Section Two: Nonlinear and Linear Equations of Motion

This section describes the equations of motion which have been implemented in the SUBMODEL program.

The nonlinear equations are in the form

$$\underline{E}\dot{\underline{x}} = \underline{f}(\underline{x},\underline{u})$$

where

$\underline{x}$ = 10 x 1 state vector
$\underline{u}$ = n x 1 control vector (n=user specified)
$\underline{f}$ = 10 x 1 vector that is a nonlinear function of the states and the controls
$\underline{E}$ = 10 x 10 matrix

The first nine differential equations are the same as the 688 nonlinear equations documented in CSDL Memo SUB 2-1083 except for three propulsion and drag terms. These changes are documented in the memo on propulsion and drag models. The nine states are ordered as stated in the main body of this thesis (Chapter Two). The tenth differential equation and state is used to describe the propulsion dynamics.

There are two propulsion models - an rps propulsion model and an eta propulsion model. The rps propulsion model contains a first order differential equation in terms of rps

(revolutions per second) and is the more accurate model of the two models. The eta propulsion model contains a first order differential equation in terms of eta (η is defined to be u/U, where U is the actual speed of the submarine and u is the commanded forward velocity) and is a slightly simplified version of the rps model. The importance of the eta model lies in the fact that it was the propulsion model that was linearized and included in the linear equations of motion. These propulsion models are documented in another Draper memo.

The controls that may be specified are bow/fairwater planes, rudder, stern planes (which may be segmented), and WSTEAM (steam flow).

Section Three: Program Description

This section describes how the four main tasks listed in the introduction are accomplished.

Before linearized dynamics can be calculated, equations of motion integrated, and/or local equilibrium points searched for, the program must be read in and can print out upon request the mass properties, the hydrodynamic coefficients, and the propulsion and drag constants. These constants and coefficients describe the dynamics of a specified submarine, and with two exceptions, are assumed to be valid for any dynamic condition. The exceptions are the propulsion variables "thrded" and "wake". The rps propulsion model calculates these variables and, therefore, values that are read in are ignored. However, in reformulating the rps propulsion model into the eta propulsion model, these two propulsion variables were assumed to be constant. A method of determining appropriate values of these constants is to integrate the nonlinear equations with the rps propulsion model using the same initial conditions that will be used to integrate the equations with the eta model. Then, use the values of "thrded" and "wake" after the initial transients of the states have "died out". The program prints out the final values of "thrded" and "wake" at the end of integrating the nonlinear equations with the rps model.

The program then proceeds to calculate the $\underline{\underline{E}}$ and $\underline{\underline{E}}^{-1}$ matrices as the $\underline{\underline{E}}^{-1}$ matrix is needed for any of the four main tasks. An indication of the accuracy of the $\underline{\underline{E}}^{-1}$ matrix is obtained by multiplying the $\underline{\underline{E}}$ and $\underline{\underline{E}}^{-1}$ matrices. The program prints each one of these matrices (i.e., $\underline{\underline{E}}$, $\underline{\underline{E}}^{-1}$, and $\underline{\underline{E}}\underline{\underline{E}}^{-1}$).

If the option to integrate the nonlinear equations of motion was selected, the initial conditions necessary to integrate the equations are read in. There is an option that can be set in the input data file containing the

initial conditions on p, q, and r from initial conditions on psidot, phidot, and thetadot. Also, the input data file contains initial conditions for both the variables rps and eta. As mentioned in section 2, there are both an rps and an eta propulsion model. If the rps model was chosen, the initial condition on rps is used and eta is calculated. If the eta model was chosen, the initial condition on eta is used and the rps initial condition is ignored.

The program proceeds to integrate the nonlinear equations of motion using a fourth order Runge Kutta routine. The values of the controls can be set in two ways. They can be either initialized and kept constant at that value throughout the run or be read from a data file. Another possibility, if the rps model is being used, is to calculate the controls using full state feedback. For this condition, the gain matrix is read by the program. Therefore, it is necessary for the program to read in the nominal point which corresponds to the linearized model used to design the gain matrix. For the purposes of calculating the controls using full state feedback only, eta is calculated from rps and u. It is subsequently used as the tenth state.

When integrating the nonlinear equations of motion, the initial time, the final time, and the integration time step must be chosen. In addition, there are options to print the states and to store the values of the states and the controls for plotting. The program writes the plotting data using an unformatted write. A plotting program, such as XPLOT4B, must be run to actually plot the data. The frequency of printing and storing data for plotting can be individually specified in terms of time steps.

Also, the program has the option to search for a local equilibrium point. If this option is selected, the program needs an initial guess of the local equilibrium point to begin the search. This initial guess can be provided in either of two ways. One way is to integrate the nonlinear equations of motion using the eta propulsion model. The program will use the final condition from integrating the nonlinear equations as the guess for the search routines. The other way is to read in an initial guess in the same manner as reading in the initial conditions to integrate the nonlinear equations of motion.

When searching for a local equilibrium point, the program uses the set of nonlinear equations with the eta propulsion model. The reason for using the eta propulsion model is that the linearized propulsion model was derived from it. Presumably, the reason for searching for a local equilibrium point is to use that point as a point about which to linearize the nonlinear equations of motion. If the vehicle is in a turn, psidot will be nonzero and

therefore the search routines will be unable to find a local equilibrium point for this case. As psi has no effect on the other differential equations, deleting the differential equation in psi allows a local equilibrium point (except in psi) to be found when the vehicle is in a turn.

To search for a local equilibrium point, the program uses two IMSL search routines - ZSPOW and ZSCNT. These routines take a supplied initial guess of the point and iterate for a specified number of times before returning a point. The number of iterations per call to a routine must be specified by the user. The program iterates by perturbing the number of variables specified by the user (maximum of eight are allowed). The point returned may or may not be closer to a local equilibrium point than the initial guess. The closeness of a point to being a local equilibrium point is determined by the sum of the squares of the derivatives.

Finally, when searching for a local equilibrium point, there is one additional option that must be specified - the number of times to call each one of the search routines. The program calls the routines in the following manner. Using the initial guess supplied by either input data or by integrating the nonlinear equations with the eta propulsion model, the program calls the ZSPOW routine. After ZSPOW returns a point, the program will cause the ZSPOW routine again using the point returned as the initial guess. The program repeatedly calls the ZSPOW routine unless: (1) the point returned is not closer than the initial guess, or (2) the specified number of times to call the search routine is exceeded. Then the program follows the same procedure with the ZSCNT routine with the first guess being the closest to a local equilibrium point available.

If the option to calculate the linearized dynamics was selected, the program would read in the nominal point about which the nonlinear equations are linearized.

If the option to integrate the linearized dynamics was chosen, the program will read in the nominal point and calculate the linearized dynamics if the option to calculate the linearized dynamics was not already chosen before. The program will then read in the initial conditions on the states and on the controls, calculate the perturbatiosn from the nominal point, and integrate the linearized equations. As with integrating the nonlinear equations of motion, the user must specify the initial time, final time, and integration time step. Also, the options to store data for plotting, to print, as well as the frequency of carrying out each step are the same as in integrating the nonlinear case.

APPENDIX C

STATE SPACE MATRICES FOR THE LINEARIZED MODELS

The elements of the $\underline{A}$, $\underline{B}$, and $\underline{C}$ matrices are presented in the standard row and column format.

APPENDIX C1

ORIGINAL MATRICES PRIOR TO SCALING

$$\underline{x}^T = [\, u \;\; v \;\; w \;\; p \;\; q \;\; r \;\; \phi \;\; \theta \;\; \psi \;\; z \,]$$

A MATRIX

-3.8245E-02	-2.1911E-02	-2.7720E-03	-1.8964E-02	-2.9363E-01	3.1674E+00	0.0000E+00	2.9326E-04	0.0000E+00	0.0000E+00
1.1461E-03	-1.5919E-01	-1.9338E-03	-1.1464E+00	1.1276E-01	-1.5397E+01	1.3004E-01	-1.7564E-03	0.0000E+00	0.0000E+00
2.4225E-05	4.6499E-04	-1.0631E-01	-1.5984E+00	1.2070E+01	8.0194E-02	0.0000E+00	7.5597E-03	0.0000E+00	0.0000E+00
2.4614E-04	-1.1680E-02	-1.3226E-03	-4.3445E-01	-2.3879E-01	-7.1773E-03	-1.5995E-01	2.1603E-03	0.0000E+00	0.0000E+00
-5.3732E-06	-1.8585E-05	1.3207E-03	-1.1380E-02	-4.0755E-01	1.0074E-04	0.0000E+00	-2.4934E-03	0.0000E+00	0.0000E+00
-2.7564E-05	-2.0277E-03	2.4063E-05	-8.1034E-03	3.6042E-03	-3.8180E-01	2.5836E-04	-3.4895E-06	0.0000E+00	0.0000E+00
0.0000E+00	0.0000E+00	0.0000E+00	1.0000E+00	1.3427E-02	-1.2348E-01	-2.0244E-10	-1.2660E-02	0.0000E+00	0.0000E+00
0.0000E+00	0.0000E+00	0.0000E+00	0.0000E+00	9.9414E-01	1.0810E-01	1.2467E-02	0.0000E+00	0.0000E+00	0.0000E+00
0.0000E+00	0.0000E+00	0.0000E+00	0.0000E+00	-1.0893E-01	1.0018E+00	1.6423E-09	1.5605E-03	0.0000E+00	0.0000E+00
1.2326E-01	-1.0728E-01	9.8656E-01	0.0000E+00	0.0000E+00	0.0000E+00	1.5702E+00	-4.8493E+01	0.0000E+00	0.0000E+00

$$\underline{u}^T = [\, \delta b \;\; \delta r \;\; \delta s_1 \;\; \delta s_2 \,]$$

B MATRIX

-1.6315E-03	-5.8396E-02	2.8022E-03	2.8022E-03
0.0000E+00	2.3119E+00	-1.6950E-01	1.6950E-01
-1.4442E+00	-1.4815E-06	-9.8476E-01	-9.8476E-01
0.0000E+00	4.2586E-02	2.0848E-01	-2.0848E-01
1.3872E-02	4.8862E-07	-2.3825E-02	-2.3825E-02
0.0000E+00	-5.8593E-02	-3.3676E-04	3.3676E-04
0.0000E+00	0.0000E+00	0.0000E+00	0.0000E+00
0.0000E+00	0.0000E+00	0.0000E+00	0.0000E+00
0.0000E+00	0.0000E+00	0.0000E+00	0.0000E+00
0.0000E+00	0.0000E+00	0.0000E+00	0.0000E+00

APPENDIX C2

MATRICES TO PERFORM UNIT TRANSFORMATIONS

Matrix used to premultiply the A and B matrices:

1.0000E+00	0.0000E+00	0.0000E+00	0.0000E+00	0.0000E+00	0.0000E+00	0.0000E+00	0.0000E+00	0.0000E+00	0.0000E+00
0.0000E+00	1.0000E+00	0.0000E+00	0.0000E+00	0.0000E+00	0.0000E+00	0.0000E+00	0.0000E+00	0.0000E+00	0.0000E+00
0.0000E+00	0.0000E+00	1.0000E+00	0.0000E+00	0.0000E+00	0.0000E+00	0.0000E+00	0.0000E+00	0.0000E+00	0.0000E+00
0.0000E+00	0.0000E+00	0.0000E+00	5.7300E+01	0.0000E+00	0.0000E+00	0.0000E+00	0.0000E+00	0.0000E+00	0.0000E+00
0.0000E+00	0.0000E+00	0.0000E+00	0.0000E+00	5.7300E+01	0.0000E+00	0.0000E+00	0.0000E+00	0.0000E+00	0.0000E+00
0.0000E+00	0.0000E+00	0.0000E+00	0.0000E+00	0.0000E+00	5.7300E+01	0.0000E+00	0.0000E+00	0.0000E+00	0.0000E+00
0.0000E+00	0.0000E+00	0.0000E+00	0.0000E+00	0.0000E+00	0.0000E+00	5.7300E+01	0.0000E+00	0.0000E+00	0.0000E+00
0.0000E+00	0.0000E+00	0.0000E+00	0.0000E+00	0.0000E+00	0.0000E+00	0.0000E+00	5.7300E+01	0.0000E+00	0.0000E+00
0.0000E+00	0.0000E+00	0.0000E+00	0.0000E+00	0.0000E+00	0.0000E+00	0.0000E+00	0.0000E+00	5.7300E+01	0.0000E+00
0.0000E+00	0.0000E+00	0.0000E+00	0.0000E+00	0.0000E+00	0.0000E+00	0.0000E+00	0.0000E+00	0.0000E+00	1.0000E+00

Matrix used to postmultiply the A matrix:

1.0000E+00	0.0000E+00	0.0000E+00	0.0000E+00	0.0000E+00	0.0000E+00	0.0000E+00	0.0000E+00	0.0000E+00	0.0000E+00
0.0000E+00	1.0000E+00	0.0000E+00	0.0000E+00	0.0000E+00	0.0000E+00	0.0000E+00	0.0000E+00	0.0000E+00	0.0000E+00
0.0000E+00	0.0000E+00	1.0000E+00	0.0000E+00	0.0000E+00	0.0000E+00	0.0000E+00	0.0000E+00	0.0000E+00	0.0000E+00
0.0000E+00	0.0000E+00	0.0000E+00	1.7452E-02	0.0000E+00	0.0000E+00	0.0000E+00	0.0000E+00	0.0000E+00	0.0000E+00
0.0000E+00	0.0000E+00	0.0000E+00	0.0000E+00	1.7452E-02	0.0000E+00	0.0000E+00	0.0000E+00	0.0000E+00	0.0000E+00
0.0000E+00	0.0000E+00	0.0000E+00	0.0000E+00	0.0000E+00	1.7452E-02	0.0000E+00	0.0000E+00	0.0000E+00	0.0000E+00
0.0000E+00	0.0000E+00	0.0000E+00	0.0000E+00	0.0000E+00	0.0000E+00	1.7452E-02	0.0000E+00	0.0000E+00	0.0000E+00
0.0000E+00	0.0000E+00	0.0000E+00	0.0000E+00	0.0000E+00	0.0000E+00	0.0000E+00	1.7452E-02	0.0000E+00	0.0000E+00
0.0000E+00	0.0000E+00	0.0000E+00	0.0000E+00	0.0000E+00	0.0000E+00	0.0000E+00	0.0000E+00	1.7452E-02	0.0000E+00
0.0000E+00	0.0000E+00	0.0000E+00	0.0000E+00	0.0000E+00	0.0000E+00	0.0000E+00	0.0000E+00	0.0000E+00	1.0000E+00

APPENDIX C2

Matrix used to postmultiply the B matrix:

1.7452E-02	0.0000E+00	0.0000E+00	0.0000E+00
0.0000E+00	1.7452E-02	0.0000E+00	0.0000E+00
0.0000E+00	0.0000E+00	1.7452E-02	0.0000E+00
0.0000E+00	0.0000E+00	0.0000E+00	1.7452E-02

Matrix used to premultiply the C matrix:

5.7300E+01	0.0000E+00	0.0000E+00	0.0000E+00
0.0000E+00	5.7300E+01	0.0000E+00	0.0000E+00
0.0000E+00	0.0000E+00	5.7300E+01	0.0000E+00
0.0000E+00	0.0000E+00	0.0000E+00	1.0000E+00

Matrix used to postmultiply the C matrix:

1.0000E+00	0.0000E+00	0.0000E+00	0.0000E+00	0.0000E+00	0.0000E+00	0.0000E+00	0.0000E+00	0.0000E+00	0.0000E+00
0.0000E+00	1.0000E+00	0.0000E+00	0.0000E+00	0.0000E+00	0.0000E+00	0.0000E+00	0.0000E+00	0.0000E+00	0.0000E+00
0.0000E+00	0.0000E+00	1.0000E+00	0.0000E+00	0.0000E+00	0.0000E+00	0.0000E+00	0.0000E+00	0.0000E+00	0.0000E+00
0.0000E+00	0.0000E+00	0.0000E+00	1.7452E-02	0.0000E+00	0.0000E+00	0.0000E+00	0.0000E+00	0.0000E+00	0.0000E+00
0.0000E+00	0.0000E+00	0.0000E+00	0.0000E+00	1.7452E-02	0.0000E+00	0.0000E+00	0.0000E+00	0.0000E+00	0.0000E+00
0.0000E+00	0.0000E+00	0.0000E+00	0.0000E+00	0.0000E+00	1.7452E-02	0.0000E+00	0.0000E+00	0.0000E+00	0.0000E+00
0.0000E+00	0.0000E+00	0.0000E+00	0.0000E+00	0.0000E+00	0.0000E+00	1.7452E-02	0.0000E+00	0.0000E+00	0.0000E+00
0.0000E+00	0.0000E+00	0.0000E+00	0.0000E+00	0.0000E+00	0.0000E+00	0.0000E+00	1.7452E-02	0.0000E+00	0.0000E+00
0.0000E+00	0.0000E+00	0.0000E+00	0.0000E+00	0.0000E+00	0.0000E+00	0.0000E+00	0.0000E+00	1.7452E-02	0.0000E+00
0.0000E+00	0.0000E+00	0.0000E+00	0.0000E+00	0.0000E+00	0.0000E+00	0.0000E+00	0.0000E+00	0.0000E+00	1.0000E+00

APPENDIX C3

MATRICES USED TO PERFORM TRANSFORMATIONS FOR CONTROL SURFACE DEFLECTION AND RELATIVE WEIGHTING OF THE OUTPUTS

$\hat{S}_u$

1.0000E+00	0.0000E+00	0.0000E+00	0.0000E+00
0.0000E+00	6.6700E-01	0.0000E+00	0.0000E+00
0.0000E+00	0.0000E+00	8.0000E-01	0.0000E+00
0.0000E+00	0.0000E+00	0.0000E+00	8.0000E-01

$\hat{S}_u^{-1}$

1.0000E+00	0.0000E+00	0.0000E+00	0.0000E+00
0.0000E+00	1.4993E+00	0.0000E+00	0.0000E+00
0.0000E+00	0.0000E+00	1.2500E+00	0.0000E+00
0.0000E+00	0.0000E+00	0.0000E+00	1.2500E+00

$\hat{S}_y$

1.0000E-01	0.0000E+00	0.0000E+00	0.0000E+00
0.0000E+00	1.0000E-01	0.0000E+00	0.0000E+00
0.0000E+00	0.0000E+00	1.0000E+00	0.0000E+00
0.0000E+00	0.0000E+00	0.0000E+00	1.0000E+00

APPENDIX C4

REDUCED AND SCALED PLANT MATRICES WITH APPROPRIATE C MATRIX MODEL WITH ROLL CONTROL

$$\underline{x}^T = [\, u \;\; v \;\; w \;\; p \;\; q \;\; r \;\; \phi \;\; \theta \,]$$

A MATRIX

-3.8269E-02	-2.1964E-02	-2.7533E-03	-3.3173E-04	2.0734E-03	5.5394E-02	0.0000E+00	5.1285E-06
1.1417E-03	-1.5939E-01	-3.3786E-05	-2.3578E-02	2.8353E-03	-2.6860E-01	2.2745E-03	-2.5914E-05
-4.7476E-04	1.3910E-03	-9.6526E-02	-2.7949E-02	2.1163E-01	7.6140E-04	0.0000E+00	1.3221E-04
1.3945E-02	-6.6430E-01	-8.0931E-02	-4.3452E-01	-2.5262E-01	-2.1920E-02	-1.6030E-01	1.8264E-03
7.1418E-05	-2.5929E-04	7.8117E-02	-1.1406E-02	-4.0815E-01	-7.7327E-04	0.0000E+00	-2.4985E-03
-1.5782E-03	-1.1622E-01	3.4035E-04	-8.0011E-03	2.2809E-03	-3.8201E-01	2.5893E-04	-2.9501E-06
0.0000E+00	0.0000E+00	0.0000E+00	1.0000E+00	1.1328E-02	-1.0538E-01	-4.9352E-10	-1.2635E-02
0.0000E+00	0.0000E+00	0.0000E+00	0.0000E+00	9.9427E-01	1.0689E-01	1.2494E-02	0.0000E+00

$$\underline{u}^T = [\, \delta b \;\; \delta r \;\; \delta s_1 \;\; \delta s_2 \,]$$

B MATRIX

-1.2666E-03	-1.5279E-03	9.8625E-05	9.8625E-05
0.0000E+00	6.0491E-02	-3.6976E-03	3.6976E-03
-2.5204E-02	-3.8763E-08	-2.1483E-02	-2.1483E-02
0.0000E+00	6.3847E-02	2.6060E-01	-2.6060E-01
1.3873E-02	7.3256E-07	-2.9781E-02	-2.9781E-02
0.0000E+00	-8.7846E-02	-4.2094E-04	4.2094E-04
0.0000E+00	0.0000E+00	0.0000E+00	0.0000E+00
0.0000E+00	0.0000E+00	0.0000E+00	0.0000E+00

APPENDIX C4

$$\underline{y}^T = [\ \phi\ \theta\ \dot{\psi}\ \dot{z}\ ]$$

C MATRIX

0.0000E+00	0.0000E+00	0.0000E+00	0.0000E+00	0.0000E+00	0.0000E+00	1.0000E-01	0.0000E+00
0.0000E+00	0.0000E+00	0.0000E+00	0.0000E+00	0.0000E+00	0.0000E+00	0.0000E+00	1.0000E-01
0.0000E+00	0.0000E+00	0.0000E+00	0.0000E+00	-1.0749E-01	9.9984E-01	4.6827E-09	1.3316E-03
1.0539E-01	-1.0629E-01	9.8873E-01	0.0000E+00	0.0000E+00	0.0000E+00	2.7119E-02	-8.4843E-01

APPENDIX C4

REDUCED AND SCALED PLANT MATRICES WITH APPROPRIATE C MATRIX
MODEL WITHOUT ROLL CONTROL

$$\underline{x}^T = [\ u\ v\ w\ p\ q\ r\ \phi\ \theta\ ]$$

A MATRIX

-3.8269E-02	-2.1964E-02	-2.7533E-03	-3.3173E-04	2.0734E-03	5.5394E-02	0.0000E+00	5.1285E-06
1.1417E-03	-1.5939E-01	-3.3786E-05	-2.3578E-02	2.8353E-03	-2.6860E-01	2.2745E-03	-2.5914E-05
-4.7476E-04	1.3910E-03	-9.6526E-02	-2.7949E-02	2.1163E-01	7.6140E-04	0.0000E+00	1.3221E-04
1.3945E-02	-6.6430E-01	-8.0931E-02	-4.3452E-01	-2.5262E-01	-2.1920E-02	-1.6030E-01	1.8264E-03
7.1418E-05	-2.5929E-04	7.8117E-02	-1.1406E-02	-4.0815E-01	-7.7327E-04	0.0000E+00	-2.4985E-03
-1.5782E-03	-1.1622E-01	3.4035E-04	-8.0011E-03	2.2809E-03	-3.8201E-01	2.5893E-04	-2.9501E-06
0.0000E+00	0.0000E+00	0.0000E+00	1.0000E+00	1.1328E-02	-1.0538E-01	-4.9352E-10	-1.2635E-02
0.0000E+00	0.0000E+00	0.0000E+00	0.0000E+00	9.9427E-01	1.0689E-01	1.2494E-02	0.0000E+00

$$\underline{u}^T = [\ \delta b\ \delta r\ \delta s\ ]$$

B MATRIX

-1.2666E-03	-1.5279E-03	1.9725E-04
0.0000E+00	6.0491E-02	0.0000E+00
-2.5204E-02	-3.8763E-08	-4.2965E-02
0.0000E+00	6.3847E-02	0.0000E+00
1.3873E-02	7.3256E-07	-5.9562E-02
0.0000E+00	-8.7846E-02	0.0000E+00
0.0000E+00	0.0000E+00	0.0000E+00
0.0000E+00	0.0000E+00	0.0000E+00

APPENDIX C4

$$\underline{y}^T = [\ \theta\ \dot{\psi}\ \dot{z}\ ]$$

C MATRIX

0.0000E+00	0.0000E+00	0.0000E+00	0.0000E+00	0.0000E+00	0.0000E+00	0.0000E+00	1.0000E-01
0.0000E+00	0.0000E+00	0.0000E+00	0.0000E+00	-1.0749E-01	9.9984E-01	4.6827E-09	1.3316E-03
1.0539E-01	-1.0629E-01	9.8873E-01	0.0000E+00	0.0000E+00	0.0000E+00	2.7119E-02	-8.4843E-01

APPENDIX D

MODAL ANALYSIS RESULTS

The matrices are presented in the standard row and column format. Additionally, the data presented consists of complex numbers. As such, the numbers are always displayed with the inaginary part directly below the real part. The eigenvectors (modal matrices) are presented as complex column vectors.

APPENDIX D1

MODAL ANALYSIS FOR DESIGN WITH ROLL CONTROL

PLANT EIGENVALUES

-1.4176E-02	-4.0661E-02	-4.2886E-02	-7.1364E-02	-1.9689E-01	-1.9689E-01	-4.5114E-01	-5.0486E-01
0.0000E+00	0.0000E+00	0.0000E+00	0.0000E+00	3.1300E-01	-3.1300E-01	0.0000E+00	0.0000E+00

TRANSMISSION ZEROS

5.8302E+07	1.2014E+07	7.8269E+06	-3.8414E-02	-2.5097E-01	-1.3680E+01	-1.3579E+01	-2.6894E+08
0.0000E+00	0.0000E+00	0.0000E+00	0.0000E+00	0.0000E+00	1.1609E+04	-1.1609E+04	0.0000E+00

EIGENVECTORS (MODAL MATRIX)

-6.8361E-03	-2.5658E-01	1.0505E-01	2.5104E-01	-1.3119E-03	-1.3119E-03	-1.0292E-03	1.7639E-02
0.0000E+00	0.0000E+00	0.0000E+00	0.0000E+00	-1.6355E-03	1.6355E-03	0.0000E+00	0.0000E+00
2.6727E-03	-2.0890E-02	2.4216E-03	1.8514E-01	-1.3216E-02	-1.3216E-02	2.9403E-02	-2.1901E-01
0.0000E+00	0.0000E+00	0.0000E+00	0.0000E+00	-1.8009E-02	1.8009E-02	0.0000E+00	0.0000E+00
4.0471E-02	1.5080E-01	1.7237E-01	8.5127E-02	-2.9186E-02	-2.9186E-02	2.1418E-01	-4.1687E-03
0.0000E+00	0.0000E+00	0.0000E+00	0.0000E+00	-6.5275E-03	6.5275E-03	0.0000E+00	0.0000E+00
-1.2341E-02	-8.9644E-03	-6.2565E-03	5.9660E-02	-2.3086E-01	-2.3086E-01	-1.4102E-01	-4.4041E-01
0.0000E+00	0.0000E+00	0.0000E+00	0.0000E+00	2.5728E-01	-2.5728E-01	0.0000E+00	0.0000E+00
1.4711E-02	3.8749E-02	4.3690E-02	1.7590E-02	-6.9174E-03	-6.9174E-03	-3.7838E-01	-4.7868E-02
0.0000E+00	0.0000E+00	0.0000E+00	0.0000E+00	-5.9444E-03	5.9444E-03	0.0000E+00	0.0000E+00
-4.3411E-04	8.8786E-03	-8.1227E-04	-7.2642E-02	5.1850E-03	5.1850E-03	4.3218E-02	-2.3648E-01
0.0000E+00	0.0000E+00	0.0000E+00	0.0000E+00	-8.4312E-03	8.4312E-03	0.0000E+00	0.0000E+00
-3.4241E-02	-6.2985E-02	-1.5239E-01	-9.4101E-01	9.2397E-01	9.2397E-01	3.5497E-01	8.2716E-01
0.0000E+00	0.0000E+00	0.0000E+00	0.0000E+00	1.5763E-01	-1.5763E-01	0.0000E+00	0.0000E+00
-9.9838E-01	-9.5150E-01	-9.6648E-01	2.8480E-02	-1.8602E-02	-1.8602E-02	8.1384E-01	1.2387E-01
0.0000E+00	0.0000E+00	0.0000E+00	0.0000E+00	-4.9793E-03	4.9793E-03	0.0000E+00	0.0000E+00

APPENDIX D1

CONTROLLABILITY MATRIX

5.6156E-01	1.7840E-01	4.1655E-01	4.8436E-01
-1.9911E-10	1.4232E-09	-3.7882E-10	4.7169E-10
-2.8596E-01	3.5042E-01	-1.2380E-01	-1.5388E-01
-6.2679E-10	2.7076E-09	7.3586E-10	-5.1437E-10
-6.4135E-01	-5.2348E-01	-2.5188E-01	-2.6555E-01
8.6262E-10	-4.1367E-09	-4.7910E-10	1.4451E-10
-5.1517E-02	5.7248E-01	1.6873E-04	-4.3806E-02
-1.0340E-09	4.5318E-09	7.6296E-10	-3.8432E-10
4.2000E-02	1.5533E-01	-1.1720E-01	1.3250E-02
1.1239E-01	-2.9618E-01	-5.9723E-01	5.7354E-01
4.2000E-02	1.5533E-01	-1.1720E-01	1.3250E-02
-1.1239E-01	2.9618E-01	5.9723E-01	-5.7354E-01
-3.9615E-01	-2.3595E-02	7.4600E-02	8.4577E-02
3.8132E-12	-1.3261E-10	-5.0678E-10	5.0520E-10
-5.6283E-02	1.3913E-01	-3.6203E-02	6.2273E-02
2.5680E-10	3.5415E-10	2.0900E-09	-2.1848E-09

OBSERVABILITY MATRIX

-3.4241E-03	-6.2985E-03	-1.5239E-02	-9.4101E-02	9.2397E-02	9.2397E-02	3.5497E-02	8.2716E-02
0.0000E+00	0.0000E+00	0.0000E+00	0.0000E+00	1.5763E-02	-1.5763E-02	0.0000E+00	0.0000E+00
-9.9838E-02	-9.5150E-02	-9.6648E-02	2.8480E-03	-1.8602E-03	-1.8602E-03	8.1384E-02	1.2387E-02
0.0000E+00	0.0000E+00	0.0000E+00	0.0000E+00	-4.9793E-04	4.9793E-04	0.0000E+00	0.0000E+00
-3.3447E-03	3.4451E-03	-6.7951E-03	-7.4483E-02	5.9029E-03	5.9029E-03	8.4965E-02	-2.3113E-01
0.0000E+00	0.0000E+00	0.0000E+00	0.0000E+00	-7.7975E-03	7.7975E-03	0.0000E+00	0.0000E+00
8.8514E-01	9.2986E-01	9.9710E-01	4.1263E-02	1.3249E-02	1.3249E-02	-4.7233E-01	-6.1643E-02
0.0000E+00	0.0000E+00	0.0000E+00	0.0000E+00	3.7872E-03	-3.7872E-03	0.0000E+00	0.0000E+00

APPENDIX D2

MODAL ANALYSIS FOR DESIGN WITHOUT ROLL CONTROL

PLANT EIGENVALUES

-1.4176E-02	-4.0661E-02	-4.2886E-02	-7.1364E-02	-1.9689E-01	-1.9689E-01	-4.5114E-01	-5.0486E-01
0.0000E+00	0.0000E+00	0.0000E+00	0.0000E+00	3.1300E-01	-3.1300E-01	0.0000E+00	0.0000E+00

TRANSMISSION ZEROS

3.0779E+07	5.5553E+03	-3.8432E-02	-1.8029E-01	-1.8029E-01	-3.1812E-01	-5.5561E+03	-1.5282E+08
0.0000E+00	0.0000E+00	0.0000E+00	3.0164E-01	-3.0164E-01	0.0000E+00	0.0000E+00	0.0000E+00

EIGENVECTORS (MODAL MATRIX)

-6.8361E-03	-2.5658E-01	1.0505E-01	2.5104E-01	-1.3119E-03	-1.3119E-03	-1.0292E-03	1.7639E-02
0.0000E+00	0.0000E+00	0.0000E+00	0.0000E+00	-1.6355E-03	1.6355E-03	0.0000E+00	0.0000E+00
2.6727E-03	-2.0890E-02	2.4216E-03	1.8514E-01	-1.3216E-02	-1.3216E-02	2.9403E-02	-2.1901E-01
0.0000E+00	0.0000E+00	0.0000E+00	0.0000E+00	-1.8009E-02	1.8009E-02	0.0000E+00	0.0000E+00
4.0471E-02	1.5080E-01	1.7237E-01	8.5127E-02	-2.9186E-02	-2.9186E-02	2.1418E-01	-4.1687E-03
0.0000E+00	0.0000E+00	0.0000E+00	0.0000E+00	-6.5275E-03	6.5275E-03	0.0000E+00	0.0000E+00
-1.2341E-02	-8.9644E-03	-6.2565E-03	5.9660E-02	-2.3086E-01	-2.3086E-01	-1.4102E-01	-4.4041E-01
0.0000E+00	0.0000E+00	0.0000E+00	0.0000E+00	2.5728E-01	-2.5728E-01	0.0000E+00	0.0000E+00
1.4711E-02	3.8749E-02	4.3690E-02	1.7590E-02	-6.9174E-03	-6.9174E-03	-3.7838E-01	-4.7868E-02
0.0000E+00	0.0000E+00	0.0000E+00	0.0000E+00	-5.9444E-03	5.9444E-03	0.0000E+00	0.0000E+00
-4.3411E-04	8.8786E-03	-8.1227E-04	-7.2642E-02	5.1850E-03	5.1850E-03	4.3218E-02	-2.3648E-01
0.0000E+00	0.0000E+00	0.0000E+00	0.0000E+00	-8.4312E-03	8.4312E-03	0.0000E+00	0.0000E+00
-3.4241E-02	-6.2985E-02	-1.5239E-01	-9.4101E-01	9.2397E-01	9.2397E-01	3.5497E-01	8.2716E-01
0.0000E+00	0.0000E+00	0.0000E+00	0.0000E+00	1.5763E-01	-1.5763E-01	0.0000E+00	0.0000E+00
-9.9838E-01	-9.5150E-01	-9.6648E-01	2.8480E-02	-1.8602E-02	-1.8602E-02	8.1384E-01	1.2387E-01
0.0000E+00	0.0000E+00	0.0000E+00	0.0000E+00	-4.9793E-03	4.9793E-03	0.0000E+00	0.0000E+00

APPENDIX D2

CONTROLLABILITY MATRIX

5.6156E-01	1.7840E-01	8.2094E-01
-1.9911E-10	1.4232E-09	1.0434E-10
-2.8596E-01	3.5042E-01	-2.5325E-01
-6.2679E-10	2.7076E-09	1.7222E-10
-6.4135E-01	-5.2348E-01	-4.7091E-01
8.6262E-10	-4.1367E-09	-2.8973E-10
-5.1517E-02	5.7248E-01	-4.0715E-02
-1.0340E-09	4.5318E-09	3.1755E-10
4.2000E-02	1.5533E-01	-9.1490E-02
1.1239E-01	-2.9618E-01	5.8204E-03
4.2000E-02	1.5533E-01	-9.1490E-02
-1.1239E-01	2.9618E-01	-5.8204E-03
-3.9615E-01	-2.3595E-02	1.4500E-01
3.8132E-12	-1.3261E-10	2.2219E-11
-5.6283E-02	1.3913E-01	2.6012E-02
2.5680E-10	3.5415E-10	-1.8620E-10

OBSERVABILITY MATRIX

-9.9838E-02	-9.5150E-02	-9.6648E-02	2.8480E-03	-1.8602E-03	-1.8602E-03	8.1384E-02	1.2387E-02
0.0000E+00	0.0000E+00	0.0000E+00	0.0000E+00	-4.9793E-04	4.9793E-04	0.0000E+00	0.0000E+00
-3.3447E-03	3.4451E-03	-6.7951E-03	-7.4483E-02	5.9029E-03	5.9029E-03	8.4965E-02	-2.3113E-01
0.0000E+00	0.0000E+00	0.0000E+00	0.0000E+00	-7.7975E-03	7.7975E-03	0.0000E+00	0.0000E+00
8.8514E-01	9.2986E-01	9.9710E-01	4.1263E-02	1.3249E-02	1.3249E-02	-4.7233E-01	-6.1643E-02
0.0000E+00	0.0000E+00	0.0000E+00	0.0000E+00	3.7872E-03	-3.7872E-03	0.0000E+00	0.0000E+00

APPENDIX E

GAIN MATRICES AND PROPERTIES OF THE CLOSED LOOP SYSTEM

For the 4-input, 4-output design the Kalman filter, control gain, and L matrices are real matrices displayed as 12x4, 4x12, and 12x4 matrices, respectively. In the case of the control gain matrices, the 12 elements of each row are displayed as two rows, containing the first six elements in one row and the last six elements in the next. The eigenvalues and transmission zeros of the open and closed loop plant are 1x24 complex matrices. The 24 elements in the row are displayed as four rows, with six elements in each row. The imaginary part of each element is directly below the real part. Similar notation is used for the 3-input, 3-output design.

APPENDIX E1

PROPERTIES OF THE ROLL CONTROL MODEL

FILTER GAIN MATRIX

-1.0282E+00	-1.8198E+01	-8.1019E-01	-2.1680E+00
1.1923E-01	7.9327E-02	-7.5141E-01	2.8994E-02
1.9031E+00	1.7664E+00	-8.6529E-01	1.5857E-01
-1.4904E+00	4.2619E-01	1.2014E+00	1.1415E-01
9.3005E-03	4.4870E-01	9.2495E-02	5.4981E-02
6.8777E-03	-3.4783E-01	-2.6354E-01	-3.8983E-02
2.4814E-02	4.1892E+00	2.1197E-01	4.9849E-01
1.8704E-01	2.4765E-01	-3.5220E-01	4.9200E-02
-3.0473E-02	-4.2343E-03	-3.1907E-02	3.5337E-04
-4.2073E-02	2.1331E-02	3.8510E-01	-4.2349E-03
5.3431E+00	2.1792E-01	-3.8501E-01	-1.5210E-01
2.1792E-01	4.9887E+00	2.8426E-01	-4.8414E-03

CONTROL GAIN MATRIX

1.3487E+00	1.4722E-03	-1.8437E-03	3.2330E-03	-2.8935E+00	2.1865E+00
-2.3081E+01	4.6679E-02	2.3366E+01	2.0238E+00	-2.3789E-01	2.5951E+01
1.4722E-03	2.0983E+00	-1.1733E-02	-4.2671E-02	-4.7100E-02	2.5212E+00
-7.6947E-01	1.9053E-01	1.7016E+00	-2.3196E+01	8.8982E-02	3.6430E-01
-1.8437E-03	-1.1733E-02	1.3132E+00	-3.5292E-01	-7.9515E-01	-1.3192E+00
-8.6155E+00	2.5982E+00	-1.9569E+00	1.4596E+00	1.4934E+00	4.8954E+00
3.2330E-03	-4.2671E-02	-3.5292E-01	1.2835E+00	-9.4105E-01	2.7612E+00
-8.7112E+00	-2.5781E+00	-5.8551E-01	6.8046E-01	-1.9771E+00	5.4309E+00

APPENDIX E1

L MATRIX

-6.0839E-01	-3.6479E+01	5.6633E-01	-4.3555E+00
1.5610E-02	8.7114E-02	-1.5284E+00	6.4870E-03
3.3627E+00	3.5527E+00	-2.4355E+00	4.4871E-01
-2.6540E+00	8.8502E-01	2.7545E+00	1.5325E-01
-2.8582E-02	8.9419E-01	8.1547E-14	1.0539E-01
2.8826E-02	-9.0182E-01	-8.2242E-14	-1.0629E-01
-2.6814E-01	8.3888E+00	7.6502E-13	9.8873E-01
0.0000E+00	0.0000E+00	0.0000E+00	0.0000E+00
4.9774E-09	1.4154E-03	-1.0629E-01	-4.4369E-13
-4.6300E-08	-1.3166E-02	9.8873E-01	4.1272E-12
1.0000E+01	-1.4691E-09	-3.8444E-17	1.2488E-11
-1.3286E-10	1.0000E+01	6.9211E-12	-5.5841E-09

OPEN LOOP EIGENVALUES

9.5843E-09	0.0000E+00	0.0000E+00	0.0000E+00	-1.4176E-02	-3.8412E-02
-4.4084E-01	-4.4084E-01	-4.5114E-01	-5.0486E-01	-5.8965E-01	-5.8965E-01
-4.0661E-02	-4.2886E-02	-7.1364E-02	-1.9689E-01	-1.9689E-01	-2.5114E-01
-9.5148E-01	-9.5148E-01	-1.0104E+00	-1.3887E+00	-1.3887E+00	-1.4462E+00
0.0000E+00	0.0000E+00	0.0000E+00	0.0000E+00	0.0000E+00	0.0000E+00
4.7901E-01	-4.7901E-01	0.0000E+00	0.0000E+00	1.1366E+00	-1.1366E+00
0.0000E+00	0.0000E+00	0.0000E+00	3.1300E-01	-3.1300E-01	0.0000E+00
1.0148E+00	-1.0148E+00	0.0000E+00	1.3186E+00	-1.3186E+00	0.0000E+00

APPENDIX E1

OPEN LOOP TRANSMISSION ZEROS

1.0000E+30	1.0000E+30	1.0000E+30	1.0000E+30	1.1625E+08	1.0192E+08
-3.9767E-02	-3.9767E-02	-1.9869E-01	-2.0469E-01	-2.0469E-01	-2.5097E-01
1.2816E+05	1.4260E+04	1.2133E+00	1.2202E+00	-1.4256E-02	-3.8414E-02
-2.8357E-01	-4.5944E-01	-1.4263E+04	-1.2816E+05	-8.6484E+07	-5.8038E+09
0.0000E+00	0.0000E+00	0.0000E+00	0.0000E+00	0.0000E+00	0.0000E+00
1.6540E-03	-1.6540E-03	0.0000E+00	2.8343E-01	-2.8343E-01	0.0000E+00
0.0000E+00	0.0000E+00	1.0851E+04	-1.0851E+04	0.0000E+00	0.0000E+00
0.0000E+00	0.0000E+00	0.0000E+00	0.0000E+00	0.0000E+00	0.0000E+00

CLOSED LOOP EIGENVALUES

-1.4220E-02	-3.8414E-02	-3.8479E-02	-4.1399E-02	-1.0317E-01	-1.0317E-01
-5.1064E-01	-5.1064E-01	-5.1516E-01	-5.2355E-01	-5.2355E-01	-7.1513E-01
-2.3970E-01	-2.3970E-01	-2.5106E-01	-2.7292E-01	-2.7292E-01	-4.1228E-01
-7.4533E-01	-7.5232E-01	-7.5232E-01	-1.0388E+00	-1.1957E+00	-1.1957E+00
0.0000E+00	0.0000E+00	0.0000E+00	0.0000E+00	1.0659E-01	-1.0659E-01
7.0401E-02	-7.0401E-02	0.0000E+00	9.2146E-01	-9.2146E-01	0.0000E+00
3.3649E-01	-3.3649E-01	0.0000E+00	2.7737E-01	-2.7737E-01	0.0000E+00
0.0000E+00	8.5953E-01	-8.5953E-01	0.0000E+00	1.1639E+00	-1.1639E+00

CLOSED LOOP TRANSMISSION ZEROS

7.5203E+10	1.1350E+04	8.6830E+03	6.7422E+03	2.5300E+02	2.5300E+02
-3.9768E-02	-3.9768E-02	-1.9869E-01	-2.0469E-01	-2.0469E-01	-2.5097E-01
1.5900E+00	1.4499E+00	2.5446E-01	7.5507E-01	-1.4253E-02	-3.8414E-02
-2.8357E-01	-4.5944E-01	-5.0698E+02	-6.7412E+03	-8.6823E+03	-1.1349E+04
0.0000E+00	0.0000E+00	0.0000E+00	0.0000E+00	4.3878E+02	-4.3878E+02
1.6527E-03	-1.6527E-03	0.0000E+00	2.8343E-01	-2.8343E-01	0.0000E+00
2.4470E+05	-2.4470E+05	1.5450E+04	-1.5450E+04	0.0000E+00	0.0000E+00
0.0000E+00	0.0000E+00	0.0000E+00	0.0000E+00	0.0000E+00	0.0000E+00

APPENDIX E2

PROPERTIES OF THE MODEL WITHOUT ROLL CONTROL

FILTER GAIN MATRIX

-1.8104E+01	-9.9739E-01	-1.9187E+00
8.3100E-02	-7.5396E-01	-2.4242E-03
1.0178E+00	2.9009E-01	1.2935E-01
4.4848E-01	9.4995E-02	4.6515E-02
-3.2777E-01	-2.9706E-01	-4.0709E-02
4.2139E+00	1.7960E-01	4.3854E-01
-8.2718E-02	1.1100E-01	-3.5626E-03
8.5074E-03	-5.1439E-02	6.8779E-05
2.0580E-02	3.8598E-01	5.4579E-03
-1.9794E-01	3.5426E-01	-5.2399E-03
5.0090E+00	2.6332E-01	-6.6166E-02

CONTROL GAIN MATRIX

1.3399E+00	2.4951E-03	-4.1531E-02	-2.8549E+00	2.1877E+00	-2.2711E+01
2.8530E-02	2.3251E+01	1.9938E+00	-2.3664E-01	2.5708E+01	
2.4951E-03	2.0950E+00	-4.4818E-02	-6.1695E-02	2.5273E+00	-9.1184E-01
8.4496E-02	1.7283E+00	-2.3191E+01	-5.5890E-02	4.6906E-01	
-4.1531E-02	-4.4818E-02	1.1898E+00	-1.3346E+00	1.2073E+00	-1.3296E+01
-7.3320E-02	-2.3292E+00	1.7524E+00	-4.3088E-01	8.1221E+00	

APPENDIX E2

L MATRIX

-3.6209E+01	4.1533E-02	-4.3257E+00
8.0193E-02	-1.5149E+00	5.7204E-03
2.0617E+00	4.6520E-01	2.8358E-01
8.9353E-01	-1.3558E-11	1.0532E-01
-9.0115E-01	1.3674E-11	-1.0621E-01
8.3826E+00	-1.2719E-10	9.8801E-01
0.0000E+00	0.0000E+00	0.0000E+00
1.4154E-03	-1.0629E-01	1.4658E-11
-1.3166E-02	9.8873E-01	-1.3635E-10
2.2992E-01	4.6272E-09	2.7099E-02
1.0000E+01	1.1950E-11	-3.4596E-10

OPEN LOOP EIGENVALUES

1.4791E-08	0.0000E+00	0.0000E+00	-1.4176E-02	-3.8430E-02	-4.0661E-02
0.0000E+00	0.0000E+00	0.0000E+00	0.0000E+00	0.0000E+00	0.0000E+00
-4.2886E-02	-7.1364E-02	-1.8012E-01	-1.8012E-01	-1.9689E-01	-1.9689E-01
0.0000E+00	0.0000E+00	3.0158E-01	-3.0158E-01	3.1300E-01	-3.1300E-01
-3.1857E-01	-4.5114E-01	-4.5954E-01	-4.5954E-01	-5.0486E-01	-1.0233E+00
0.0000E+00	0.0000E+00	4.9673E-01	-4.9673E-01	0.0000E+00	1.1072E+00
-1.0233E+00	-1.0643E+00	-1.3940E+00	-1.3940E+00		
-1.1072E+00	0.0000E+00	1.3186E+00	-1.3186E+00		

APPENDIX E2

OPEN LOOP TRANSMISSION ZEROS

1.0000E+30	1.0000E+30	1.0000E+30	1.7438E+11	2.5380E+10	1.2540E+08
0.0000E+00	0.0000E+00	0.0000E+00	0.0000E+00	0.0000E+00	0.0000E+00
2.4318E+04	1.3204E+04	-1.4324E-02	-3.8432E-02	-3.9719E-02	-3.9719E-02
0.0000E+00	0.0000E+00	0.0000E+00	0.0000E+00	9.8294E-04	-9.8294E-04
-1.5509E-01	-1.8029E-01	-1.8029E-01	-1.9034E-01	-1.9034E-01	-3.1812E-01
0.0000E+00	3.0164E-01	-3.0164E-01	3.1017E-01	-3.1017E-01	0.0000E+00
-3.5414E-01	-4.5896E-01	-1.3205E+04	-2.4309E+04		
0.0000E+00	0.0000E+00	0.0000E+00	0.0000E+00		

CLOSED LOOP EIGENVALUES

-1.4259E-02	-3.8432E-02	-3.8768E-02	-4.0957E-02	-1.3245E-01	-1.3245E-01
0.0000E+00	0.0000E+00	0.0000E+00	0.0000E+00	1.0424E-01	-1.0424E-01
-1.7991E-01	-1.7991E-01	-1.9902E-01	-1.9902E-01	-2.8854E-01	-2.8854E-01
3.0178E-01	-3.0178E-01	3.0667E-01	-3.0667E-01	2.9348E-01	-2.9348E-01
-3.1880E-01	-4.5868E-01	-4.8610E-01	-5.2124E-01	-6.8742E-01	-7.5761E-01
0.0000E+00	0.0000E+00	0.0000E+00	0.0000E+00	0.0000E+00	0.0000E+00
-8.4879E-01	-8.4879E-01	-1.1972E+00	-1.1972E+00		
9.4987E-01	-9.4987E-01	1.1636E+00	-1.1636E+00		

CLOSED LOOP TRANSMISSION ZEROS

1.0000E+30	7.5842E+08	3.0352E+04	1.3159E+04	5.1442E+02	-1.4324E-02
0.0000E+00	0.0000E+00	0.0000E+00	0.0000E+00	0.0000E+00	0.0000E+00
-3.8432E-02	-3.9718E-02	-3.9718E-02	-1.5509E-01	-1.8029E-01	-1.8029E-01
0.0000E+00	9.8524E-04	-9.8524E-04	0.0000E+00	3.0164E-01	-3.0164E-01
-1.9034E-01	-1.9034E-01	-3.1812E-01	-3.5414E-01	-4.5896E-01	-2.5748E+02
3.1017E-01	-3.1017E-01	0.0000E+00	0.0000E+00	0.0000E+00	4.4566E+02
-2.5748E+02	-1.3166E+04	-3.0347E+04	-8.0668E+09		
-4.4566E+02	0.0000E+00	0.0000E+00	0.0000E+00		